ICRF Heating of Tokamaks

D.T. Blackfield

January 1979

UWFDM-278

FUSION TECHNOLOGY INSTITUTE

UNIVERSITY OF WISCONSIN

MADISON WISCONSIN

ICRF Heating of Tokamaks

D.T. Blackfield

Fusion Technology Institute
University of Wisconsin
1500 Engineering Drive
Madison, WI 53706

http://fti.neep.wisc.edu

January 1979

UWFDM-278

ICRF HEATING OF TOKAMAKS

Donald T. Blackfield

Nuclear Engineering Department
University of Wisconsin
Madison, Wisconsin 53706

January 1979

UWFDM-278

This work was supported by DOE Contract ET-78-S-02-4636.

ABSTRACT

In this paper the radiofrequency (RF) heating of tokamaks by means of the fast magnetosonic wave in the ion cyclotron range of frequencies (ICRF) is examined. Using linear weak damping theory the RF heating expressions for each species are derived. Possible mode conversion processes which may occur in tokamak reactors are then examined. Next, various parametric processes are examined for reactor conditions. Except possibly near the RF launching structure, no instabilities are calculated to be excited. Next, experimental results are surveyed for various RF heated tokamaks.

In the next section, a space-averaged, time-dependent startup model is used to describe the role of RF heating to ignition of a tokamak reactor. The computational point model code simultaneously solves the ion and electron energy balance equations. Conduction, convection and radiative losses are compared with ion and electron wave heating processes together with alpha particle heating from fusion reactions. The model shows that 150-225 MJ (75 MW, 2-3 sec) of RF power is needed to ignite a 700 MW_e fusion reactor when the RF heating is overlapped with the current-rise phase of operation.

Since RF heating at the second ion harmonic is a non-Maxwellian process, in the third section quasi-linear theory is used to derive RF velocity space diffusion terms which are then inserted in a two dimensional velocity space Fokker-Planck code. Using this code, only an 11% difference in the

reactor Q is found from a purely Maxwellian case. Due to the collisionality of reactor plasmas, it appears that high energy ion tail formation is suppressed.

TABLE OF CONTENTS

		Page
	ABSTRACT	i
I.	REVIEW OF ICRF HEATING.	1
	A. Introduction	1
	B. Review of Vlasov Plasma Theory	4
	1. Cold Plasma Theory.	4
	2. Hot Plasma Theory	10
	C. Mode Conversion Processes.	24
	D. Parametric Instabilities	28
	E. Experimental Results	39
	References.	47
II.	POINT MODEL	54
	A. Reactor Startup.	54
	B. NUWMAK Point Code Results.	67
	References.	91
III.	FOKKER-PLANCK THEORY AND RF HEATING	92
	A. Fokker-Planck Theory	93
	B. Quasi-linear Theory.	95
	C. Numerical Results for NUWMAK Using HYBRID III. .	105
	References.	121

APPENDICES. 123
A. Ion-Ion Hybrid Resonance and Fundamental Minority Species Heating in Reactor Tokamaks . 123
B. The Fokker-Planck Collision Operator 126
C. 136
D. Low Frequency Alfven Wave Heating. 138
1. Theory of Alfven Wave Heating 138
2. Fast Alfven Wave Electron Heating of TETR Plasma 142

References. 154

TABLES. 155
1. Tokamak Parameters 155
2. Experimental RF Parameters 157
3. Proposed RF Parameters 159
4. Reactor Parameters 160
5. Tokamak Parameters 161
6. Plasma Parameters. 161

I REVIEW OF ICRF HEATING

I-A INTRODUCTION

For a fusion reactor to reach the required ignition temperature of 7-10 keV, it appears that ohmic heating alone will be insufficient. The power supplied to the plasma through ohmic heating is

$$P_{oh} = E_\phi J_\phi = \eta J_\phi^2 \qquad (1)$$

where η is the plasma resistivity. Neoclassical theory predicts that the plasma resistivity will be[1]

$$\eta_{nc} = \eta_{sp}(1-.95(r/R)^{1/2} + 1.95(r/R))^{-1} \qquad (2)$$

where η_{sp} is the Spitzer resistivity,[2]

$$\eta_{sp} = 6.53\times10^3 T_e^{-3/2} \ln\Lambda \qquad \text{(cgs)}. \qquad (3)$$

The ohmic heating expression is proportional to $T_e^{-3/2}$ and for $T_e > 1$ keV, becomes negligible (see figs.(II-B-8,16)).

The two main candidates for providing the additional power are neutral beams and radiofrequency (RF) heating. A comparison of the relative merits of neutral beams and radiofrequency heating, utilizing the fast magnetosonic wave at the second harmonic of deuterium, may be found in an EPRI report by Scharer, Conn, and Blackfield.[3] The difficulty with neutral beams, whose physics is well understood, lies in the feasibility of obtaining sources. Neutral beams must have high energy (150-300 keV) for plasma penetration, large current (1-3 A/cm^2) while having an overall efficiency $\gtrsim$ 50%.

Due to the rapidly decreasing electron stripping cross section with increasing ion energy, negative ion sources must be used. Much experimental work remains to be done im the area of source development.

Several RF frequency ranges appear to be attractive for supplying auxiliary heating power and are reviewed in papers by Scharer, Blackfield and others[3-6]. A particularly attractive regime, from the standpoint of available power supplies and present day experiments, is the ion cyclotron range of frequencies (ICRF). Most of the theoretical work, briefly reviewed in Secs. I-B,C,D , has been done by Adam and Samain[7-9] at Fontenay-aux-Roses; Weynants, Messiaen and Vandenplas[10-18] at the Ecole Royale Militaire in Belg m; Stix, Perkins et al at Princeton[19-25]; Swanson and Ngan[26-27] at USC, and Scharer, Mau, McVey and Blackfield[3-6,28-37] at Wisconsin.

ICRF heating experiments have been performed on several tokamaks including ST, ATC, TFR, TO-1, TM-1Vch, T-4 and PLT.[38-45] Other experiments are being planned for ALCATOR, T-10, DIVA, and JET. In section I-E, past experimental results and future heating proposals are surveyed.

In Sec.I-B, expressions for RF heating with the fast magnetosonic wave at the second harmonic of deuterium are derived using Vlasov theory. These expressions are then added to fluid energy balance equations in Sec.II-A. Through space averaging of these equations, a point model computer code is used to investigate several possible RF startup scenarios for NUWMAK[35,46] in Sec.II-B.

Possible mode conversion processes which might occur

within a reactor are discussed in Sec.I-C and Appendix A. In Sec.I-D parametric instabilities which may result from the plasma being heated by the RF are examined.

In Sec.III-A the derivation of the Fokker-Planck equation to which are added RF induced quasi-linear diffusion terms is (Sec.III-B) is reviewed. The resulting equation is solved using a two dimensional velocity space Fokker-Planck code, HYBRID III. In Sec.III-C several RF startup scenarios using HYBRID III are examined.

I-B REVIEW OF VLASOV PLASMA THEORY

I-B-1 Cold plasma theory

To optimize an auxiliary heating scheme, the supplementary heating power should be deposited in the core of the plasma. Conn and Kesner[50] have shown that ignition criteria are lowered when the density and temperature profiles are peaked at the center. Physically, as space-time studies have verified[51], when the profiles are peaked at the plasma center, ignition can occur there. A burn wave is formed and propagates outwards, igniting the remaining plasma. Through the use of core heating, the power requirements for supplementary heating can be reduced.

For a reactor to reach ignition, approximately 50-100 MW of additional power will be needed. In the ICRF range (f~25-200 MHz), power supplies on the order of megawatts are already available. This, and the fact that core heating is feasible, makes ICRF heating desirable.

In cold plasma theory, both the fast and slow waves can propagate parallel to an externally applied magnetic field, B_o (see fig.(I-B-1)). To minimize heating and radiation damage to the RF launching structure, either a waveguide or coil must be placed outside of the plasma (fig.(I-B-2)). Therefore, any ICRF wave launched must propagate across magnetic field lines in order to heat the center. In the tokamak configuration (fig.(I-B-3)), ions rotate about field lines in a left-handed sense. To have ion cyclotron heating, it is desirable to have a large left-handed component of the wave electric field. Ion

cyclotron heating occurs when the electric field rotates with the ions and the field oscillates with the local gyroperiod (Doppler shifted in a hot plasma). When this occurs, the ions are accelerated with a corresponding damping of the wave. The slow or ion cyclotron wave is a left-handed polarized wave, so on first impression one would expect this to be a desirable heating mode. In fact, this wave was used to heat the Model C stellerator at Princeton.

In a tokamak, a slow wave excited at the plasma edge must proceed up a steep density gradient. The perpendicular wave-number, $k_\perp$, increases as the wave propagtes up this gradient. Near the plasma surface, the slow wave reaches a cutoff where $k_\perp \to \infty$, called the perpendicular ion cyclotron resonance. Here the slow wave may be mode converted into an outwardly propagating electrostatic ion cyclotron or ion Bernstein wave (I.B.).[4,20,54,55] The resultant electrostatic wave may then be quickly damped by electron Landau damping, causing undesirable heating near the plasma surface. Surface heating leads to enhanced radiation losses and increased wall sputtering.

Through the proper adjusting of the RF generating frequency and matching of the loading impedance, ion heating at the plasma center can be achieved using the fast wave. The fast wave, in a hot plasma, propagates at all angles to the external magnetic field (fig.(I-B-4)). For this reason, this paper will concentrate on fast wave heating, specifically at the second harmonic. Fundamental heating is briefly discussed in Appendix A.

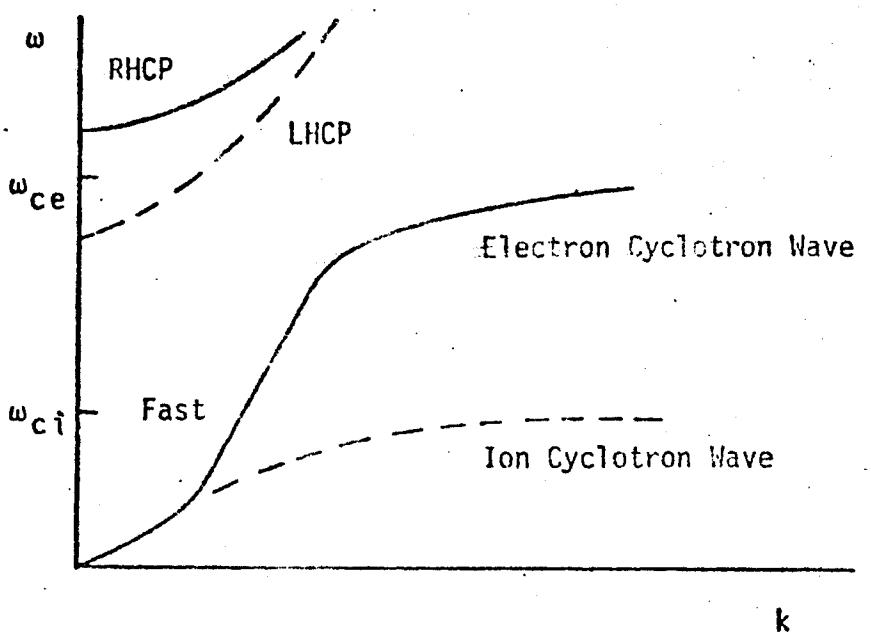

Fig. I-B-1 Principal cylcotron waves $\vec{k} \| \vec{B}$ (reproduced from Ref. 37)

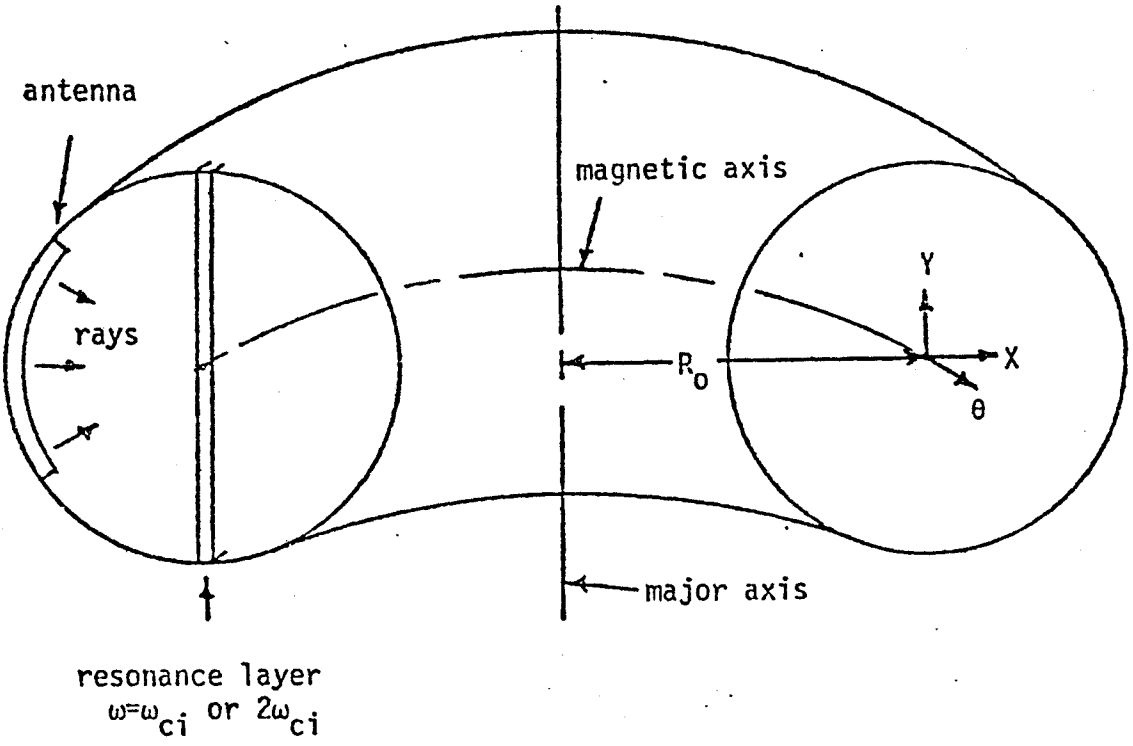

minor cross-sectional coordinates

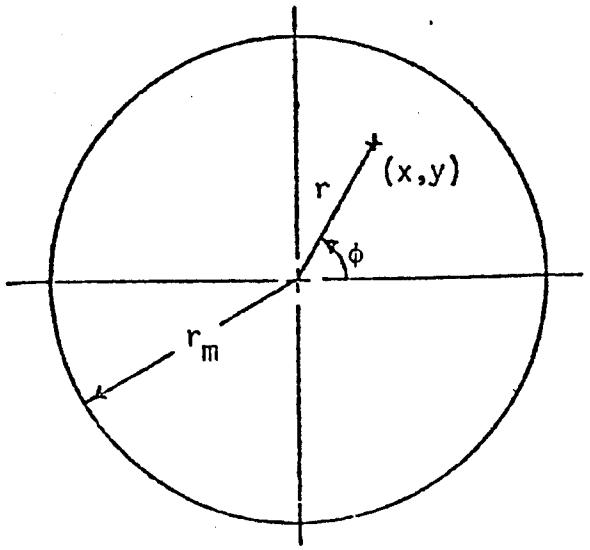

Fig. I-B-2 Axisymmetric tokamak with RF wave launching attenna on the LFS (reproduced from Ref. 37)

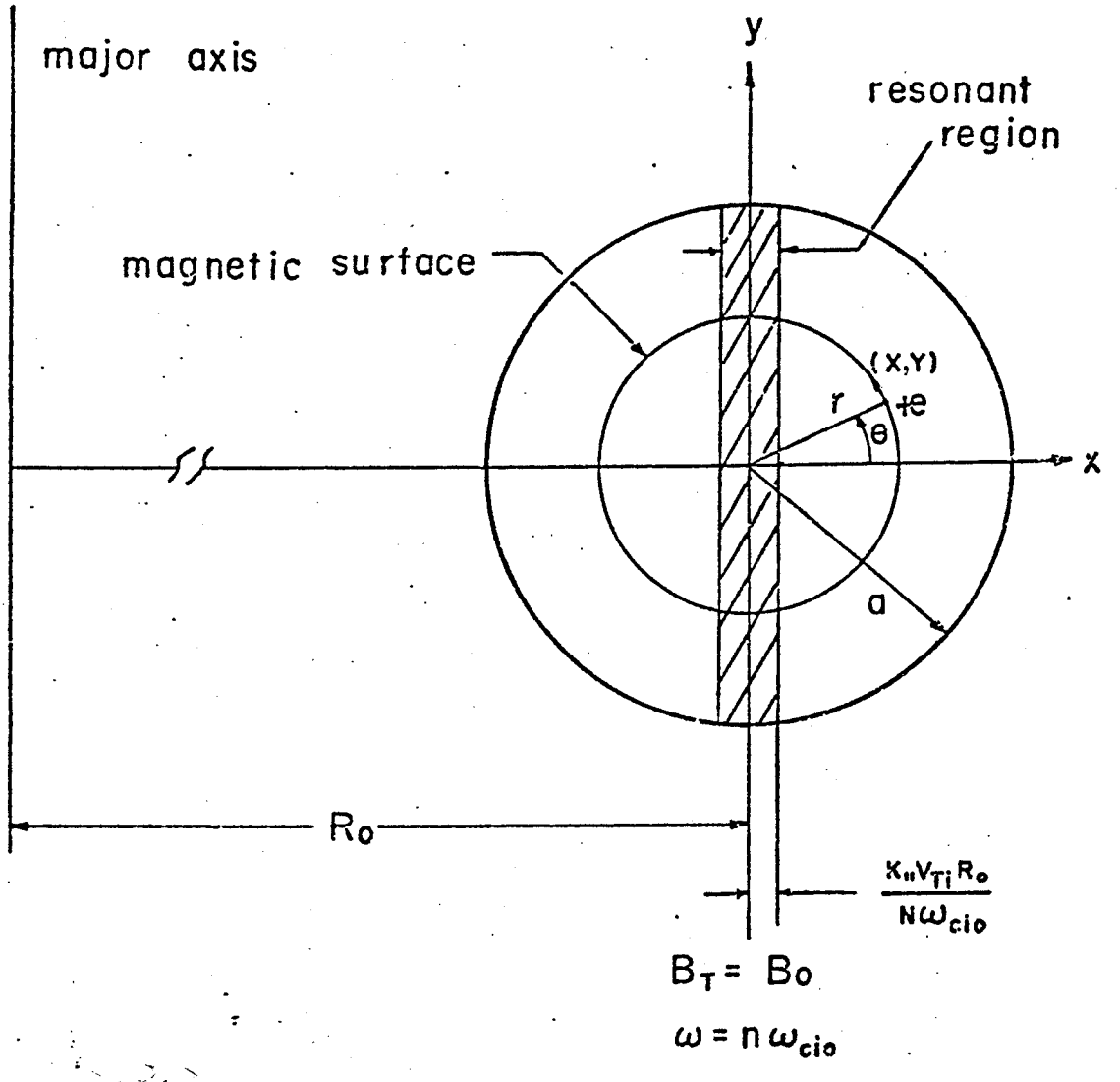

Fig. I-B-3 Fast wave cyclotron heating scheme in the tokamak configuration. B_o is the magnetic field on axis and ω_{cio} is the corresponding ion gyro-frequency. (reproduced from Ref.6)

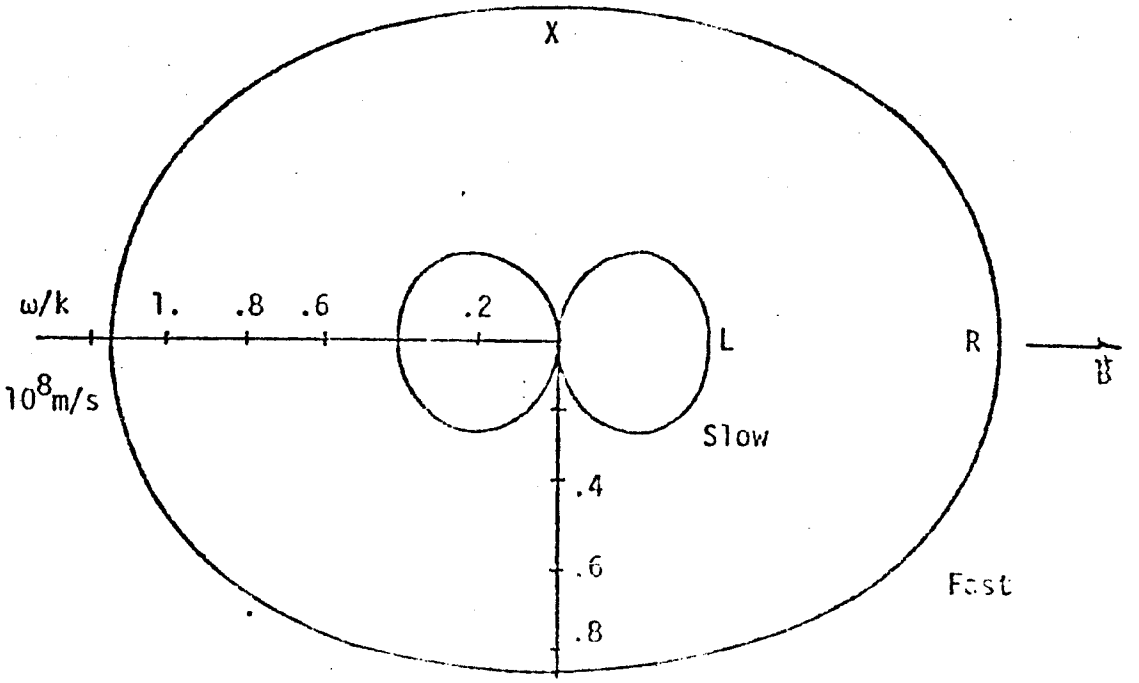

Fig. I-B-4 Wave-normal surfaces (reproduced from Ref. 37)

I-B REVIEW OF VLASOV PLASMA THEORY

I-B-2 Hot plasma theory

When the RF driving frequency $\omega=\omega_{ci}$, the fast wave is mainly a right-handed circularly polarized wave which undergoes little ion cyclotron damping. On solving the wave equation for an unbounded plasma, for higher harmonics (n=2,3), an appreciable left-handed component appears. In NUWMAK with $\omega=2\omega_{cd}$, fig.(III-B-11) shows that $|E_+|/|E_-| \sim O(1)$.

In hot plasma theory, ions are heated by the fast wave through finite ion gyroradius effects, shown in fig.(I-B-5). The electric field vector of a left-handed circularly polarized wave, $|E_+|$, is plotted in both space and time. The direction of the D.C. external magnetic field and the sense of the ion gyromotion are also shown. At various points along the ion trajectory, the ion velocity may be synchronous with the wave electric field vector. At these points energy may be exchanged between the particle and wave, depending upon the ion velocity space distribution. For point and space-time calculations, Maxwellian particle distributions are assumed. For second harmonic heating, energy exchange is possible when the ion gyroradius equals one quarter of the wavelength of the fast wave. Hence, harmonic heating preferentially heats ions with finite gyroradius.

Perkins[19] has shown that only the fast wave can become a normal mode of a tokamak when $\omega=n\omega_{ci}$ (n=1,2,3) is located in the center. An eigenmode structure enhances the heating proper-

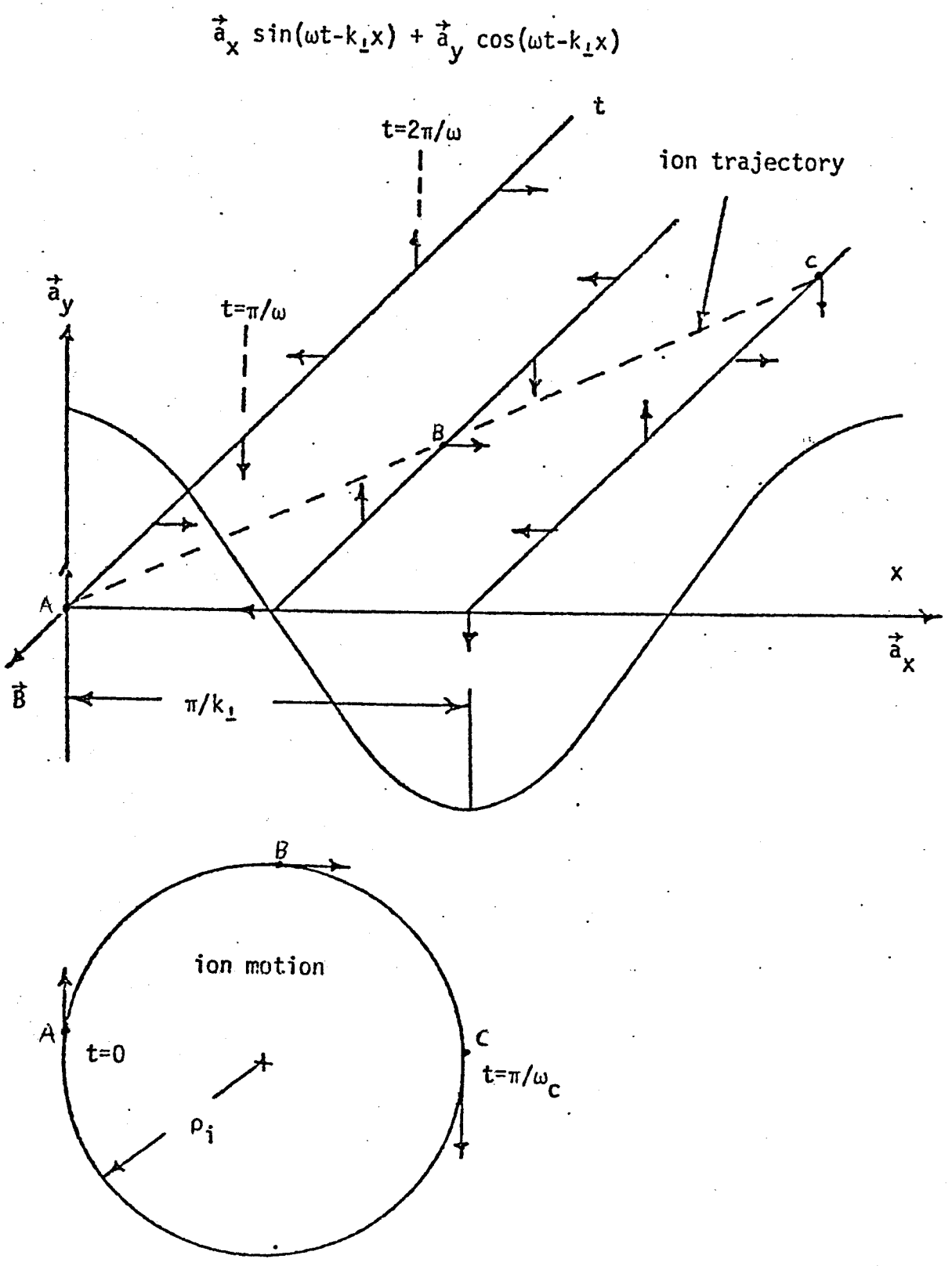

Fig. I-B-5 LHCP ion cyclotron wave in x and t space
The ion may be heated at points A,B and C.
(reproduced from Ref. 37)

ties of the fast wave. Eigenmodes enhance the wave electric field and increases the loading resistance of the launching structure.[18] Besides heating ions, the fast wave may also heat electrons through Landau and transit time damping when $v_{\phi_{\parallel}} \leq v_{the}$ (see Appendix D).

Unlike neutral beams, the fast magnetosonic wave does not have a maximum density cutoff, therefore, wave penetration is not a problem. However, there is a low density cutoff, below which no eigenmode is possible.[5,56,57] For small values of $k_{\parallel}$[5]

$$k_{\perp} \sim \frac{\omega_{pi}}{c} \frac{\omega}{\omega_{ci}} \quad . \tag{4}$$

For a radial eigenmode to be formed $k_{\perp} \geq \pi/2a$, From eq.(4), the minimum or critical density needed is

$$n_c = 1.64\times10^{12} (m_i/m_e) (\Omega a)^{-2} \quad cm^{-3} \tag{5}$$

where $\Omega=\omega/\omega_{ci}$ and a= the plasma minor radius (cm). For NUWMAK with $\omega=2\omega_{cd}$, $n_c \sim 1.2 \times 10^{11}$ cm^{-3}, which is easily met.

Linear wave theory will be used to calculate the power flow to each species, since the wave damping mechanisms are weak and mode conversion and parametric processes are neglected. In weak damping theory, the power deposited in the plasma from oscillating electric fields is[24,58]

$$P = \omega \vec{E} \cdot (\overline{\overline{K}}^a \cdot \vec{E})/2 \qquad (W/cm^3) \tag{6}$$

where $\overline{\overline{K}}^a$ is the anti-hermitian part of the dielectric tensor. $\overline{\overline{K}}$ and $\vec{E}$ will now be obtained for an unbounded hot plasma starting from the Vlasov-Maxwell equations[59]

$$\frac{\partial f_\alpha}{\partial t} + \vec{v} \cdot \frac{\partial f_\alpha}{\partial \vec{r}} + \frac{q_\alpha}{m_\alpha c} (c\vec{E} + \vec{v}\times\vec{B}) \cdot \frac{\partial f_\alpha}{\partial \vec{v}} = 0 \tag{7}$$

where α = species (e,d,t) and

$$n_\alpha(\vec{r},\vec{t}) = n_{o_\alpha} \int f_\alpha(\vec{r},\vec{v},t)\, d\vec{v} \tag{8}$$

$$\vec{\nabla} \times \vec{E} + \frac{1}{c}\frac{\partial \vec{B}}{\partial t} = 0 \ , \tag{9a}$$

$$\vec{\nabla} \times \vec{B} - \frac{1}{c}\frac{\partial \vec{E}}{\partial t} = \frac{4\pi \vec{J}}{c} \ , \tag{9b}$$

$$\vec{\nabla}\cdot\vec{E} = 4\pi\rho \ , \tag{9c}$$

$$\vec{\nabla}\cdot\vec{B} = 0 \ . \tag{9d}$$

Expanding $\vec{E},\vec{B}$ and f about their equilibrium positions

$$\begin{aligned} f &= f_o + f_1 \ , \\ \vec{B} &= B_o + B_1 \ , \\ \vec{E} &= E_o + E_1 \ , \end{aligned} \tag{10}$$

to zeroth order , eq.(7) becomes

$$\frac{\partial f_{o_\alpha}}{\partial t} + \vec{v}\cdot\vec{\nabla} f_{o_\alpha} + \frac{q_\alpha}{m_\alpha c}\left(c\vec{E}_o + \vec{v}\times\vec{B}_o \right)\cdot\vec{\nabla}_v f_{o_\alpha} = 0 \ . \tag{11}$$

Assuming that $f_o = f_o(\vec{v})$,

$$\frac{q_\alpha}{m_\alpha c}\,(cE + \vec{v}\times B_o)\cdot\vec{\nabla}_v f_{o_\alpha} = 0 \ , \tag{12}$$

so that to first order

$$\frac{df_{1_\alpha}}{dt} = \frac{\partial f_{1_\alpha}}{\partial t} + \frac{q_\alpha}{m_\alpha c}(cE_o + \vec{v}\times B_o)\cdot\vec{\nabla}_v f_{1_\alpha} = -\frac{q_\alpha}{m_\alpha c}(cE_1 + \vec{v}\times B_1)\cdot\vec{\nabla}_v f_{o_\alpha} \ . \tag{13}$$

With $f_{1_\alpha}(t\to\infty) \to 0$ as an initial condition, and

$$\begin{aligned} E_o &= 0 \ , \\ E_1 &= E_1 e^{i(\vec{k}\cdot\vec{x}-\omega t)} \ , \\ B_1 &= B_1 e^{i(\vec{k}\cdot\vec{x}-\omega t)} \ , \end{aligned} \tag{14}$$

using integration along the unperturbed orbit, that

$$f_{k_\alpha} = -\frac{q_\alpha}{m_\alpha}\int_0^\infty \frac{\partial f_{o_\alpha}}{\partial \vec{v}} \cdot \left[\left(1 - \frac{\vec{k}\cdot\vec{v}(\tau)}{\omega}\right)\overline{\overline{I}} + \frac{\vec{k}\vec{v}(\tau)}{\omega}\right] \cdot E_1 e^{-i\Phi(\tau)} d\tau \tag{15}$$

with $\tau = t-t'$, $\Phi(\tau) = \vec{k}\cdot(\vec{x}-\vec{x}')$, and $f_{1_\alpha} = f_{k_\alpha} e^{i(\vec{k}\cdot\vec{x}-\omega t)}$.

Assuming that there are no density gradients and orientating the coordinate axis so that $k_y=0$, the unperturbed particle orbit is

$$\vec{v}' = v_\perp \cos(\omega_{c\alpha}\tau+\theta)\hat{x} + v_\perp \sin(\omega_{c\alpha}\tau+\theta)\hat{y} + v_\parallel \hat{z} \quad . \tag{16}$$

Defining the current density $\vec{J}_k$ as

$$\vec{J}_k = \sum_\alpha q_\alpha n_\alpha \langle v_\alpha \rangle \quad , \qquad \langle v_\alpha \rangle \equiv \int \vec{v} f_{k_\alpha} \, d\vec{v} \quad , \tag{17}$$

Maxwell's eqs. yield the following expression for $\vec{J}_k$

$$\vec{J}_k = \frac{i\omega}{4\pi}\,(\overline{\overline{\varepsilon}} - \overline{\overline{I}})\cdot E_1 \tag{18}$$

where

$$\overline{\overline{\varepsilon}}(\vec{k},\omega) = \overline{\overline{I}} + \sum_\alpha \frac{\omega_{p_\alpha}^2}{i\omega}\int_0^{2\pi} d\theta \int_0^\infty v_\perp dv_\perp \int_{-\infty}^{\infty} v_\parallel dv_\parallel \int_0^\infty d\tau \; \vec{v}\frac{\partial f_{o_\alpha}}{\partial \vec{v}'}\cdot\left[\left(1-\frac{\vec{k}\cdot\vec{v}}{\omega}\right)\overline{\overline{I}} + \frac{\vec{k}\vec{v}'}{\omega}\right] e^{-i\Phi(\tau)} \tag{19}$$

Expressing $e^{-i\Phi(\tau)}$ as[59]

$$\sum_{n=-\infty}^{\infty}\sum_{n'=-\infty}^{\infty} J_n(k_\perp\rho_\alpha) J_{n'}(k_\perp\rho_\alpha) e^{-i\left[n(\omega_{c\alpha}\tau+\theta) - n'\theta + (k_\parallel v_\parallel - \omega)\tau\right]}$$

where $\rho_\alpha = v_\perp/\omega_{c\alpha}$,

the dielectric tensor may be written as

$$\overline{\overline{\varepsilon}}(\vec{k},\omega) = \left(1-\frac{\omega_p^2}{\omega^2}\right)\overline{\overline{I}} - \sum_\alpha \frac{\omega_{p_\alpha}^2}{\omega^2}\sum_{n=-\infty}^{\infty}\int d\vec{v}\left[\frac{n}{\rho_\alpha}\frac{\partial f_{o_\alpha}}{\partial v_\perp} + \frac{k_\parallel \partial f_{o_\alpha}}{\partial v_\perp}\right]\frac{\Pi_\alpha(v_\perp, v_\parallel; n)}{n\omega_{c_\alpha} + k_\parallel v_\parallel - \omega} \tag{20}$$

where

$$\Pi_\alpha = \begin{bmatrix} \frac{n^2\omega_{c\alpha}^2}{k_\perp^2} J_n^2 & \frac{iv_\perp n\omega_{c\alpha}}{k_\perp} J_n J_n' & \frac{v_\parallel n\omega_{c\alpha}}{k_\perp} J_n^2 \\ \frac{-iv_\perp n\omega_{c\alpha}}{k_\perp} J_n J_n' & v_\perp^2 (J_n')^2 & -iv_\parallel v_\perp J_n J_n' \\ \frac{v_\parallel n\omega_{c\alpha}}{k_\perp} J_n^2 & iv_\parallel v_\perp J_n J_n' & v_\parallel^2 J_n^2 \end{bmatrix} \quad (21)$$

where $\int d\vec{v} \equiv 2\pi \int_0^\infty v_\perp dv_\perp \int_{-\infty}^\infty dv_\parallel$, $J_n = J_n(\xi)$, $J_n' = \frac{dJ_n(\xi)}{d\xi}$, and

$\xi \equiv k_\perp \rho_\alpha$.

The wave equation may be written as

$$\frac{c^2}{\omega^2} (\vec{k} \times (\vec{k} \times E_1) + \overline{\overline{\varepsilon}} \cdot E_1) = 0 , \quad (22)$$

or in matrix form

$$\begin{bmatrix} K_{xx} - n_\parallel^2 & K_{xy} & K_{xz} + n_\parallel n_\perp \\ K_{yx} & K_{yy} - n^2 & K_{yz} \\ K_{zx} + n_\parallel n_\perp & K_{zy} & K_{zz} - n_\perp^2 \end{bmatrix} \cdot \begin{bmatrix} E_1 \end{bmatrix} = 0 , \quad (23)$$

defining $\overline{\overline{K}} = \frac{c^2 \overline{\overline{\varepsilon}}}{\omega^2}$, $\vec{n} \equiv \frac{c\vec{k}}{\omega}$ and assuming a bi-Maxwellian

$$f_{o_\alpha} = f_{o_\alpha} e^{-\frac{m_\alpha}{2}(v_\perp^2/T_{\perp_\alpha} + v_\parallel^2/T_{\parallel_\alpha})} . \quad (24)$$

To third order in $\lambda = k_\perp^2 \rho_\alpha^2/2$ the tensor elements are[5,6,37,60,61]

$$K_{xx} = A_o + A_1 n_\perp^2 + A_2 n_\perp^4 + A_3 n_\perp^6 + \ldots$$

$$K_{xy} = C_o + C_1 n_\perp^2 + C_2 n_\perp^4 + C_3 n_\perp^6 + \ldots$$

$$K_{yy} = B_o + B_1 n_\perp^2 + B_2 n_\perp^4 + B_3 n_\perp^6 + \ldots$$

$$K_{yz} = F_o + F_1 n_\perp^2 + F_2 n_\perp^4 + F_3 n_\perp^6 + \ldots \qquad (25)$$

$$K_{xz} = E_o + E_1 n_\perp^2 + E_2 n_\perp^4 + E_3 n_\perp^6 + \ldots$$

$$K_{zz} = G_o + G_1 n_\perp^2 + G_2 n_\perp^4 + G_3 n_\perp^6 + \ldots$$

where

$$A_o = 1 + \sum_\alpha \rho_\alpha S_1^\alpha \qquad C_2 = i\sum_\alpha \rho_\alpha \eta_\alpha^2 \left(\tfrac{15}{2}D_1^\alpha - 6D_2^\alpha + \tfrac{3}{2}D_3^\alpha\right)$$

$$A_1 = -2\sum_\alpha \rho_\alpha \eta_\alpha (S_1^\alpha - S_2^\alpha) \qquad C_3 = i\sum_\alpha \rho_\alpha \eta_\alpha^3 \left(-\tfrac{28}{3}D_1^\alpha + \tfrac{28}{3}D_2^\alpha - 4D_3^\alpha + \tfrac{2}{3}D_4^\alpha\right)$$

$$A_2 = \sum_\alpha \rho_\alpha \eta_\alpha \left(\tfrac{5}{2}S_1^\alpha - 4S_2^\alpha + \tfrac{3}{2}S_3^\alpha\right) \qquad F_o = -i\sum_\alpha \gamma_\alpha (-S_o'^\alpha + S_1'^\alpha)$$

$$A_3 = \sum_\alpha \rho_\alpha \eta_\alpha \left(-\tfrac{7}{3}S_1^\alpha + \tfrac{14}{2}S_2^\alpha - 3S_3^\alpha + \tfrac{2}{3}S_4^\alpha\right) \qquad F_1 = -i\sum_\alpha \gamma_\alpha \eta_\alpha (3S_o'^\alpha - 4S_1'^\alpha + S_2'^\alpha)$$

$$B_o = A_o \qquad F_2 = -i\sum_\alpha \gamma_\alpha \eta_\alpha^2 \left(-5S_o'^\alpha + \tfrac{15}{2}S_1'^\alpha - 3S_2'^\alpha + \tfrac{1}{2}S_3'^\alpha\right)$$

$$B_1 = \sum_\alpha \rho_\alpha \eta_\alpha (4S_o^\alpha - 6S_1^\alpha + 2S_2^\alpha) \qquad F_3 = -i\sum_\alpha \gamma_\alpha \eta_\alpha^3 \left(\tfrac{53}{6}S_o'^\alpha - \tfrac{28}{3}S_1'^\alpha + \tfrac{22}{3}S_2'^\alpha - \tfrac{4}{3}S_3'^\alpha + \tfrac{1}{3}S_4'^\alpha\right)$$

$$B_2 = \sum_\alpha \rho_\alpha \eta_\alpha^2 \left(-12S_o^\alpha + \tfrac{37}{2}S_1^\alpha - 8S_2^\alpha + \tfrac{3}{2}S_3^\alpha\right) \qquad E_o = \sum_\alpha \gamma_\alpha D_1'^\alpha \qquad (26)$$

$$B_3 = \sum_\alpha \rho_\alpha \eta_\alpha^3 \left(20S_o^\alpha - \tfrac{97}{3}S_1^\alpha + \tfrac{50}{3}S_2^\alpha - 5S_3^\alpha + \tfrac{2}{3}S_4^\alpha\right) \qquad E_1 = \sum_\alpha \gamma_\alpha \eta_\alpha (-2D_1'^\alpha + D_2'^\alpha)$$

$$C_o = i\sum_\alpha \rho_\alpha D_1^\alpha \qquad E_2 = \sum_\alpha \gamma_\alpha \eta_\alpha^2 \left(\tfrac{5}{2}D_1'^\alpha - 2D_2'^\alpha + \tfrac{1}{2}D_3'^\alpha\right)$$

$$C_1 = i\sum_\alpha \rho_\alpha \eta_\alpha (-4D_1^\alpha + 2D_2^\alpha) \qquad E_3 = \sum_\alpha \gamma_\alpha \eta_\alpha^3 \left(-\tfrac{7}{3}D_1'^\alpha + \tfrac{11}{3}D_2'^\alpha - D_3'^\alpha + \tfrac{1}{6}D_4'^\alpha\right)$$

$$G_o = 1 + \sum_\alpha \rho_\alpha W_o^\alpha \qquad G_2 = 4\sum_\alpha \rho_\alpha \eta_\alpha^2 \left(\tfrac{3}{2}W_o^\alpha - 2W_1^\alpha + \tfrac{1}{2}W_2^\alpha\right)$$

$$G_1 = 4\sum_\alpha \rho_\alpha \eta_\alpha (-W_o^\alpha + W_1^\alpha) \qquad G_4 = 4\sum_\alpha \rho_\alpha \eta_\alpha^3 \left(-\tfrac{5}{3}W_o^\alpha + \tfrac{5}{2}W_1^\alpha - W_2^\alpha + \tfrac{1}{6}W_3^\alpha\right)$$

where

$$\eta_\alpha = \frac{v_{\perp\alpha}^2 \omega^2}{4\omega_{c\alpha}^2 c^2}, \quad \rho_\alpha = \frac{\omega_{p_\alpha}^2}{2\omega v_{\parallel\alpha} k_\parallel} (T_{\perp\alpha}/T_{\parallel\alpha}) \ , \ v_{\parallel\alpha} = (2T_{\parallel\alpha}/m_\alpha)^{1/2} \ ,$$

$$v_{\perp\alpha} = (2T_{\perp\alpha}/m_\alpha)^{1/2} \ , \ S_n^\alpha = Z_n^\alpha + Z_{-n}^\alpha - \frac{k_\parallel v_{\parallel\alpha}}{\omega}(1-T)(Y_n^\alpha + Y_{-n}^\alpha) \ ,$$

$$D_n^\alpha = Z_n^\alpha - Z_{-n}^\alpha - \frac{k_\parallel v_{\parallel\alpha}}{\omega}(1-T)(Y_n^\alpha - Y_{-n}^\alpha) \ ,$$

$$W_n^\alpha = \xi_n^\alpha Y_n^\alpha + \xi_{-n}^\alpha Y_{-n}^\alpha - \frac{n\omega_{c\alpha}}{\omega}(1-T)(\xi_n^\alpha Y_n^\alpha - \xi_{-n}^\alpha Y_{-n}^\alpha) \ , \tag{27}$$

$$S'^\alpha_n = Y_n^\alpha + Y_{-n}^\alpha - \frac{n\omega_{c\alpha}}{\omega}(1-T)(Y_n^\alpha - Y_{-n}^\alpha) \ , \quad Y_n^\alpha = 1 + \xi_n^\alpha Z_n^\alpha \ ,$$

$$D'^\alpha_n = Y_n^\alpha - Y_{-n}^\alpha - \frac{n\omega_{c\alpha}}{\omega}(1-T)(Y_n^\alpha + Y_{-n}^\alpha) \ , \quad T = (T_{\parallel\alpha}/T_{\perp\alpha}) \ ,$$

with $\xi_n^\alpha \equiv \frac{\omega - n\omega_{c\alpha}}{k_\parallel v_{\parallel\alpha}}$ and Z_n^α is the Fried-Conte Integral[62]

$$Z_n^\alpha \equiv \pi^{-1/2} \int_{-\infty}^{\infty} \frac{e^{-x^2}}{x - \xi_n^\alpha} dx \ . \tag{28}$$

From Onsager's relations[63], the remaining elements are

$$\begin{aligned} K_{xy} &= -K_{yx} \\ K_{yz} &= -K_{zy} \\ K_{zx} &= K_{xz} \ . \end{aligned} \tag{29}$$

Eq.(23) has a nontrivial solution when[64]

$$\det\left[\overline{\overline{K}}\right] = 0 \ . \tag{30}$$

Eq.(30), the dispersion equation, has the following form

$$An_\perp^6 + Bn_\perp^4 + Cn_\perp^2 + D = 0 \ . \tag{30'}$$

Using the solution for a cubic equation[65], eq.(30') may be solved for complex $k_\perp^2$ given a real $k_\parallel$ and ω. Assuming that the plasma density has the parabolic profile $n(r)=n_o(1-(r/a)^2)$, and magnetic field neglecting poloidal

field effects is $B=B_o(R_o/(R_o+r))$, eq.(30') can be solved locally, at each point along the minor cross section. Fig.(I-B-6) displays $k_\perp^2$ for NUWMAK (see Table(III)).

The smallest root of the dispersion equation corresponds to the fast wave root while the next smallest root corresponding to an Ion Bernstein (I.B.) wave. Mau[6] has examined eq.(30') taking into account the effects due to gradients in density, temperature and magnetic field. For parabolic density and temperature profiles, the fast wave root is unchanged while the I.B. wave becomes evanescent on the inside of the torus. The effect of gradients in UWMAK III[109] is shown in fig.(I-B-7).

To obtain the RF heating terms which will be added to the fluid energy balance equations in Sec.II-A, eqs.(6) and (25) are used together with the observation that for ions (with n=2,3)

$$|K_{zz}| >> |K_{xz}|, |K_{yz}| . \qquad (31)$$

Therefore, the 3×3 tensor $\overline{\overline{K}}$ can be approximated by the following 2×2 tensor

$$\overline{\overline{K}} \simeq \begin{bmatrix} K_{xx} & K_{xy} \\ K_{yx} & K_{yy} \end{bmatrix} . \qquad (32)$$

Defining E_+ as that component of the electric field which rotates in the same sense as the ions,

$$E_+ = E_x + iE_y . \qquad (33)$$

From eq.(25)

$$K^a_{xx} = -iK^a_{xy} = K^a_{yy} . \qquad (34)$$

On combining eqs.(6),(25),(29),(32-34), the following

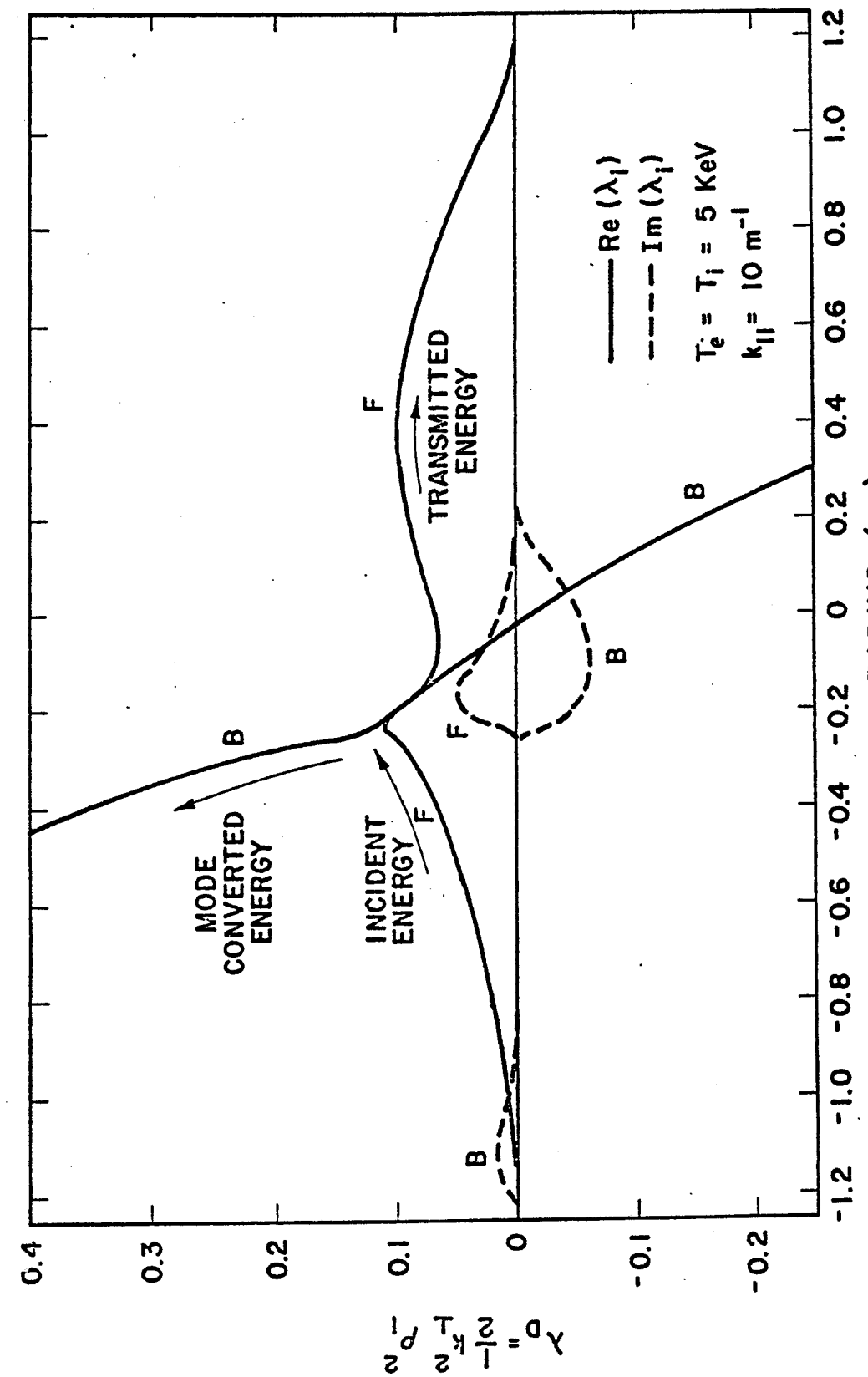

Fig. I-B-6 Local fast magnetosonic dispersion relation for a plasma profile given by $n_e = 2n_D = 2n_T = 4 \times 10^{14}$ $(1-(r/a)^2)cm^{-3}$, $T_e = T_i = 5\ (1 - 0.9(r/a)^2)^2$ keV, $k_{||} = 10\ m^{-1}$, f = 92 MHz and B_o = 60 kG on axis.

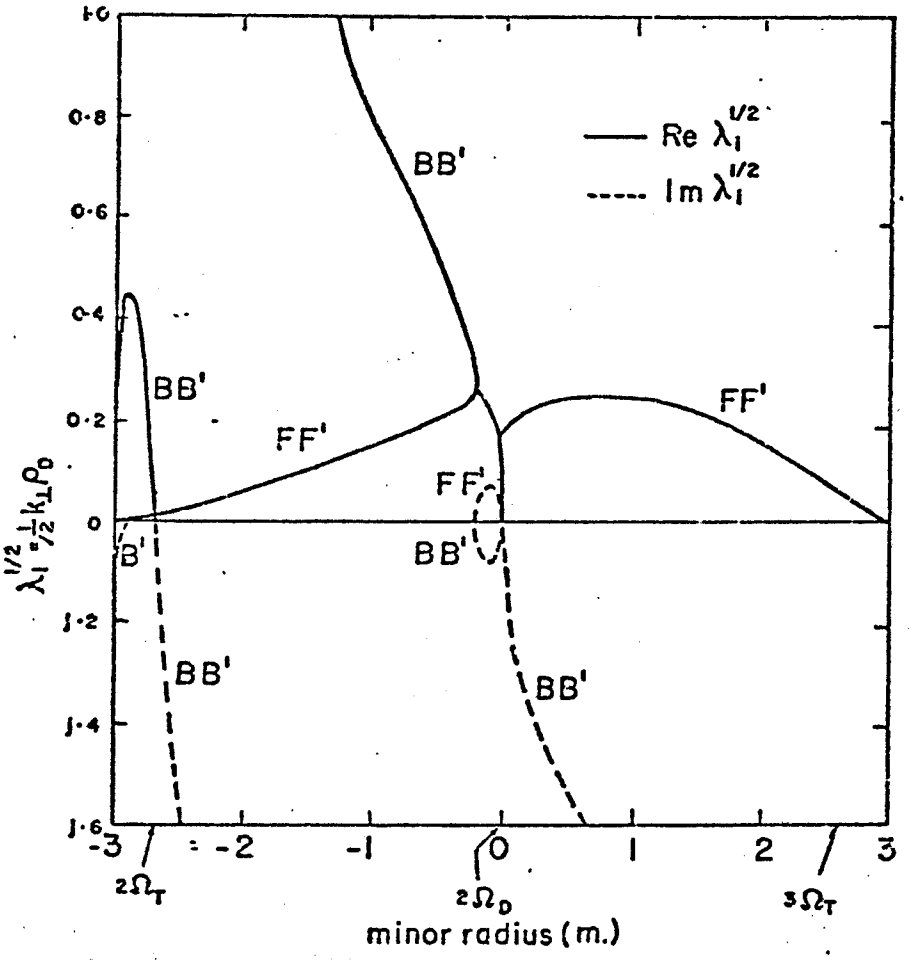

Fig. I-B-7 Comparison of the dispersion relation in the local and drift approximation for a 50-50 D-T plasma in UWMAK III over the minor cross-section. Parabolic profiles are used with $n_e = 2n_d = 2n_t = 1.2 \times 10^{14}$ cm^{-3} and $T_e = T_i = 8$keV as the peak values on axis. f=61 MHz, $k_\parallel = 0$ and $B_o = 40$kG. F and B represent the local fast and ion-Bernstein roots when F' and B' are the corresponding drift approximations. (reproduced from Ref.6)

expression for the power deposited in the ions from finite ion gyroradius heating , with $T_{\perp\alpha} = T_{\parallel\alpha} = T_i$ (i=d,t) is obtained

$$P^i_{RF} = \frac{\pi^{1/2}\varepsilon_o\omega^2_{pi}Re|\lambda_i|^{n-1}}{4k_\parallel v_{thi}} |E_+|^2 e^{-\left[(\omega-n\omega_{ci})/k_\parallel v_{thi}\right]^2} \quad (W/m^3) \ , \tag{35}$$

with n = 2 for d
= 3 for t .

Expressing the toroidal magnetic field, assuming large aspect ratio as

$$B = \frac{B_o}{1+(r/R)\sin\theta} \simeq B_o\left(1 - \frac{r\sin\theta}{R}\right) \ , \tag{36}$$

eq.(35) becomes

$$P^i_{RF}(r,\theta) = \frac{\pi^{1/2}\varepsilon_o\omega^2_{pi}Re|\lambda_i|^{n-1}}{4k_\parallel v_{thi}} |E_+|^2 e^{-\gamma^2\sin^2\theta} \quad (W/m^3) \tag{37}$$

where $\gamma = \frac{n\omega_{cio}r}{Rk_\parallel v_{thi}}$, $\omega_{cio} = q_iB_o/m_i$ and $\omega = n\omega_{cio}$.

For electron heating, $|K_{xx}|$ is the dominant term in the dielectric tensor, so the following reduced 2×2 tensor may be used in eq.(6), (with n=0)

$$\overline{\overline{K}} \simeq \begin{bmatrix} K_{yy} & K_{yz} \\ K_{zy} & K_{zz} \end{bmatrix} \ . \tag{38}$$

The power deposited to the electrons from Landau and transit time damping (Appendix D) with $T_{\perp e} = T_{\parallel e} = T_e$ is

$$P^e_{RF} = \frac{\pi^{1/2}\varepsilon_o\omega^2_{pi}Re|k_\perp|^2 v_{the}}{\omega^2_{ce}4k_\parallel} |E_y|^2 e^{-(\omega/k_\parallel v_{the})^2} \quad (W/m^3) , \tag{39}$$

where eqs.(23) and (38) have been used to express E_z in terms of E_y. Using eqs.(23) and (32) to express E_y in terms of E_+ ,

$$|E_+|^2 = |1 - \chi|^2 |E_y|^2 \ , \tag{40}$$

where

$$\chi = -iE_x/E_y \simeq -iK_{xy}/(K_{xx}-n_\parallel^2) \quad . \tag{41}$$

For a single ion species,

$$|E_y|^2 \simeq |1+x^2||E_+|^2 \ , \text{ where } x^2 = \frac{3\pi^{1/2}k_\perp^2 v_\perp^2}{8k_\parallel v_{thi}\omega_{ci}} \quad . \tag{42}$$

Averaging over a magnetic flux surface and assuming that $|E_+| = |E_+(r)|$, eq.(37) becomes

$$\langle P^i_{RF}(r)\rangle_\theta = \frac{1}{2\pi}\int_0^{2\pi} P^i_{RF}\, d\theta = \frac{\pi^{1/2}\varepsilon_o\omega_{pi}^2 |Re\lambda_i|^{n-1}}{4k_\parallel v_{thi}} I_o(\gamma^2/2)|E_+|^2 \quad (W/m^3) \ . \tag{43}$$

For $\gamma^2/2 >> 1$, eq.(43) becomes

$$\langle P^i_{RF}(r)\rangle_\theta \simeq \frac{\varepsilon_o\omega_{pi}^2 R|Re\lambda_i|^{n-1}}{4n\omega_{cio}r}|E_+|^2 \quad . \tag{44}$$

Eqs.(43) and (44) show that the ion heating is strongly peaked at the plasma center. For harmonics n>1, ion finite gyroradius heating preferentially heats ions with large $v_\perp$. This heating process will tend to produce a high energy ion tail in the perpendicular velocity distribution. For this reason, ion higher harmonic heating is inherently a non-Maxwellian heating process. Fundamental (n=1) and electron heating are Maxwellian processes since tails are not produced. Since fluid codes assume that the heating process is Maxwellian, this assumption will be examined in Sec.III.

Thermal effects and the 1/R variation in the B field lead to ion heating over a finite width of the plasma's minor cross section, called the cyclotron resonance layer.

From eqs.(43) and (44) this width ,ΔR, is (fig.(I-B-3)

$$\Delta R \simeq \frac{r}{(\gamma/2)} = \frac{2k_{\parallel}v_{thi}R}{n\omega_{cio}} \quad , \; n = 1,2,3, \ldots \tag{45}$$

In eq.(30'), assume now that $k_{\perp}^2$ is real and that ω has a small imaginary component, $\gamma_{n\omega_{ci}}$. For second harmonic heating , with $\frac{n_e m_e T_e}{n_i m_i T_i} \ll 1$, using eq.(30) and magnetic flux surface averaging,

$$\gamma_{2\omega_{ci}} \simeq \frac{\eta_i k_{\perp}^2 T_i}{4m_i\omega_{ci}} \quad , \; \eta_i = n_i/n_e \text{ , and } i=d,t^{(4)} \; . \tag{46}$$

For electron heating[4]

$$\gamma_e = \frac{8e^{-1}\pi^{1/2}k_{\perp}T_i}{3m_i\omega_{ci}} \; . \tag{47}$$

Since these damping decrements are found to be large compared to possible parametric instabilities (Sec.I-D), these possible instabilities can be neglected when modelling the RF heating of a reactor.

Fig.(I-B-6) shows that there is a finite region of the tokamak cross section where the real parts of $k_{\perp}$ of the fast and I.B. waves coalesce. Within this region possible mode conversion processes[22,26,27,30,31,37] may compete with the weak linear damping processes. These heating mechanisms will now be examined.

I-C MODE CONVERSION PROCESSES

Since the fast wave root coalesces with the ion Bernstein (I.B.) root over a finite region of the plasma, it has been proposed[17,26,32,66] that some of the fast wave energy may couple to the I.B. wave (fig.(I-B-6)). In experiments, the cavity Q has been approximately one order of magnitude lower than predicted by weak damping theory. In experiments using deuterium plasmas, impurity hydrogen has always been present in concentrations of several percent. A smaller Q can be explained[34,37] by mode conversion occuring at the ion-ion hybrid resonance layer (see Appendix A) present in these experiments. Perkins[22] has theorized that this effect will be small when the proton concentration η_p

$$\eta_p < \frac{n}{2R\omega_{cp}} (2T_i/m_p)^{1/2} \sim \frac{n}{200} T_{keV}^{1/2} \qquad (48)$$

where n is the toroidal mode number.
In NUWMAK where $n \simeq 50$, η_p needs to be less than 25% which is easily satisfied.

Three possible heating mechanisms involving mode conversion in the ICRF range have been investigated.[22,27,37,107,108] In this section the possibility of mode conversion occurring in a D-T reactor when $\omega/\omega_{cd} = \Omega_d = 2$ is discussed. The two other processes both involve the presence of the two ion hybrid resonance surface within the plasma. Ion-ion hybrid resonance heating ($\Omega_d=1$) and fundamental minority species heating ($\Omega_d=1$) are examined in Appendix A.

The dispersion equation (30) derived earlier assumed that various modes propagate independently within the plasma.

To investigate the mode conversion problem, the wave equation is used. For small variations in the plasma parameters over a wavelength[27,37], eq.(30) may be inverse Fourier transformed by replacing

$$k_{\perp} \rightarrow i\frac{d}{dx} \tag{49}$$

for a slab model with $k_y=0$.

The wave equation takes the following form

$$a(x)\frac{d^4E_y(x)}{dx^4} - b(x)\frac{d^2E_y(x)}{dx^2} + c(x)E_y(x) = 0 , \tag{50}$$

and a WKB solution found in the regions far from the confluence zone ($|b|^2 >> |4ac|$).

Examining the WKB solution of eq.(50) at the two edges of the confluence region, McVey[37] obtains the following transmission coefficient

$$|T| = e^{-\pi\eta/2} \tag{51}$$

and reflection coefficient

$$|R| = |1-e^{-\pi\eta}| \tag{52}$$

where

$$\eta \propto \frac{R_o\omega_{pd}\beta}{2c} \quad \text{and} \quad \beta = nT/B_o^2 . \tag{53}$$

Due to the 1/R variation in the toroidal field, mode conversion processes are not symmetric about the plasma center for waves incident from either side. Therefore, a high field side (HFS), where $B>B_{\text{res layer}}$ and a low field side (LFS) where $B<B_{\text{res layer}}$ will be defined. The mode coupling process depends upon the value of $k_{\parallel}$ excited. The effect of the poloidal field on $k_{\parallel}$ is discussed in Sec.IV.

For $k_{\parallel}=0$, a fast wave incident from the LFS is coupled

to an I.B. wave in the resonance layer. The I.B. wave is evanescent on the HFS. Energy is recoupled to the fast wave which propagates towards the LFS and is reflected at the reactor wall. Therefore, the resonance layer acts as a reflecting wall for a fast wave propagating from the LFS. A standing wave forms, but the eigenmode has a reduced cavity width. Surface heating of electrons may result. The fraction of incident fast wave energy coupled to the I.B. wave is

$$A_\ell = 1 - |T|^2 - |R|^2 = e^{-\pi\eta} - e^{-2\pi\eta} \tag{54}$$

where

$$\eta \propto Rn_e^{3/2}(B_o^2/T)^{-1} \quad . \tag{55}$$

When a fast wave with $k_{\parallel}=0$ is incident from the HFS, there is strong coupling at the harmonic resonance layer to an I.B. wave with a coincident phase velocity. In this case, the second harmonic layer appears as an absorbing layer and heating occurs in its vicinity. The fraction of incident energy coupled to the I.B. wave in this case is

$$A_h = 1 - |T|^2 = 1 - e^{-\pi\eta} \quad . \tag{56}$$

Eqs.(54-56) show that coupling to I.B. waves appears to be the dominant heating mechanism in reactor plasmas.

For $k_{\parallel} \lesssim 0.05\text{cm}^{-1}$, the above coupling picture does not change. For intermediate values of $k_{\parallel}$ ($\sim 0.15\text{cm}^{-1}$), the confluence region, and therefore the coupling between the fast and I.B. waves, decreases. For reactor plasmas and large $k_{\parallel}$ ($>0.3\text{cm}^{-1}$), the confluence region shrinks to a point, thereby uncoupling these two modes. For large values of $k_{\parallel}$ ($>0.2\text{cm}^{-1}$), finite ion gyroradius effect is the

dominant heating mechanism, with the I.B. wave being strongly evanescent in the coupling region.

In smaller machines the confluence width is smaller, thereby reducing the minimum value of $k_{\parallel}$ needed to avoid mode conversion. In PLT and TFTR, $k_{\parallel}$ need only be larger than $0.12 cm^{-1}$.

Since the fast and I.B. waves are uncoupled for large $k_{\parallel}$, this range of $k_{\parallel}$ would appear to be suitable for reactor heating. However, McVey[37] has shown that for large $k_{\parallel}$ in a reactor, the fast wave is almost totally absorbed through ion finite gyroradius effects within one pass of the wave across the minor cross section. It appears that there can be only a small enhancement of the eigenmode for this range of $k_{\parallel}$.

For second harmonic heating of a reactor, an intermediate value of $k_{\parallel}$ ($\sim 0.1 cm^{-1}$) seems preferable. Mode conversion processes, if present, should not be the dominant heating mechanism. Toroidal eigenmodes, though perhaps reduced in Q, will be excited to enhance plasma heating and increase the loading resistance. Ion heating of the plasma core should be possible.

Before examining the experimental results obtained from ICRF heating experiments, the possibility of parametric instabilities being excited by the RF which can lead to undesirable surface heating will now be briefly surveyed.

I-D PARAMETRIC INSTABILITIES

In the presence of a fast magnetosonic wave, electrostatic oscillations may be excited, grow in amplitude, and heat the plasma through various linear and nonlinear processes. Such instabilities may be caused by parametric effects whereby an RF pump wave decays into either two I.B. waves[69,70] or an I.B. and an ion acoustic wave.[68,69,72,73] Instabilities may also result from nonlinear Landau damping effects[69,70] when the pump wave is in resonance with the plasma oscillations through particle motion. The additional effects of two ion species,[71,74-76] density, temperature, and magnetic field gradients,[75] and saturation mechanisms[76] have been explored. Experimentally, parametric excitation of ion-ion hybrid modes[77], I.B. modes[78] and drift waves[80] in low density linear plasmas have been observed in good agreement with theory in the Princeton L-4 device (fig.(I-D-1)). For a single ion species in L-4, the parametric excitation of a non-resonant ion cyclotron quasi-mode has been seen[79] when the RF pump frequency $\omega_o \geq 2\omega_{ci}$. This process may take place near the plasma surface during the RF heating phase of a reactor.[79] Unfortunately, most of the theoretical work in the ICRF range deals with pump frequencies at the fundamental ion frequencies for deuterium and hydrogen. These results will be briefly reviewed. The subject of parametric instabilities is far from complete, and much additional work

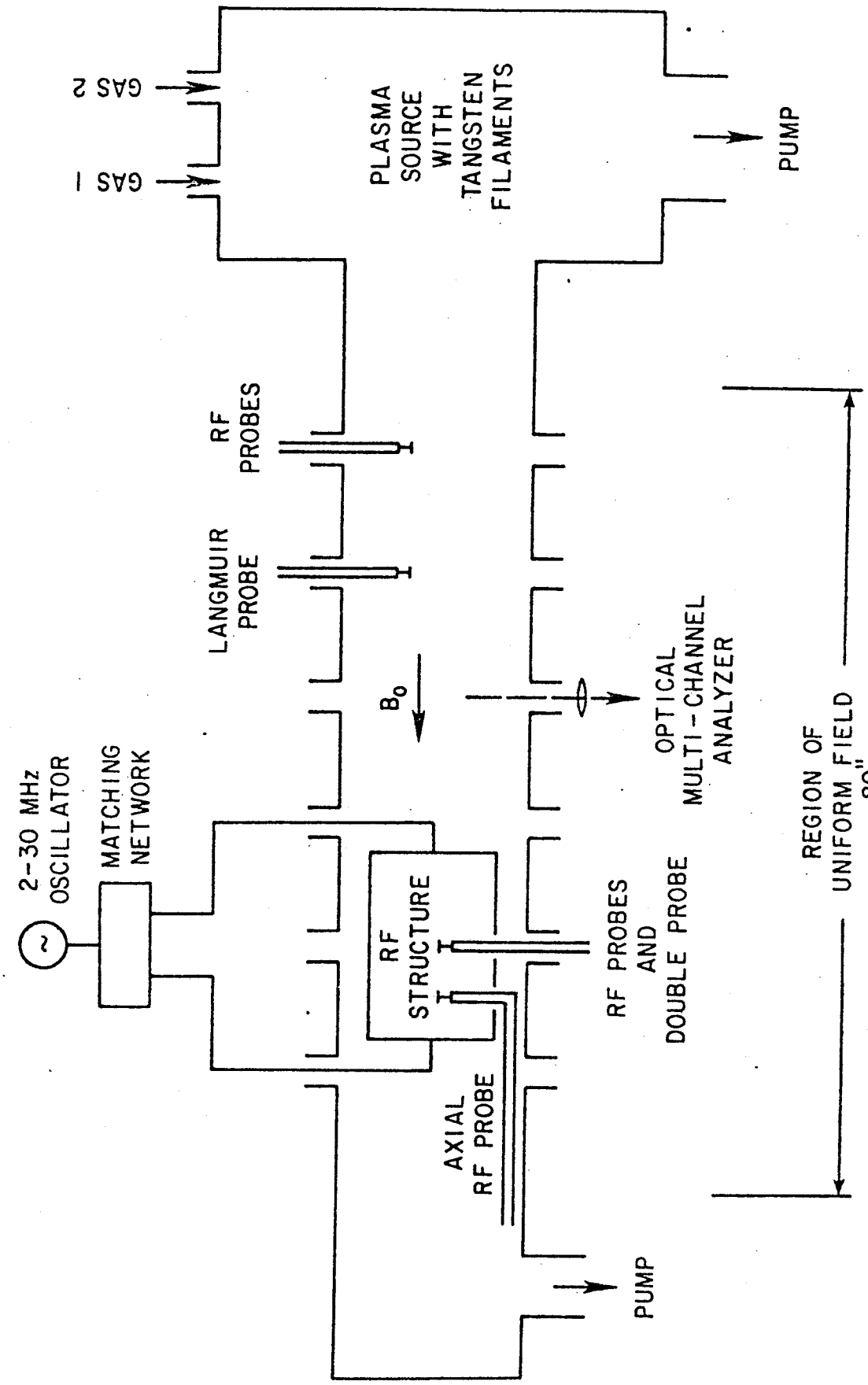

Fig. I-D-1 Simplified schematic of the experimental set-up of the Princeton linear device L-4 (reproduced from Ref.77)

needs to be done experimentally as well as theoretically for a D-T plasma with pump frequency $\omega=2\omega_{cd}$.

In a thermal plasma, to have unstable oscillations which could lead to plasma heating, the excited plasma modes must have a frequency ω smaller than the pump frequency ω_o.[69] In addition, the modes must have large $k_\perp$ to be coupled to the pump wave[69], limiting the possible excited modes to either I.B. or drift waves.

The dominant nonlinear mechanisms depend upon the ratio of the electron drift velocity induced by the pump wave to the plasma sound speed U_e/c_s . When $U_e/c_s > 1$, as in collisionless shock waves, fast high frequency beam instabilities may be excited[70]. In fusion reactors, $U_e/c_s < 1$, otherwise the magnetic field associated with such a large amplitude pump wave would disturb the magnetic surfaces and lead to enhanced particle losses[70]. Therefore, only the slower instabilities driven by three wave interactions or inverse nonlinear Landau damping are thought to occur within a reactor. First, the possible instabilities present in a single ion species are investigated. These instabilities are driven by the relative velocity between ions and electrons. Later, the additional effects produced by the presence of a second ion species are examined.

I.B. waves may be excited by direct resonant amplification[68,70] or by off resonant excitation via inverse nonlinear Landau damping[69,70] in a single ion species. Martin and Samain[69] investigate I.B. oscillations in a toroidal configuration, taking into account the existence of the magnetic

surfaces as well as the nonuniformity of the static magnetic field. They assume that $T_i/T_e \simeq 1$ and that the mode undergoes no linear Landau damping, that is $|\omega - n\omega_{ci}| >> k_{\parallel} v_{thi}$ and $\omega >> k_{\parallel} v_{the}$ where ω is the excited mode frequency. Finally, only the case where the excited mode wavenumber $\vec{k}=(k_{\perp}, k_{\parallel})$, $k_{\perp}\rho_{the} << 1$ with the harmonic number $n << k_{\perp}\rho_{thi} << \omega_{pi}/\omega_{ci}$ is examined. An upperbound is calculated for the heating rate γ_h so as to not itself induce nonlinear effects. With $E_n/n_e T << 1$, they find that

$$\gamma_h << \omega_o (R/r)^{1/2} (\rho_{thi}/r) (\omega_{ci}/\omega_{pi})^{5/2} \qquad (57)$$

where r is the radius of heating and $\rho_{thi} = v_{thi}/\omega_{ci}$.
For NUWMAK,

$$\gamma_h << 80 \text{ sec}^{-1} . \qquad (58)$$

For the electric field of the pump wave E_θ to produce effective heating

$$E_\theta \gtrsim 20B (v_{thi}/c) (\omega_{ci}/\omega_{pi}) (\rho_{thi}/R)^{1/2} \text{ (CGS)}. \qquad (59)$$

For NUWMAK, $E_\theta > 300$V/cm, which is larger than the average RF induced electric field (see fig.(III-B-11)). If the RF electric field is highly nonuniform, this process may compete with linear damping.

Harms et al[71] examine both the resonant amplification of one I.B. and one ion acoustic wave or of two I.B. waves, and the off resonant excitation of these modes via inverse nonlinear Landau damping. They find that the threshold for excitation of acoustic waves by a magnetosonic pump wave is too high for this process to occur in reactors. However, the

threshold for I.B. excitation is much lower and will now be examined for the reactor regime.

Harms et al[71] assume that $k_o\rho_{the} << k\rho_{the} << 1$ and that $\omega_{ci} < \omega_o < \omega_{lh}$, and $\omega < \omega_{lh}$, where lh designates lower hybrid, the pump wave is (k_o, ω_o) and the electrostatic oscillations are $(\vec{k}, \omega)$. Only cases where the pump wave propagates perpendicular to the external magnetic field and where $\omega_1 - \omega_2 = \omega_o$ for the excited modes (ω_1, ω_2) are considered. For the amplification of I.B. waves, $\omega_r / k_\perp c_s << 1$ with r=1,2, they find possible instabilities when $|\omega_r - n\omega_{ci}| << \omega_{ci}$. For resonant amplification, an additional condition is that $Re\omega_2 - \omega_o \simeq Re\omega_1$.

However, the I.B. wave, $(\omega_1, \vec{k}_1)$, which is excited, undergoes strong Landau damping when $k_\perp$ is large. The instability disappears when

$$|\omega_1 / k_z c_s| \lesssim (2\pi)^{1/2} k_1 \rho_{thi} (m_e/m_i)^{1/2} (T_i/T_e)^{1/2} \qquad (60)$$

This instability has a sharp cutoff when $k_\perp \lambda_{Di} \simeq 1$, where $\lambda_{Di} = (T_i / 4\pi n_i e^2)^{1/2}$; therefore, there is no instability when

$$k_\perp \lambda_{Di} > \alpha (2\pi)^{-1/2} (T_e/T_i)^{1/2} \frac{(\omega_{ce}\omega_{ci})^{1/2}}{\omega_{pi}} \qquad (61)$$

where α is a numerical factor less than 1.

Inverse nonlinear ion Landau damping can be important only when $|\omega_2 \pm \omega_o - n\omega_{ci}| < k_\parallel c_s$. This nonlinear process is small compared to electron nonlinear Landau damping which suffers the same cutoff for $k_\perp$ as given in eq. (61).

Since Landau damping increases with increasing $k_\perp$, three wave decay processes can only be important when the pump wave excites modes with small $k_\perp$. Using eq. (61), these

processes can be neglected when

$$(2\pi)^{-1/2}(T_e/T_i)^{1/2}\frac{(\omega_{ce}\omega_{ci})^{1/2}}{\omega_{pi}} < 1, \qquad (62)$$

which is the case for reactors.

When eq.(62) is applicable, off resonant excitation of I.B. waves may occur when $|\omega_o|/2 < |\omega_1| < |\omega_o|$. A destabilizing process is inverse nonlinear electron damping. At this time, it is unclear whether electrostatic modes with small enough $k_\perp$ will be excited to avoid cutoff. Two ion species effects will now be reviewed.

Harms et al[72] investigate two cases where I.B. waves are excited and propagate parallel (case A), or nearly perpendicular (case B) to the pump wave. They assume an infinite, homogeneous, collisionless background plasma with pump frequency greater than any excited mode frequency. The I.B. waves may become unstable through either the ion cyclotron decay instability or nonlinear Landau instability for low values of the pump electric field $|\vec{E}_p|$. In two species plasmas these instabilities are excited by the relative drift motion of the different ion species induced by the pump wave.

The ion cyclotron decay instability results from a fast wave decaying into two I.B. waves whose frequencies corresponds to the two ion gyrofrequencies[74,76]. Sperling[76] finds that the threshold for this instability decreases as T_e/T_i increases and is smaller than the instabilities which might be present in a single ion species plasma when $T_i/T_e \ll 1$.

Returning to the work of Harms et al[72], for case A, $\vec{k}=\vec{k}_\perp||\vec{k}_o$, the relative motion of the two ion species produces the instability. For case B, $k_\perp \perp k_o$ and $k_\parallel \neq 0$, the instability arises from the electron-ion drift so the threshold is similar to that obtained for a single species.

For case A, the growth rate for the resonant instability is

$$\Gamma_A \simeq (2\pi)^{-1/2}\left|\frac{\omega_1\omega_2}{\omega_{pi}^2}\right| (\rho_{thd}\rho_{tht})^{-1/2} \left|\frac{\omega_{cd}-\omega_{ct}}{\omega_{cd}+\omega_{ct}}\right| |E_{py}| \quad (63)$$

$$\simeq 3.5\times10^4 |E'_{py}| (T'_i)^{-1/2} \quad \text{sec}^{-1} \quad (64)$$

for a D-T plasma with

$$\frac{|E'_{py}|}{\sqrt{T'_i}} << 100H' \frac{(k_\perp\rho_{thd})_{min}}{k_\perp\rho_{thd}}$$

$H' = H/\text{Tesla}$
$T' = T/\text{keV}$
$E'_{py} = E_{py}\text{cm}/100\text{V}.$

For a reactor with $T_i=T_e$

$$(k_\perp\rho_{thd})_{min} \simeq 6 \leq k_\perp\rho_{thd} \lesssim 25 . \quad (65)$$

For case B,

$$\Gamma_B \simeq (2\pi)^{-1/2}\left[\frac{\bar{\omega}_1\bar{\omega}_2}{\omega_{pi}^2}\right]^{1/2} \frac{(\rho_{thd}\rho_{tht})^{-1/2}}{(\omega_{cd}+\omega_{ct})} \omega_{pi}[S'(\xi_{e,1})-S'(\xi_{e,2})]E_{py}$$

where $S'(\xi)= \frac{d}{d\xi}\left[\exp(-\xi^2)\int_o^\xi e^{t^2}dt\right]$, $|\xi| = \left|\frac{\omega-\bar{\omega}}{k_z v_i}\right| >>1$, and $\bar{\omega}\gtrsim\omega = n\omega_{ci}$. (66)

For reactor plasmas

$$\Gamma_B \simeq 2.7\times10^4 E'_{py}(T'_i) \quad \text{sec}^{-1} \quad (67)$$

with

$$\frac{E'_{py}}{\sqrt{T'_i}} << 10H' \frac{(k_\perp\rho_{thd})_{min}}{k_\perp\rho_{thd}} . \quad (68)$$

In Harms' analysis, collisional damping is neglected. For this to be the case, E_{py} must be so large that $\Gamma >> \gamma_c$ so that

$$E'_{py} >> 2N'_e \frac{(k_\perp \rho_{thd})^2}{T'_i (k_\perp \rho_{thd})_{min}} \qquad \text{with } N'_e = n_e cm^3/10^{14} \tag{69}$$

For NUWMAK, an average value of $E'_{py} \simeq .3$ (see fig.(III-B-11)). The growth rates for cases A and B are

$$\Gamma_A \simeq 3.5\times10^3 \text{ sec}^{-1} \tag{70}$$

and

$$\Gamma_B \simeq 4.0\times10^3 \text{ sec}^{-1}. \tag{71}$$

From eq.(46), the average damping rate due to harmonic heating is

$$\gamma_{2\omega_{cd}} \simeq 6.5\times10^6 \text{ sec}^{-1}. \tag{72}$$

Since $\gamma_{2\omega_{cd}} >> \Gamma_A, \Gamma_B$, resonant instabilities for I.B. waves are not expected to be significant heating mechanisms. In addition for $T_i \gtrsim 1$ keV, case B can not occur since eqs.(80) and (81) cannot both be satisfied,

$$E'_{py} << 60 \text{ and } E'_{py} >> 70. \tag{73}$$

Since inverse nonlinear damping occurs only for case B, this process will not cause significant plasma heating either.

Besides examing heating rates, the threshold electric field needed to cause an instability can also be calculated. Sperling and Perkins[74] calculate the threshold for the ion cyclotron decay instability in an H-D plasma for $\omega_{ch}/k_\parallel << (T_e/m_e)^{1/2}$. Their results are reviewed and applied to a D-T plasma under the assumption that they do not vary greatly. For the above range of $k_\parallel$, the electron susceptibility is

only weakly affected by the pump field so nonlinear effects due to electron-ion drift are smaller than those caused by ion-ion motion. Hence, the threshold for two ion instabilities are lower. The threshold for two I.B. waves to become unstable is given by[74,81]

$$v_h^2=(3\pi A_d)^2\frac{(T_e m_e)}{m_h^2}\frac{\ln(T^3 m_h/m_e)}{2T^4}\left|\frac{1}{q_d}+\frac{1}{q_h A_d}^{1/2}\right|^2\frac{c_s^2}{c_{sd}^2} \qquad (74)$$

where v_h is the relative ion velocity and

$$m_d= A_d m_h \qquad T= T_e/T_i$$
$$q_i= n_i/n_e \qquad c_s^2 = \sum_i q_i T_e/m_i .$$

The threshold for this instability is determined principally by ion damping of the I.B. waves.

To determine the above threshold, the relative ion velocity needs to be calculated. For a fast wave propagating essentially orthogonal to B_o, this velocity is

$$\frac{v_h B}{cE} = \omega_o(\omega_{ch}-\omega_{cd})(\omega_o^2-q_h\omega_{cd}^2-q_d\omega_{ch}^2)^{-1} . \qquad (75)$$

When $\omega_o \simeq 1.5\omega_{ch}$ and E is the maximum electric field,

$$v_h \simeq cE/B . \qquad (76)$$

Combining eqs. (74) and (76), the minimum value of the electric field needed to obtain this instability is

$$E = \frac{6\pi B}{c}\left|\frac{T_e m_e}{2m_h^2}\right|^{1/2}\frac{(\ln(m_h/m_e))^{1/2}\, c_s}{c_{sd}} \qquad (\ )$$

for a 50-50 D-T plasma with T= 1. For NUWMAK, E would be

$$E \simeq 3\text{kV/cm} . \qquad (78)$$

Except possibly near the RF exciting structure, this insta-

bility should not occur if the calculations for a D-T plasma do not differ greatly from those done for D-H.

Sperling and Perkins[75] show that while temperature and density gradients do not greatly affect this threshold for reactors, magnetic field gradients may introduce a mismatch in the wavenumber which, if large, can increase the threshold.

Ono et al[79] investigate the parametric excitation of an ion cyclotron quasi-mode. For typical edge parameters- $T_i=T_e=20eV$, $B_o=20-30kG$, and neutral density of $10^{13}cm^{-3}$- this instability will occur when

$$E > 60 \text{ V/cm.} \qquad (79)$$

This instability might occur in the vicinity of the launching structure and cause surface heating.

Finally, a general review was written by Porkolab[81] of all the parametric processes which might occur in a reactor. In this paper, he states that the threshold for ion cyclotron drift wave excitation is

$$E \geq \frac{2(\omega^* \omega_{ci})^{1/2} B}{kc} \qquad \text{where } \omega^* \text{ is the drift frequency.} \quad (80)$$

For NUWMAK, to excite drift waves, E> 70V/cm, which is larger than the expected average RF-induced electric field.

In summary, the fast magnetosonic wave may couple to drift or acoustic waves[68,81], decay into I.B. waves[70,81] or ion cyclotron waves,[71,74,75,78,81] in multi-species plasmas, or decay into ion cyclotron quasi-modes near the plasma surface.[78,79,81] The coupling to drift waves may occur

near the plasma surface, where the pump wave electric field is expected to be large. Hence, undesirable surface heating may result[81]. Excitation in two ion species of an I.B. wave may result in this wave decaying into a low frequency ion acoustic wave and an ion cyclotron quasi-mode, which is then damped by nonlinear ion cyclotron damping, resulting in strong perpendicular heating[81]. More experimental work and theoretical work in the area of fusion plasmas needs to be done. No parametric instabilities have been observed in any of the ICRF experiments reviewed in Sec.I-E. At this time, it appears that parametric effects can be ignored except possibly in the vicinity of the RF launching structure.

I-E EXPERIMENTAL RESULTS

Fast wave experiments have been performed on several tokamaks throughout the world (see Tables I-IV). The first ICRF heating of a tokamak in the US was performed on the ST machine at Princeton (1972-74). Fundamental and second harmonic heating was examined in two phases. In phase I,[82-84,86] low levels of power (P_{RF}<500 W) were used to investigate the wave generation problem. Using an RF frequency of 25MHz, a single half turn coil was encapsuled in ceramic, electrostatically shielded from the plasma, and placed in the shadow of the limiter on the HFS. Poloidal modes m=0,1 were excited and a wave damping length of 1m was measured for fundamental heating. For second harmonic heating, T_i of the main body increased from 120eV to 175eV and a 1keV ion tail was observed. Wave generation efficiencies of 40% for fundamental and 50% for second harmonic heating were obtained.

In phase II[84-86], higher RF power levels (P_{RF}<1 MW) were used. This time two 1/2 turn coils seperated by $\pi/8$ radians (43cm) obtained wave generation efficiencies $\geq$ 90%. Poloidal mode m=-1 and toroidal modes with $4 \leq |n| \leq 9$ were excited with an attenuation length approximately three times the circumference of ST. For RF pulses of 75-150kW for 5-10ms, $\Delta T_{i_{\perp body}} \sim 100$eV and $\Delta T_{i_{\perp tail}} \sim 500$eV within 1ms after the RF was first on. $T_{i_{\parallel}}$ had no tail but increased from 100eV to 200eV, indicating that global ion heating was obtained with an overall heating efficiency of 20%.[84,86] For later studies,[85] $\Delta T_{i_{\perp body}} \sim 3$ times.

To heat at the deuterium second harmonic with an RF frequency of 25MHz, the toroidal B field had to be lowered to 16kG. For stability , the Ohmic heating current was lowered to 65kA. Due to this degraded operation, the dominant loss mechanism for the heated ions was through the particle orbit loss cones. The RF driven tail, containing 8-40% of the total ion energy was subject to these cones and subsequently, 20-200kW of power was lost, reducing the overall heating efficiency. Disruptive instabilities caused by increased impurity influx prevented the use of RF pulses longer than 1-2ms for RF energy > 100J. Even with this degraded operation of ST, the RF overall heating efficiency was comparable with that of neutral beam heating on ATC. Eigenmodes, ion heating and tail formation were observed to be in general agreement with theory.

In TFR[87-89] low power (P_{RF}<1kW) experiments were performed using a V-shaped coil, 40cm long, 60cm wide, located at a plasma minor radius of 19cm. The power was supplied by a tuneable amplifier of frequency 50-75MHz. A two-stub matching network transformed the loading impedance to 50Ω from a resistance of 1Ω. Toroidal eigenmodes were observed but the measured cavity Q of 50 was lower than predicted. A stronger than anticipated absorption occured when the cyclotron resonance layer was located at the plasma center. When the toroidal B field was changed from 34-49kG, with a resultant sweep of the resonance layer across the plasma cross section, asymmetric wave damping occured in the deuterium plasma but not in hydrogen. Jacquinot et al[67]

theorize that these phenomena are caused by mode conversion at the two ion hybrid resonance surface due to the presence of impurity hydrogen (see Sec.I-C). Similar effects were found in ATC, TM-1, and T-4.

For the high power experiments in TFR[88], 100kW 20ms pulses were used. With better impurity control than on ST, the electron density increase during heating was less than 10%, indicating that little additional impurities entered the plasma from the RF. A high power (120kW), 50-90MHz, power generator was used with a 55% efficiency. Two 1/2 turn coils, 98cm long, excited the m=0 mode when 180^{o} out of phase, or m=1 when in phase. An RF pulse 5-27ms was supplied 100ms after plasma initiation. During heating, the loading resistance increased from 1Ω to 4-8Ω.

With the m=0 mode, toroidal eigenmodes were excited. Whereas a wave cavity Q of up to 10^5 was expected, Q was typically less than 10^4, indicating that two ion resonant absorption might have been occuring.

Preliminary results show that T_i increases by 150eV to 200eV with no significant tail formation for ion temperatures up to 5keV. If mode conversion processes are dominant, little tail formation would be observed.

Experiments on ATC[90,91] used the ST 25MHz generator. ATC, with a toroidal B field of 17kG, was well suited for deuterium second harmonic heating, which requires B of 16.4kG for an RF frequency of 25MHz. Unlike ST, ATC was operated at full current so that an order of magnitude more RF energy was supplied.

Fast waves were launched in ATC with a 1"× 1/4" cross section, 135^{o} arc length, copper strip encased in a ceramic sheath. For peak RF power of 200kW, the pulse length of 10ms was comparable to the ion energy confinement time of 5-11ms. The power dropped substantially during the pulse so that the average RF power supplied was only 145kW. The RF pulse length, being long compared to the equipartition time for both the ion main body (.1ms) and tail (2ms),led to the determination that the heating was not limited to tail production nor to minority ion heating.

An ion body temperature increase from 200-400eV in both the parallel and perpendicular directions indicated an overall heating efficiency of 10-40%. A 1keV high energy ion tail was observed. The amount of RF energy supplied was limited by the occurance of the m=2 MHD oscillation which led to plasma disruption. During heating, n_e increased less than 30%.

In ATC it was unclear whether the deuterons were directly heated by the RF or indirectly heated by impurity protons. Experiments in T-4[100] observed proton heating while deuteron heating occurred only in the vicinity of the attenna. However, on T-4 power could only be coupled during the occurrence of toroidal eigenmodes lasting only a few hundred microseconds. This time length was much shorter than either the deuterium or hydrogen equipartition time as well as the deuteron heating time.

The Russians have studied fundamental and second harmonic heating on T0-1, TM-1Vch and T-4. In T0-1[92-95], the ion temperature increased 30eV from 90±30eV to 150±30eV using

fundamental heating.

In TM-1Vch[96-99], for low power experiments ($\leq$20kW), a single loop launched a fast wave with a frequency of 22MHz. For fundamental heating, a low Q of 5-16 was measured. For second harmonic heating, toroidal eigenmodes were excited with an RF pulse length (.4ms) comparable to the energy confinement time (.3ms). The wave generation efficiency was 40-50%.

For the high power experiments, two asymmetrically placed coupling coils obtained generating efficiencies of 80-90% for power amplifier input levels of 150kW ($\omega/\omega_{ci}=\Omega=2$) and 1MW ($\Omega=1$). With m=0, toroidal eigenmodes were again excited. In the deuterium plasma, the mode quality was again decreased, due possibly to the presence of a 1% concentration of impurity protons. The pulse was increased for these experiments to .8ms, being limited, as in ST, by impurities. High energy proton tails led to unconfined bannana orbits with a resulting loss in heating efficiency. For RF power greater than 100kW, an unconfined, high energy deuteron tail was formed.

In T-4[100], $P_{RF}\simeq$1MW, f=23MHz, ICRF heating for $1\leq\Omega\leq2$ was examined when B varied from 10kG to 35kG. To simulate a possible reactor launching structure, an uninsulated stainless steel loop was placed between two limiters to prevent possible shorting. 50kW of power produced a high energy ion tail at the second harmonic. Again, where a Q of 3000 was predicted, a Q of only 300 was measured again an indication of possible mode conversion being present.

In the Japanese tokamak DIVA[101], second harmonic heating of a deuterium plasma with and without impurity protons,

using a mode tracking feedback system similar to the one on TFR is planned. A 1/2 turn coil, similar to those on ATC and ST will deliver up to 200kW for f=25-30MHz (Ω=1) and f=48-60MHz (Ω=2) corresponding to B_o=16-20kG.

For a base ion temperature of 150eV, preliminary experiments have already increased T_i 1.5 times, 1ms after the RF was applied. During heating n_e increased less than 20%. 65% of the input power went to the plasma with 30% being absorbed by the bulk ions resulting in an overall heating efficiency of 20%. Toroidal eigenmodes of short duration (20-30μs) compared to the pulse length of 1ms were excited. The antenna loading resistance increased during this time by a factor of 2-3.

Low power antenna coupling experiments are being carried out on ERASMUS[103], MICROTOR and MACROTOR[102]. Antenna designs are being tested and the coupling and mode selection problems investigated.

Finally, high power experiments are being planned for PLT. ICRF experiments with B_o from 25-46kG will be performed by Colestock, Hosea et al[104] with a goal of improving on the present heating efficiencies of 20-40%. They plan to minimize the density buildup now occurring which is thought to be caused by surface heating in smaller devices. They will attempt to clarify the importance of mode conversion processes by operating in D-He^3 at the second harmonic of He^3, thereby eliminating all possible hydrogen resonances. The concentration of protons in a deuterium plasma will be varied and RF together with beams will be used to heat a $10^{14}cm^{-3}$ plasma to over 5keV.

PLT will use two 1/2 turn coils to excite m=0,$\pm$1,$\pm$3

poloidal modes. The larger machine is expected to have a longer ion confinement time and have a greater number of excited toroidal modes. Preliminary experiments have excited high Q modes, even in the presence of several percent hydrogen. Mode tracking will be used to optimize coupling. Mode tracking times of over 200ms during the discharge have already been achieved.

In summary, ICRF experiments with absorbed power up to 200kW with overall heating efficiencies up to 40% have been accomplished. Wave generation efficiencies over 80% are easily achieved using simple loop antennas. Bulk ion heating without a decrease in the ion energy confinement time has been observed. Direct ion heating, rather than increased ohmic heating from increases in impurity concentrations has doubled T_i. Ion tail formation in $v_\perp$ indicates second harmonic heating is occurring. Toroidal eigenmodes have been seen to agree well with cold plasma theory and mode tracking has been successfully carried out on TFR and PLT. ICRF heating has been shown to be as efficient as the neutral beam heating of ATC.

However, it is still unclear as to whether deuterons are heated directly by the RF or by energetic protons which may not be present in reactors. Lower than expected Q's have been measured. This decrease in Q or enhancement in damping at the second deuterium harmonic is thought to be caused by the presence of impurity hydrogen. Hydrogen impurity may lead to enhanced cyclotron damping or Landau damping at the two ion hybrid resonance surface. ICRF heating may also lead to an influx of impurities and energetic ions in the tail may be lost.

Though much has been accomplished, the exact heating

mechanism(s) is not known. It is not clear how present experiments scale up to reactor conditions. The launching structure has not been optimized and no experiments used waveguides which have been proposed for reactors.

As machines get larger, it is expected that impurities and unconfined tail ions will not be serious problems. Though an expected increase in the number of modes present may hinder tracking, mode tracking may not even be needed. Efficient heating has been accomplished without coupling to eigenmodes. Obviously, more experimental work needs to be done.

Having surveyed the various heating processes which may occur within a plasma, in Secs. II and III and Appendix D, various possible ICRF heated reactor plasmas are simulated using fluid codes (Sec.II and Appendix D) or a Fokker-Planck code (Sec.III). The only heating processes that are assumed to occur are the linear finite ion gyroradius and electron Landau and transit time damping. Sec. I has shown that this assumption appears to be a reasonable one as far as reactor plasmas are concerned.

References

(1) R. Hazeltine, F. Hinton, M. Rosenbluth, Phys. of Fluids 16, 1973, p. 1645.

(2) Lyman Spitzer, Jr., Physics of Fully Ionized Gases, Interscience Publishers, 1962, p. 139.

(3) J.E. Scharer, R.W. Conn, and D.T. Blackfield, Study of Fast Magnetosonic Wave Heating and Neutral Beam Heating at Large Tokamaks, EPRI ER-268, Sept. 1976.

(4) D.T. Blackfield and J.E. Scharer, "Preliminary Study of Supplementary RF Heating in a Tokamak Reactor," University of Wisconsin FDM-118, January 1975.

(5) B. McVey, "Supplementary RF Heating of a Tokamak Plasma in the Ion Cyclotron Range of Frequencies," University of Wisconsin Report PLP-716, February 1977.

(6) Tak Kuen Mau, "Radio-Frequency Heating and Propagation in Tokamak Plasmas in the Ion Cyclotron Range of Frequencies", University of Wisconsin (Ph.D. Thesis), 1977.

(7) J. Adams and A. Samain, "Chauffage par Absorption Cyclotronique", Rappert du Groupe d'etude du Chauffage d'un Plasma Confine dans une Configuration Magnetique de Type Tokamak Report EUR-CEA-FC-579.

(8) J. Adams, "Ion Heating Mechanisms Based on the Absorption of the Fuse Hydromagnetic Wave Around the Ion Cyclotron Frequency", Symposium on Plasma Heating and Injection, Varenna, Italy (1972).

(9) J. Adams, "Etudes des Possibilities de Chauffuge du Plasma de TFR par Absorption de L'onde Hydronagnetique Rapide", Report EUR-CEA-FC-711, October (1973).

(10) A.M. Messiaen, P.E. Vandenplas, "Comprehensive Theory of Radio-Frequency Absorption by a Magnetized, Hot Electron-Ion Plasma Column", Nuc. Fusion 11, 556 (1971).

(11) A. Messiaen, P. Vandenplas, "Comprehensive Theory of RF Energy Absorption by a Hot Ion-Electron Plasma Cylinder Excited by an Arbitrary Electromagnetic Field", Plasma Phys. 15, 505 (1973).

(12) A. Messiaen, P. Vandenplas, "Bounded Plasma Theory of Radio-Frequency Heating of Toroidal Machines", Report 61, Lab. Phys. Plasmas, Ecale Royale Militaire (Brussels, 1974).

(13) A. Messiaen, P. Vandenplas, "Bounded Plasma Aspects of the RF Heating in Toroidal Devices (Varenna, Italy, 1974).

(14) A. Messiaen, P. Vandenplas, "Toroidal Plasma Resonances and Electron Transit Time Damping for Heating Large Thermonuclear Tori", Phys. Letters 49A, 475 (1974).

(15) A. Messiaen, P. Vandenplas, "The Present State of Research Into Plasma Heating and Injection Methods", Euratom Advisory Group on Heating and Injection, pp. 62-62A (1974).

(16) A. Messiaen, P. Vandenplas, "Radio-Frequency Heating of Large Thermonuclear Tori", Fifth Conf. on Plasma Physics and Controlled Nuclear Fusion Research (Tokyo, 1974), Paper IAEA-CN-33/C4-2.

(17) R.R. Weynants, "Ion Heating at Twice the Ion Cyclotron Frequency in Reactor Oriented Machines", Phys. Rev. Letters 33, 78 (1974).

(18) R.R. Weynants, "A High-Temperature, High Density Reduction of Harmonic Ion-Cyclotron Heating Efficiency", Symposium on Plasma Heating in Toroidal Devices (Varenna, Sept. 1974).

(19) F.W. Perkins, "Hydromagnetic Wave Heating of Tokamak Plasmas, "Symposium on Plasma Heating and Injection (Varenna, Italy), 1972.

(20) F.W. Perkins, M. Chance, J.M. Kindel, "Hydromagnetic Wave Heating of Tokamak Plasmas", Third International Symposium on Toroidal Confinement (Garching, 1973).

(21) M.S. Chance, F.W. Perkins, J.L. Sperling, "Ion Cylotron Heating of Tokamaks-Theoretical Considerations", Princeton University, Plasma Physics Laboratory (unpublished).

(22) F.W. Perkins, Nucl. Fusion 17, 1197 (1977).

(23) T.H. Stix, Nucl. Fusion 15, 737 (1975).

(24) T.H. Stix, "Fast Wave Heating of a Two Component Plasma", Princeton University, PPPL MATT-1113.

(25) T.H. Stix, Third Symposium on Plasma Heating in Toroidal Devices, Varenna (1976), PPPL Report 1309.

(26) D.G. Swanson and Y.C. Ngan, Phys. Rev. Letters 35, 517 (1975).

(27) D.G. Swanson, Phys. Rev. Letters 36, 316 (1976).

(28) J.E. Scharer, T.K. Mau, D.T. Blackfield, B.D. McVey, "Fast Magnetosonic Wave Heating at the Second Ion Cyclotron Harmonic in Tokamak Plasmas", Proc. Seventh European Conference on Controlled Fusion and Plasma Physics, p. 145, Lausanne, Sept. 1975.

(29) T.K. Mau, "Preliminary Studies on RF Heating of Ions in Tokamak-Type Plasma", University of Wisconsin Report PLP 599 (1975).

(30) J.E. Scharer, B.D. McVey and T.K. Mau, Nuc. Fusion 17, 297 (1977). J.E. Scharer, and T.K. Mau, 3rd Int'l Meeting on The. and Exp. Aspects of Heating Tor. Plasmas, Grenoble (1976) Vol. 1 p. 179.

(31) J. Jacquinot et al, Phy. Rev. Letters 39, (1977) 88.

(32) J.E. Scharer, J. Beyer and D.T. Blackfield, "Scaling of Ion Cyclotron Frequency Range Heating to Reactor Size", Proc. 3rd Top. Conf. on RF Plasma Heating, (Pasadena, 1978) paper D7-1.

(33) J.E. Scharer and D.T. Blackfield, Bull. Am. Phys. Soc. 21, (1976) 1158.

(34) J.E. Scharer and D.T. Blackfield, Bull. Am. Phys. Soc. 22, (1977) 1185.

(35) J.E. Scharer, D.T. Blackfield, T.K. Mau and J.B. Beyer, "Fast Magnetosonic Wave Heating of the NUWMAK Tokamak Reactor", Submitted to Nuc. Fusion

(36) D.T. Blackfield, et al., Bull. Am. Phys. Soc. 23, (1978) 821.

(37) Brian McVey, "A Ray Tracing Analysis of Fast Wave Heating of Tokamaks", University of Wisconsin Report PLP 755 (May 1978) (PhD. Thesis).
B.D. McVey and J.E. Scharer, Proc. 3rd Top. Conf. RF Plasma Heating, (Pasadena, 1978), Paper D6-1.

(38) J. Adam, et al., "Wave Generation and Heating in the ST Tokamak at the Fundamental and Harmonic Ion Cyclotron Frequencies", Proc. 5th Int'l Conf. on Plasma Phys. and Contr'l. Nuc. Fusion Res. (Tokyo, 1974) Paper IAEA-CN-33/A 3-2

(39) V.L. Vdovin, N.V. Shapotkovskii and V.D. Rusanov, Proc. 3rd Int'l Meeting on The. and Exp. Aspects of Tor. Plasmas (Grenoble, 1976), Vol. 2, p. 347.

(40) H. Takahasi et al., Phys. Rev. Letters 39, (1977) 31.

(41) V.V. Buzankin et al., "Experiments in Magnetoacoustic Heating of Plasma in Tokamak T-4", 6th Int'l Conf. on Plasma Phys. and Cntr'l. Fus. Res. (Berchtesgaden, 1976) Paper IAEA CN35/G10 Vol III p. 61.

(42) TFR Group, "Magnetosonic Wave Generation and Damping in the TFR Tokamak Near the Ion Cyclotron Frequencies", 6th Conf. on Pl. Phys. and Nuc. Fus. Res. (Berchesgaden, 1976), Paper IAEA-CN-35/G8, IAEA (Vienna,1977) Vol. III p. 39.

(43) see 38.

(44) J.C. Hosea, Princeton University Report MATT-1129 (May 1975).

(45) H. Takahashi, Princeton Univ. Report MATT-1140 (Oct. 1975).

(46) B. Badger et al., University of Wisconsin Dept. of Nuc. Engineering Report FDM-330.

(47) Hasegawa et al., Phys. Rev. Letters 35, (1975) 370.

(48) F.W. Perkins and C.F. Karney, "Axisymmetric Alfven Resonance Heating of Tokamaks", Bull. Am. Phys. Soc. 23, (1978) 864.

(49) B. Badger et al., University of Wisconsin Fusion Design Memo Report UWFDM-191 (Dec. 1977).

(50) J. Kesner and R.W. Conn, Nuc. Fus. 16, (1976) 397

(51) K. Audenaerde, R.W. Conn and M. Gordinier, "Periodic Gas Puffing (PGP) Mode for Long Burn Operation of Divertorless Tokamaks", Bull. Am. Phys. Soc. 23, (1978) 909.

(52) B.W. Reed et al., Princeton Univ. Report PPPL-1410 (Dec. 1977).

(53) S.J. Buchsbaum, Phys. of Fluids 3, (1960) 418.

(54) D.G. Swanson, Phys. of Fluids 18, (1975) 1269.

(55) G. Cattanei, Phys. Rev. Letts. 27, (1971) 980.

(56) J. Hosea and R. Sinclair, Phys. Fluids 13, (1970) 701.

(57) W.M. Hooke and J. Hosea, "Wave Generation and Heating Near the Ion Cyclotron Frequency in the ST Tokamak", Vth Europ. Conf. Contr'l Fus. and Plas. Phys. (Grenoble, 1972).

(58) G. Bekefi, Radiation Processes in Plasmas, John Wiley & Sons, Inc., N.Y. (1966) pp. 9-12.

(59) S. Ichimara, Basic Principles of Plasma Physics, A Statistical Approach, W.A. Benjamin, Inc., Reading, Mass. (1973).

(60) T.H. Stix, The Theory of Plasma Waves, McGraw-Hill, N.Y. (1962).

(61) D.G. Swanson, Phys. Fluids 10, (1967) 428.

(62) B.D. Fried and S.D. Conte, The Plasma Dispersion Function, Academic Press, New York (1961).

(63) L.D. Landau and E.M. Lifshitz, Electrodynamics of Continuous Media, Pergamon Press, Oxford (1975).

(64) B. Noble, Applied Linear Algebra, Prentice-Hall Inc., New Jersey (1969).

(65) M. Abramowitz and I.A. Stegun, Handbook of Mathematical Functions, Dover, New York (1964).

(66) Y.C. Ngan and D.G. Swanson, Phys. Fluids 20, (1977) 1920.

(67) J. Jacquinot, B.D. McVey and J.E. Scharer, Phys. Rev. Letters 39, (1977) 88.

(68) A.A. Ivanov and V.V. Parail, JETP Letters 35, (1972) 494.

(69) N. Martinov and A. Samain, Plasma Physics 15, (1973) 783.

(70) K.D. Harms, G. Hasselberg and A. Rogister, Nuc. Fusion 14, (1974) 251.

(71) K.D. Harms, G. Hasselberg and A. Rogister, Nuc. Fusion 14, (1974) 657.

(72) A.B. Kitsenko and K.N. Stepanov, Sov. Phys. Tech. Phys. 18, (1974) 902.

(73) A.B. Kitsenko, V.I. Panchenko and K.N. Stepanov, Sov. Phys. Tech. Phys. 18, (1974) 905,911.

(74) J.L. Sperling and F.W. Perkins, Phys. Fluids 17, (1974) 1857.

(75) J.L. Sperling and F.W. Perkins, Phys. Fluids 19, (1976) 281.

(76) J.L. Sperling, Phys. Fluids 20, (1977) 2104.

(77) M. Ono, R.P.H. Chang and M. Porkolab, Princeton Univ. Report PPPL-1325 (Feb. 1977).

(78) M. Ono, M. Porkolab, and R.P.H. Chang, Phys. Rev. Letters 38, (1977) 962.

(79) M. Ono, M. Porkolab and R.P.H. Chang, Princeton Univ. Report PPPL-1395 (Dec. 1977).

(80) M. Ono, M. Porkolab and R.P.H. Chang, Princeton Univ. Report PPPL-1434 (April 1978).

(81) M. Porkolab, Nuc. Fus. 18, (1978) 367.

(82) W.M. Hooke and J.C. Hosea, Princeton Univ. Report MATT-940 (Nov. 1972).

(83) J.C. Hosea and W.M. Hooke, Phys. Rev. Lett. 31, (1973) 150.

(84) see 44.

(85) see 45.

(86) see 38.

(87) TFR Group, "Excitation and Damping of the Fast Magnetosonic Waves in TFR Near the Harmonic Cyclotron Frequency", 3rd Int'l. Meeting on The. and Exp. Aspects of Heating Tor. Plasmas (Grenoble, 1976), Vol. I, p. 87.

(88) TFR Group, "ICRF Heating in TFR Preliminary Observations and Prospects for Further Developments", Joint Varenna-Grenoble Int'l. Sym. on Heating Tor. Plasmas (Grenoble, 1978).

(89) see 42.

(90) see 40.

(91) H. Takahashi, Princeton Univ. Report MATT-1374 (Oct. 1977).

(92) N.V. Ivanov, I.A. Kovan and E.V. Los', JETP Letters 14, (1971) 138.

(93) N.V. Ivanov, I.A. Kovan and E.V. Los',"Excitation of the Spectrum of Natural Oscillations of the Plasma Pinch in the Tokamak TO-1", Translated from Atomaya Energiya 32, (1972) 453.

(94) N.V. Ivanov, I.A. Kovan, et al., JETP Lett. 16, (1972) 60.

(95) N.V. Ivanov, et al., JETP Lett. 20, (1972) 39.

(96) V.L. Vdovin, et al., JETP Lett. 14, (1971) 149.

(97) V.L. Vdovin, et al., JETP Lett. 17, (1973) 2.

(98) V.L. Vdovin, V.D. Rusanov and N.V. Shapotkovskii, 5th Conf. Plas. Phys. and Nuc. Fus. Res. (Tokyo, 1974).

(99) see 39.

(100) see 41.

(101) DIVA Group, "Preliminary Results of ICRF Heating in Diva", Joint Varenna-Grenoble Int'l. Sym. Heating Tor. Plas. (Grenoble, 1978).

(102) G.J. Morales and R.J. Taylor, "ICRF Heating in the MACROTOR Tokamak", Joint Varenna-Grenoble Int'l. Sym. Heating Tor. Plas. (Grenoble, 1978).

(103) V.P. Bhatnagar, et al., "Magnetosonic Resonance Heating In The ERASMUS Tokamak", Joint Varenna-Grenoble Int'l. Sym. Heating Tor. Plas. (Grenoble, 1978).

(104) P.L. Colestock, J.C. Hosea, et al., "ICRF Heating in PLT", Joint Varenna-Grenoble Int'l. Sym. Heating Tor. Plas. (Grenoble, 1978).

(105) W.M. Hooke, F.W. Perkins, et al., "Propsal for the High-Power ICRH Wave-Heating Facility for the PLT Tokamak", Draft Copy (April 3, 1978).

(106) J. Adam, "Design Study for ^{o}Ion Cyclotron Heating in JET", Fonteny-aux-Roses Report n^{o} 1147 (Feb. 1976).

(107) F. Fidone and L. Gomberhoff, Plasma Phys. 20, (1978) 689.

(108) R. Klima, et al., Nuc. Fusion 15, (1975) 1157.

(109) B. Badger, et al., Univ. of Wisconsin Fusion Design Memo Report UWFDM-150 (July 1976).

II POINT MODEL

II-A REACTOR STARTUP

In this section, we examine various ways in which a reactor may be heated to ignition using RF auxiliary heating. Time varying temperature as well as various heating and loss mechanism curves are obtained by solving the time dependent ion and electron energy balance equations. The RF heating terms are calculated assuming a linear, weak damping, finite Larmor radius theory. A computer point code, based on a spatially independent, "0-D" model is used to solve the energy balance equations. The energy balance equations can be obtained from the Boltzman equation,[1,2,3]

$$\frac{df_j}{dt} + \vec{v} \cdot \vec{\nabla} f_j + \frac{e_j}{m_j} (\vec{E} + \vec{v} \times \vec{B}) \cdot \vec{\nabla}_v f_j = C_j \qquad (1)$$

where C_j is the Fokker-Planck collision operator.[4]
By taking the second velocity or energy moment of Eq. 1 we obtain

$$\frac{\partial}{\partial t} (\frac{3}{2} n_j kT_j) = - \vec{\nabla} \cdot (\frac{3}{2} kT_j \vec{\Gamma}_j + \vec{Q}_j) - n_j kT_j \vec{\nabla} \cdot \vec{V}_j$$
$$+ n_j e_j \vec{E} \cdot \vec{V}_j + m_j \int v^2 C_j d^3v \qquad (2)$$

$$\vec{Q}_j \equiv \int \vec{v} (\vec{v} - \vec{V}_j)^2 f_j d^3v \qquad (3)$$

where use has been made of both the particle and momentum conservation equations.[1]

Averaging over a magnetic flux surface yields the spatially dependent fluid energy equations for both electrons and ions. For electrons we have

$$\frac{\partial}{\partial t}\left(\frac{3}{2} n_e k T_e\right) = \frac{n_i^2 \langle \sigma v \rangle_{DT}}{4} E_\alpha U_{\alpha e} + \frac{1}{r}\frac{\partial}{\partial r}\left[r\left(Q_e + \frac{3}{2} k T_e \Gamma_e\right)\right]$$

$$- Q_{ei} - P_{rad} + P_{Ohm} + P^e_{INJ} + P^e_{RF} \qquad (4)$$

where a source term for an external injection of power either from RF or beams as well as loss terms from Bremsstrahlung and synchrotron radiation have been added. The radiation loss terms are calculated assuming that a local Maxwellian temperature occurs for the electrons over time scales much longer than the relaxation scale in Eq. 1.

The ion equation is

$$\frac{\partial}{\partial t}\left(\frac{3}{2} n_i k T_i\right) = \frac{n_i^2 \langle \sigma v \rangle_{DT}}{4} E_\alpha U_{\alpha i} + \frac{1}{r}\frac{\partial}{\partial r}\left[r\left(Q_i + \frac{3}{2} k T_i \Gamma_i\right)\right]$$

$$+ Q_{ei} + P^i_{INJ} - P_{cx} + P^i_{RF} \qquad (5)$$

where

n_e, n_i = electron and ion densities, with $n_i = n_D + n_T$

T_e, T_i = electron and ion temperatures, with $T_D = T_T$ due to the short ion-ion equilibration time

$U_{\alpha e}$, $U_{\alpha i}$ = fraction of alpha energy to electrons and ions

Q_{ei} = electron-ion rethermalization term

P_{rad} = Bremsstrahlung, line, recombination and synchrotron radiation losses

P_{Ohm} = Ohmic heating

P^e_{INJ}, P^i_{INJ} = electron and ion heating sources from beams

P_{cx} = charge exchange energy loss

Γ_e, Γ_i = electron and ion particle fluxes

Q_e, Q_i = electron and ion energy conduction terms

P^e_{RF}, P^i_{RF} = electron and ion RF power absorption terms

To obtain the particle flux terms in Eqns. 4 and 5 we examine the particle conservation equation of the zeroth moment of Eq. 1

$$\frac{\partial n_i}{\partial t} = \frac{1}{r}\frac{\partial}{\partial r}(r\Gamma_i) - \frac{n_i^2 \langle\sigma v\rangle_{DT}}{2} + S_p(r,t) \tag{6}$$

where $S_p(r,t)$ is the particle source due to neutral beams, pellet injection, or gas puffing and we may write[1]

$$\Gamma_i = D_i \frac{\partial n_i}{\partial r} \tag{7}$$

$$Q_{e,i} = \chi_{e,i} \frac{\partial (kT_{e,i})}{\partial r} \tag{8}$$

To obtain the ion-electron equilibration term in Eqns. 4 and 5 we use the classical expression which is in agreement with experimental results,

$$Q_{ei} = \frac{3n_e}{\tau_{ei}} \frac{m_e}{m_i} k(T_e - T_i) , \tag{9}$$

where τ_{ei} is the electron-ion equilibration time which for the neoclassical banana regime is given by[5]

$$\tau_{ei} = \frac{3\, m_e^{1/2}\, T_e^{3/2}}{4(2\pi)^{1/2} e^4 n_i \ell n \Lambda} . \tag{10}$$

The Ohmic heating term is evaluated from the neoclassical model

$$P_{Ohm} = E_\phi J_\phi \tag{11}$$

$$E_\phi = \eta_{nc} J_\phi \tag{12}$$

where η_{nc} is the neoclassical resistivity obtained from the Spitzer resistivity by[1,6]

$$\eta_{nc} = \eta_{sp} [1 - 1.95(r/R)^{1/2} + .95(r/R)]^{-1} \tag{13}$$

The energy loss from Bremsstrahlung may be written as[2,5]

$$P_B = 4.8 \times 10^{-31} Z_{eff} n_e^2 T_e^{1/2} \text{ watts/cm}^3 \tag{14}$$

with T_e in keV.

The synchrotron loss term is[8]

$$P_{syn} = 1.55 \times 10^{-14}(1 - r_w)^{1/2}[5. + .17(5-A)]^3 \frac{n_e^{1/2} B_T^{5/2}}{a^{1/2}} T_e^{2.1} \text{ W/cm}^3 \tag{15}$$

where

A = aspect ratio

r_w = wall reflectivity

T_e in keV

B_T = toroidal field in Tesla

a = minor radius

Finally Eqns. 4 and 5 become[9]

$$\frac{\partial n_e T_e}{\partial t} = 4.28 \times 10^{-11} n_e n_i \frac{(T_i - T_e)}{T_e^{3/2}} + \frac{1}{1.5r} \frac{\partial}{\partial r} (r n_e \chi_e \frac{\partial T_e}{\partial r}) - \frac{1}{r} \frac{\partial}{\partial r} (r n_e V_e T_e)$$

$$+ 4.17 \times 10^{15} \{n_D n_T \langle \sigma v \rangle U_{\alpha e} + \bar{E} \cdot \bar{J} + P_{inj}(U_{be} + f(\frac{E_\alpha}{E_b}) U_{\alpha e})$$

$$- P_B - P_S\} + P_{RF}^e \tag{16}$$

and

$$\frac{\partial n_i T_i}{\partial t} = -4.28 \times 10^{-11} n_i n_e \frac{(T_i - T_e)}{T_e^{3/2}} + \frac{1}{1.5r}\frac{\partial}{\partial r}\left(r n_i \chi_i \frac{\partial T_i}{\partial r}\right) - \frac{1}{r}\frac{\partial}{\partial r}\left(r n_i V_i T_i\right)$$

$$+ 4.17 \times 10^{15} \{n_D n_T \langle\sigma v\rangle_{DT} U_{\alpha i} + P_{inj}\left(U_{bi} + f\left(\frac{E_\alpha}{E_B}\right)U_{\alpha i}\right)\} + P_{RF}^i \qquad (17)$$

$T_{e,(i)}$ is the electron (ion) temperature (eV), B_p is the poloidal magnetic field (Gauss), $n_{e,(i)}$ is the electron (ion) density (cm^{-3}), V_i is the ion velocity (cm/ms), J is the toroidal current density (amp/cm^2), E is the toroidal electric field (volt/cm), r is the radius (cm), t is time (ms), $\chi_{e,(i)}$ is the electron (ion) thermal diffusivity (cm^2/ms), η_{NC} is the neoclassical resistivity (ohm-cm), D is the diffusion coefficient (cm^2/ms), $U_{bi,(e)}$ is the fraction of beam energy going to ions (electrons), and f is the fraction of deuterons in the neutral beam which undergo fusion as they slow down in a tritium target plasma. P_B, P_S, represent Bremsstrahlung, synchrotron radiation, respectively (watts), and E_B is the beam energy, and $P_{RF}^{i,e}$ is the ion (electron) power absorption (watts).

Since the point code is spatially independent, we need to eliminate the gradients in both the conduction and convection terms. Therefore, we may replace the conduction term by[10]

$$\frac{2}{3}\frac{\partial}{\partial r}\left[rn\chi\frac{\partial T}{\partial r}\right] \rightarrow \frac{nT}{\tau_c} \qquad (18)$$

where τ_c is a characteristic thermal conduction time. For the convection term we have[10]

$$\frac{1}{r}\frac{\partial}{\partial r}\left(r\, nVT\right) \rightarrow \frac{nT}{\tau_D} \qquad (19)$$

where τ_D is a characteristic thermal diffusion time.

Qualitatively, we can replace τ_c and τ_D by

$$\tau_c^{i,e} \rightarrow \frac{a^2}{\chi_{i,e}} \tag{20}$$

$$\tau_D \rightarrow \frac{a^2}{D} \tag{21}$$

where a is the plasma minor radius and D is the diffusion coefficient, and χ is the thermal conduction coefficient.

To calculate D and $\chi_{i,e}$[11] we first must examine single particle orbits. Particles may travel along magnetic field lines which, if closed and in the absence of drifts, result in no particle losses. However, due to the 1/R variation in the magnetic field, as a particle travels along a given field line it passes through regions of varying field strengths. For a maximum magnetic field strength on that line of B_{max} particles with energy $E < \mu B_{max}$ will be reflected from the high magnetic field regions and become trapped in weak magnetic wells, undergoing periodic motion between reflection points. The bounce frequency for this periodic motion is approximately

$$\omega_b \simeq \frac{v_T}{Rq} \sqrt{2\varepsilon} \tag{22}$$

where $\varepsilon = r/R$ and q is the safety factor

$$q = \frac{rB_T}{RB_p} \quad . \tag{23}$$

Besides this bounce motion, particles also experience an effective gravitational force again caused by the inhomogeneity in the magnetic

field. The resultant drift of particles may be characterized by the velocity

$$V_D \simeq (mv_{\parallel}^2 + \mu B) \frac{B \times \nabla B}{eB^3} \sim \frac{m}{eB} \frac{v_T^2}{R} \tag{24}$$

The combination of bounce motion with drift produces a banana-shaped orbit whose width is given by

$$\Delta r_T \simeq \frac{2V_D}{\omega_b} \simeq 2\rho_\theta \sqrt{\varepsilon} = 2q\ \rho/\sqrt{\varepsilon} \tag{25}$$

where $\rho_\theta = \frac{V_T m}{eB_p}$.

A general particle diffusion coefficient may be defined by $D \sim (\Delta x)^2/\Delta t$ where Δx is the mean spatial step size caused by the scattering process during the time Δt. In the absence of bounce motion and drifts, simple Coulomb collisions produce particle transport. For low β machines, the classical diffusion coefficient is written[11] as

$$D \sim \nu_{ei} \rho^2 \tag{26}$$

where ρ, the gyroradius, is the step size and

$$\nu_{ei} = \frac{4\sqrt{2\pi}\ n_i Z^2\ e^4 \ell n \Lambda}{3\sqrt{m_e}\ T_e^{3/2}} = \text{electron-ion collision frequency.} \tag{27}$$

However, when banana orbits are present in tokamaks, this simple diffusion picture becomes more complicated.

For low ν, the trapped particles have a step size on the order of the banana width rather than their gyroradius. This step size is valid when the collision frequency for the scattering of trapped particles

out of the region of trapped particle velocity space is small compared to the bounce frequency. Since Coulomb collisions are small angle processes we define

$$\nu_{eff} \sim \frac{\nu_{90°}}{(\Delta\theta)^2} \sim \frac{\nu_{ei}}{\varepsilon} \tag{28}$$

The condition for trapped particles to be considered "collisionless" is that

$$\nu_{eff} < \omega_b \text{ or } \nu < \varepsilon^{3/2} V_T/Rq \tag{29}$$

In this "neoclassical" regime, the diffusion coefficient due to trapped particles is

$$D \sim \nu_{eff} (\Delta r_T)^2 f_T \sim \nu \rho^2 q^2 \varepsilon^{-3/2} \tag{30}$$

where f_T is the fraction of trapped particles

$$f_T \equiv \frac{B_{max}}{B_{min}} - 1 \equiv \sqrt{2\varepsilon} \tag{31}$$

For ions in this neoclassical regime $\chi_i \sim D$.

Since plasmas in tokamaks are neither spatially uniform nor Maxwellian, they are subject to both macroinstabilities and microinstabilities. Microinstabilities may be driven by velocity space anisotropy or temperature, density and pressure gradients. Microinstabilities lead to enhanced or "anomalous" transport of which, for tokamaks, the most important kind are those driven by the various gradients present in all tokamaks.

In an inhomogeneous plasma, there is an apparent drift of particles in the $\vec{B}X\nabla n$ direction given by

$$V_d = \frac{T}{eB}\frac{1}{n}\frac{dn}{dr} = \frac{\rho}{r_n} v_T \tag{32}$$

where r_n = effective plasma radius = $(\frac{1}{n}\frac{dn}{dr})^{-1}$.

When there exists an E_θ in the $\bar{B}X\nabla n(\theta)$ direction, with wave number k_θ, this field produces a drift wave with frequency

$$\omega_* = k_\theta V_D \cdot \tag{33}$$

Since $\frac{1}{r} < k_\theta < \rho_i^{-1}$ we may have a range of drift frequencies with

$$\omega_{*min} \simeq \frac{V_d}{r} \sim \frac{v_{thi}}{r}\frac{\rho_i}{r_n} \tag{34}$$

$$\omega_{*max} \simeq \frac{V_d}{\rho_i} \sim \frac{v_{thi}}{r_n} \cdot \tag{35}$$

There is no energy or momentum exchange between species since E_θ causes both ions and electrons to drift in the $\bar{E}_\theta X\bar{B}$ direction, hence no instability develops. However, various mechanisms exist which may retard one of the drifting species, resulting in a net exchange of either momentum or energy with the drift wave causing an instability to grow. These mechanisms which result in enhanced transport may be classified between various natural frequencies in the plasma ω_{*min}, ω_{*max}, ω_b and the curvature drift frequency $\omega_D \equiv k_\theta v_D$. In tokamaks, we usually have

$$\omega_{Dmin} < \omega_{*min} << \omega_{bi} << \omega_{*max} < \omega_{be} \cdot$$

Therefore, we may order the various types of instabilities due to drift waves in order of decreasing collision frequency.

For $\nu_{eff} > \omega_{be}$ but $\nu < \omega_{*max}$, i.e., trapped particles collide before a full bounce period is completed, drift dissipative modes develop and we have the following "pseudoclassical" transport coefficients

$$\chi_e \sim C_o \nu_{ei} \rho_{\theta e}^2 \qquad \text{and} \qquad D \sim C_1 \nu_{ei} \rho_{\theta e}^2 \tag{36}$$

with $C_o = 10$ and $C_1 = 10/3$ for NUWMAK.

For $\nu_{eff_e} < \omega_{be}$, $\nu_{eff_e} > \omega_{*min}$ trapped particles bounce before undergoing Coulomb collisions, hence are "collisionless". When a temperature gradient exists, these collisions do not retard the $\overline{E \times B}$ drift of the trapped electrons and the dissipative trapped electron mode develops with transport coefficients

$$\chi_e \sim \frac{3\,\varepsilon^{3/2}\, r^2\, \omega_{*min}\, \omega_{*min}^T}{\nu_{ei}} \qquad \text{with } \omega_{*min}^T = \frac{1}{e\,Br}\frac{\partial T}{\partial r} \tag{37}$$

$D \sim \varepsilon \chi_e \sim \chi_i$.

For $\nu_{eff_e} < \omega_{be}$, $\nu_{eff_e} < \omega_o \sim 0.1\,(r/\rho_{\theta e})\,\omega_{*min}$ again we have a dissipative trapped electron mode instability developing. However, in this lower collision frequency regime the effective wave number k of this mode is determined by the magnetic shear and we obtain

$$\chi_e \sim C_2 \nu_{ei} \rho_{\theta e}^2 \qquad \text{where } C_2 = 0.06\,\varepsilon^{1/2}\,\frac{d\ell nT}{d\ell nn}\,\frac{m_i}{m_e}\,\frac{B_p}{\theta B} \tag{38}$$

$D \simeq \varepsilon \chi_e \sim \chi_i$. = constant of order 10^2 depending upon the magnetic shear

$$\theta \equiv r_n/L \rightarrow \theta = r_n/L_S$$

Finally for $\nu_{eff_i} \ll \omega_{bi}$ the frequency of this mode is below the ion bounce frequency. The drift wave in this case is supported by only trapped particles and we have

$$D \sim \chi_e \sim \chi_i \sim \frac{\varepsilon^{5/2} r^2 \omega_{*min}^2}{\nu_{ei} (1 + T_e/T_i)^2} \tag{39}$$

In the point code, all of the above transport coefficients are first calculated and the largest values for D and $\chi_{i,e}$ are used in the energy balance equations.

To eliminate the spatial dependency in density and temperature, we use the following expressions for the average density and temperature[9,10]

$$\bar{n} = 2 \int_o^a \frac{n(r) r dr}{a^2} \tag{40}$$

$$\bar{T} = \frac{\int_o^a n(r)\, T(r)\, r dr}{\int_o^a n(r)\, r dr} \tag{41}$$

where both T(r) and n(r) are assumed of parabolic form

$$n(r) = 2\, n_o \left(1 - \frac{r^2}{a^2}\right)^{\alpha} \tag{42}$$

$$T(r) = 2\, T_o \left(1 - \frac{r^2}{a^2}\right)^{\beta} \tag{43}$$

where α and β are set equal to 1 for the cases we analyze.

Since NUWMAK is noncircular, a shape factor S is defined[10] by

$$S = \frac{\text{circumference of plasma}}{\text{circumference of prescribed circular plasma}} \tag{44}$$

so that the stability factor q is given by

$$q = \frac{S}{A} \frac{B_T}{B_p} \tag{45}$$

where A is the aspect ratio of the smaller inscribed circular plasma and B_p is the poloidal field at the plasma edge.

In the point code, we assume that through some fueling mechanism, such as low energy neutral beams or pellets, the density of deuterium and tritium remains constant, although the ratio of the two species may vary if neutral deuterium beams are used. The resultant alphas from both main body and TCT fusions are calculated and we may find the resultant electron density by the charge neutrality condition

$$n_e = n_D + n_T + 2n_\alpha \tag{46}$$

We now spatially average the RF heating expressions (Sec. I, Eqs. 39, 44) and assuming the parabolic expressions (42,43) and define

$$PRFI = \sum_{\ell=2}^{3} \int_0^a \frac{\varepsilon_o \omega_{pi}^2(r)}{4\ell\, \omega_{cio}} \frac{R}{r} \left[\frac{\langle k_\perp^2\rangle v_{thi}^2(r)}{2\omega_{ci}^2(r)}\right]^{\ell-1} |E_+|^2 r dr \Big/ \int_0^a r dr \tag{47}$$

where $\ell = \frac{\omega}{\omega_{ci}} = 2$ for deuterium and 3 for tritium :

$$PRFE = \frac{\int_0^a \frac{\pi^{1/2}\varepsilon_o}{4 k_\parallel} \frac{\omega_{pe}^2(r)}{\omega_{ce}^2(r)} \langle k_\perp^2\rangle v_{the}(r) (1 + x^2(r)) |E_+|^2 e^{-\left(\frac{\ell^2\omega^2_{cio}}{k_\parallel^2 v_{the}^2(r)}\right)} r dr}{\int_0^a r dr} \tag{48}$$

In the expressions for PRFI and PRFE we have previously averaged $k_\perp^2$ over the resonant heating zone whose width is given for both ion species by

$$\Delta R = \frac{2\, k_{\parallel}\, v_{thi}\, R}{\ell\, \omega_{cio}} \tag{49}$$

while for the electrons, ΔR is taken to be the entire plasma cross section since electron Landau heating as well as transit time magnetic pumping occur over the entire plasma radius. With this model we have neglected possible effects due to coupling problems as well as multiple modes. With this we find that

$$PRFI = \sum_{\ell=2}^{2} \frac{|E_+|^2}{2\ell\omega_{cio}a^2}\, \varepsilon_o R \int_0^a \omega_{pi}^2(r) \left[\frac{\langle k_\perp^2\rangle\, v_{thi}^2(r)}{2\,\omega_{ci}^2(r)}\right]^{\ell-1} dr \tag{50}$$

$$= PRFI'\ |E_+|^2$$

$$PRFE = \langle k_\perp^2\rangle \frac{|E_+|^2}{2k_{\parallel}a^2}\, \pi^{1/2} \int_0^a \frac{\omega_{pe}^2(r)}{\omega_{ce}^2(r)}\, v_{the}(r)\, (1 + x^2(r))\, e^{-\ell^2\omega^2_{cio}/k_{\parallel}^2 v^2_{the}} dr \tag{51}$$

$$= PRFE'\ |E_+|^2 \tag{52}$$

$$\text{TOTAL RF INJECTED POWER} = |E_+|^2 \times (PRFI' + PRFE') \times \text{VOLUME}\ . \tag{53}$$

In the point code, we input the total power deposited in the plasma; therefore, we normalize $|E_+|^2$ such that

$$|E_+|^2 = \frac{\text{TOTAL RF INJECTED POWER}}{(PRFI' + PRFE') \times \text{VOLUME}}\ . \tag{54}$$

II-B NUWMAK POINT CODE RESULTS

There are several possible scenarios for an RF heated reactor startup[12-14]. As shown in Table 4, we first examine a non-circular tokamak of minor radius 1.25 m, major radius of 5.00 m, non-circularity factor of 1.33, toroidal B field on axis of 60 kG which determines the RF frequency used as 92 MHz and plasma current of 6.48 MA which results in a thermal energy output of 2300 MW. The average electron density is approximately 2.00×10^{14} cm^{-3}, while the plasma is a 50-50 mix of D and T. Also initially, $T_i=T_e=1.0$ keV for Figs. 1 thru 9, while for the latter figures $T_i=T_e=300$ eV.

First of all, in Fig. II-B-1, a moderate amount of power may be supplied for a relatively long time, or left on during the entire burn time in the case of a driven reactor. In Fig. II-B-1 we supply RF power levels of 50, 70, 80 and 100 MW for a full 3 seconds. We notice that for power levels of 80 MW and above, an equilibrium ion temperature of 15 keV can be achieved within 3 seconds.

By going to higher RF power levels supplied over a shorter time, we may increase the duty cycle of the power reactor. In Fig. II-B-2, for power levels above 125 MW supplied for 1 second, an equilibrium ion temperature of 13.5 keV may be achieved as early as 1.5 seconds after the RF heating phase, thereby decreasing the startup phase by as much as 1.5 seconds. The equilibrium temperature in Fig. II-B-1 is higher than the one in Fig. II-B-2 because the continuous supply of RF power in the driven case causes the plasma to reach a higher equilibrium. If the RF was shut off in the driven case, the plasma would then relax to the equilibrium value of the undriven case. In addition Fig. II-B-2

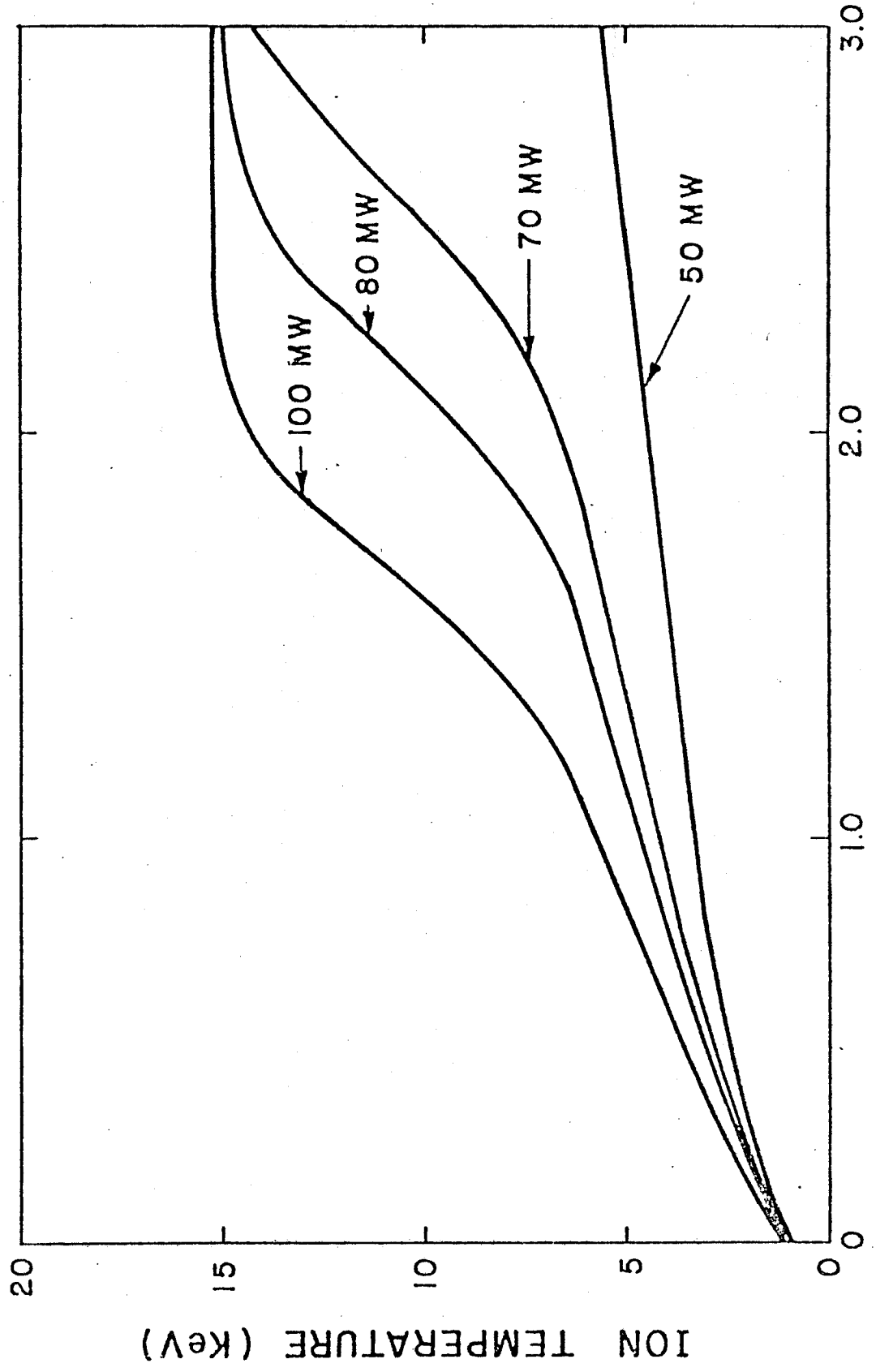

Fig. II-B-1 Magnetosonic wave heating for RF power levels of 50, 70, 80 and 100 MW applied for 3 sec.

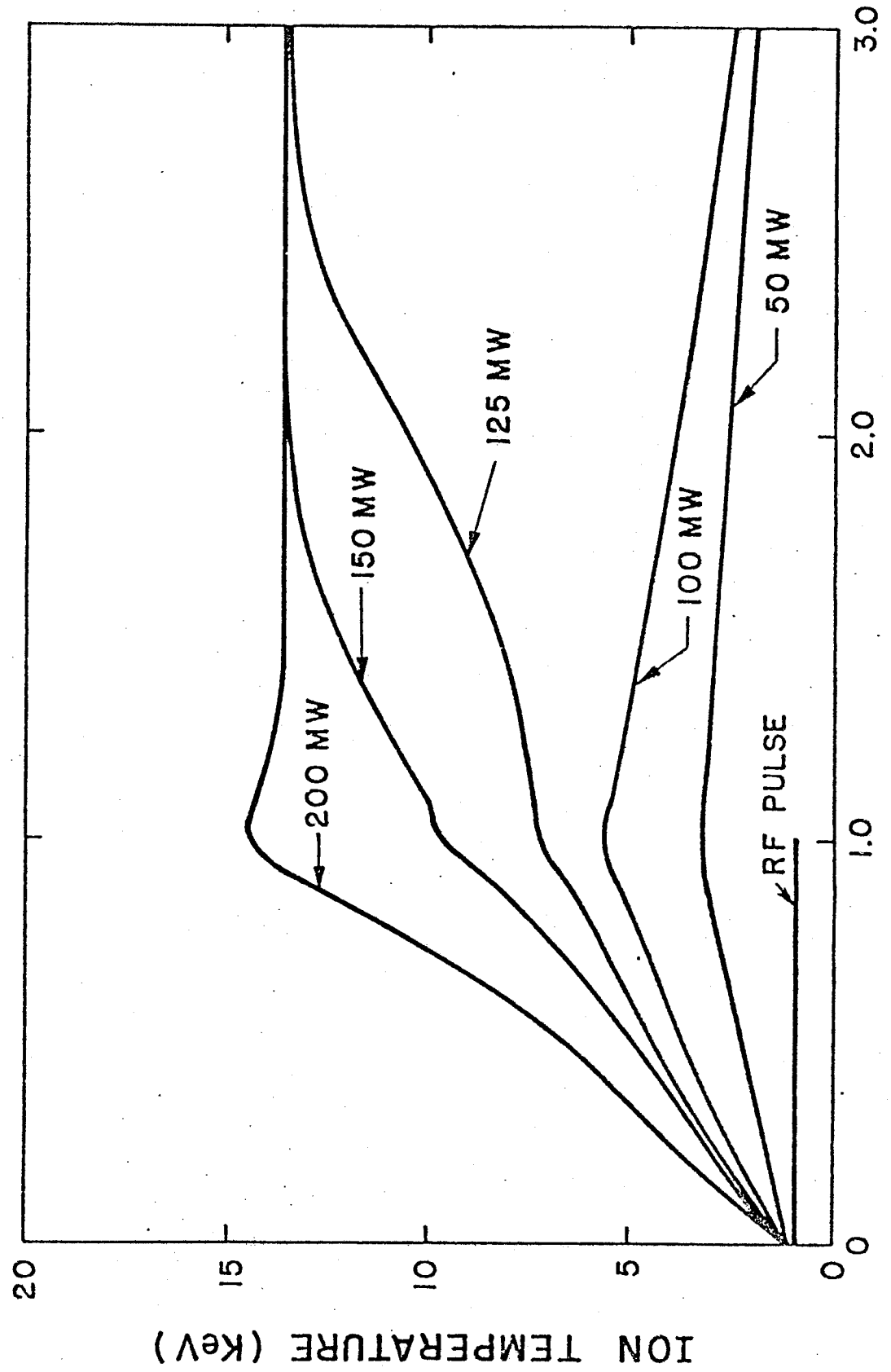

Fig. II-B-2 Magnetosonic wave heating for RF power levels of 50, 100, 125, 150 and 200 MW applied for 1 sec.

shows that for power levels of 100 MW and below the plasma never reaches ignition and the plasma temperature subsequently drops once the RF is turned off.

In Figs. II-B-3 thru 9 we deal with the case of 175 MW supplied for 1 second. In Fig. II-B-3, we notice that in the first second of operation T_i is greater than T_e because most of the RF power is supplied to the ions (see Fig. II-B-7). However, 800 ms after the RF is turned on, T_i becomes so high that a significant number of fusions occur. The resultant alphas deposit most of their energy in the electrons as they thermalize causing T_e to become greater than T_i, reaching a steady state value of 15 keV as compared to that of 13.5 keV for the ions. The alpha power to the electrons as shown in Fig. II-B-3 rises sharply after 800 ms and eventually reaches an equilibrium value of 360 MW. The kink in the alpha curve corresponds to the sudden loss of RF heating power at the time of shut off.

In Eqs. (50) and (51) an averaged value for $k_\perp^2$ was used. In Fig. II-B-4 we have the averaged value $\langle k_\perp^2 \rangle^{1/2}$ for each species when $k_\perp^2$ is averaged over either the resonant heating zone of each ion species as shown in Fig. II-B-5 or, for the case of the electrons, over the entire plasma cross section. In Fig. II-B-5, the resonant width for deuterium increases from 6.6 cm to 23 cm while that of tritium spreads from 5.5 cm to 18.8 cm as T_i increases.

Figure II-B-6 displays the magnitude of the spatially averaged electric field $|E_+|$. We notice that $|E_+|$ drops from a peak value of 1040 V/m to that of 280 V/m with increasing time. As time increases, the plasma conductivity increases, hence the magnitude of E_+ must decrease if we wish to supply a constant amount of power to the plasma.

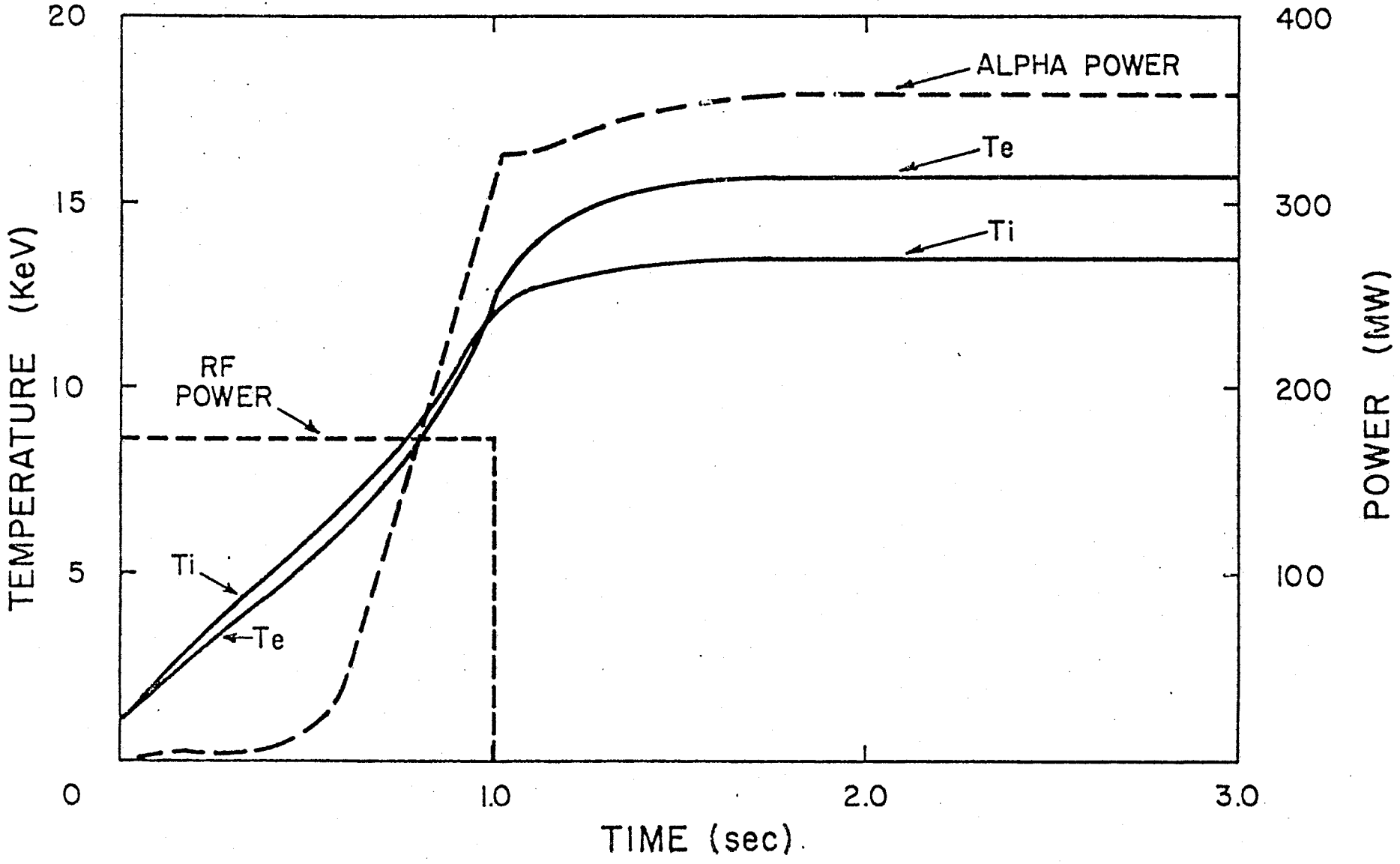

Fig. II-B-3 Magnetosonic wave heating to reactor ignition and alpha power deposited in the electrons for an RF pulse of 1 sec, at 175 MW.

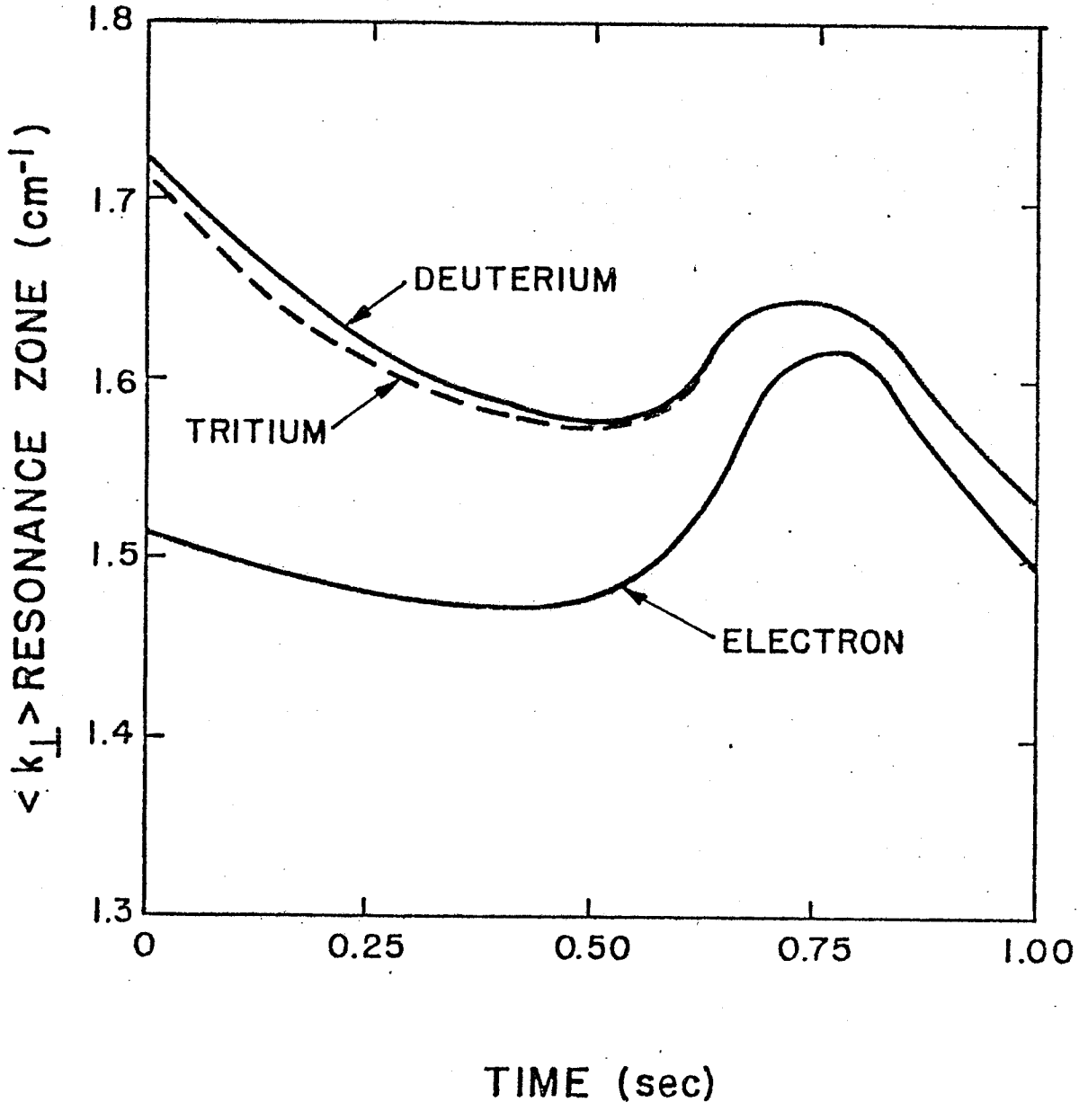

Fig. II-B-4 $k_\perp$ averaged over the resonance zone of each species for an RF power level of 175 MW.

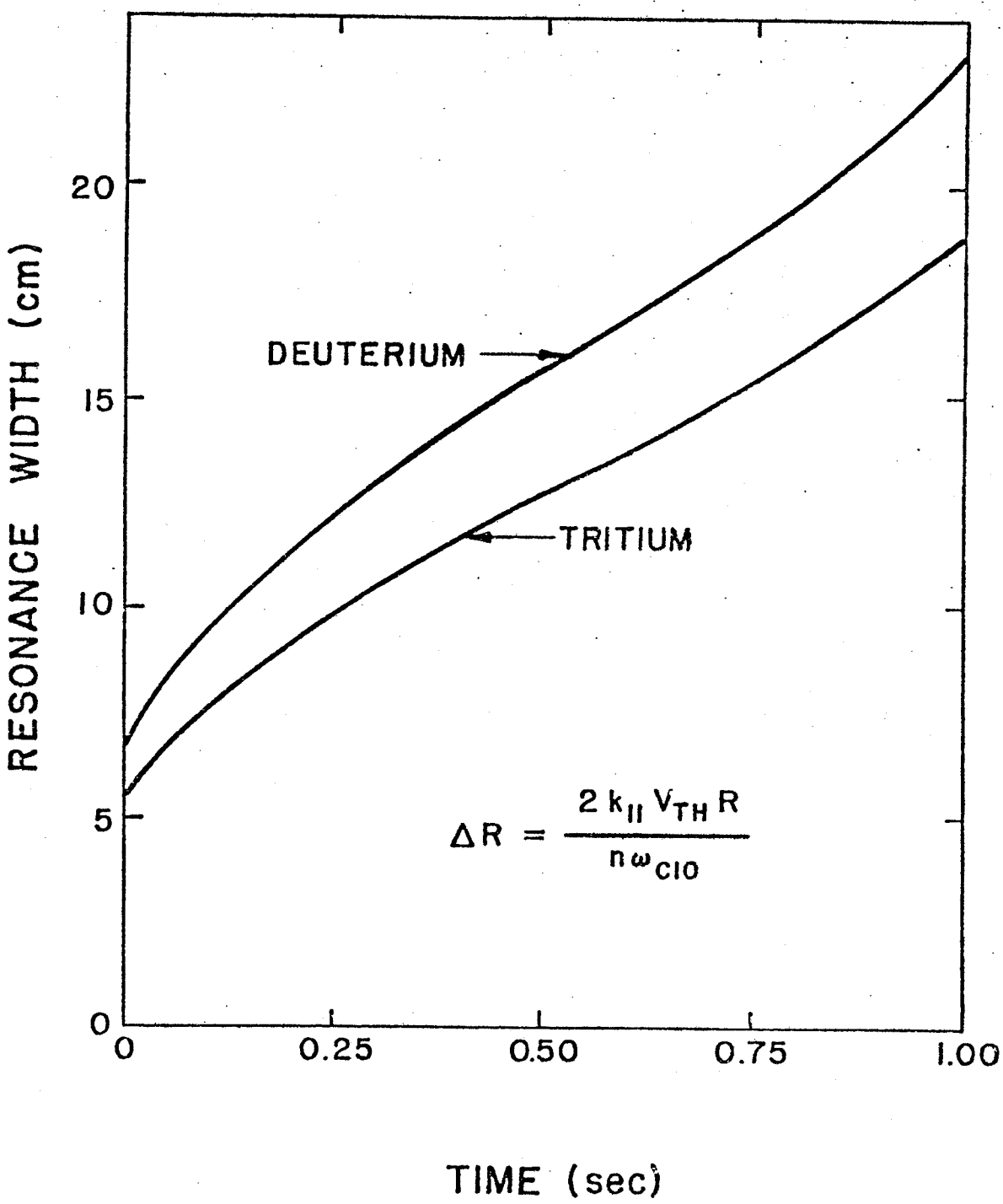

Fig. II-B-5 Deuterium and tritium resonance widths for an RF power level of 175 MW.

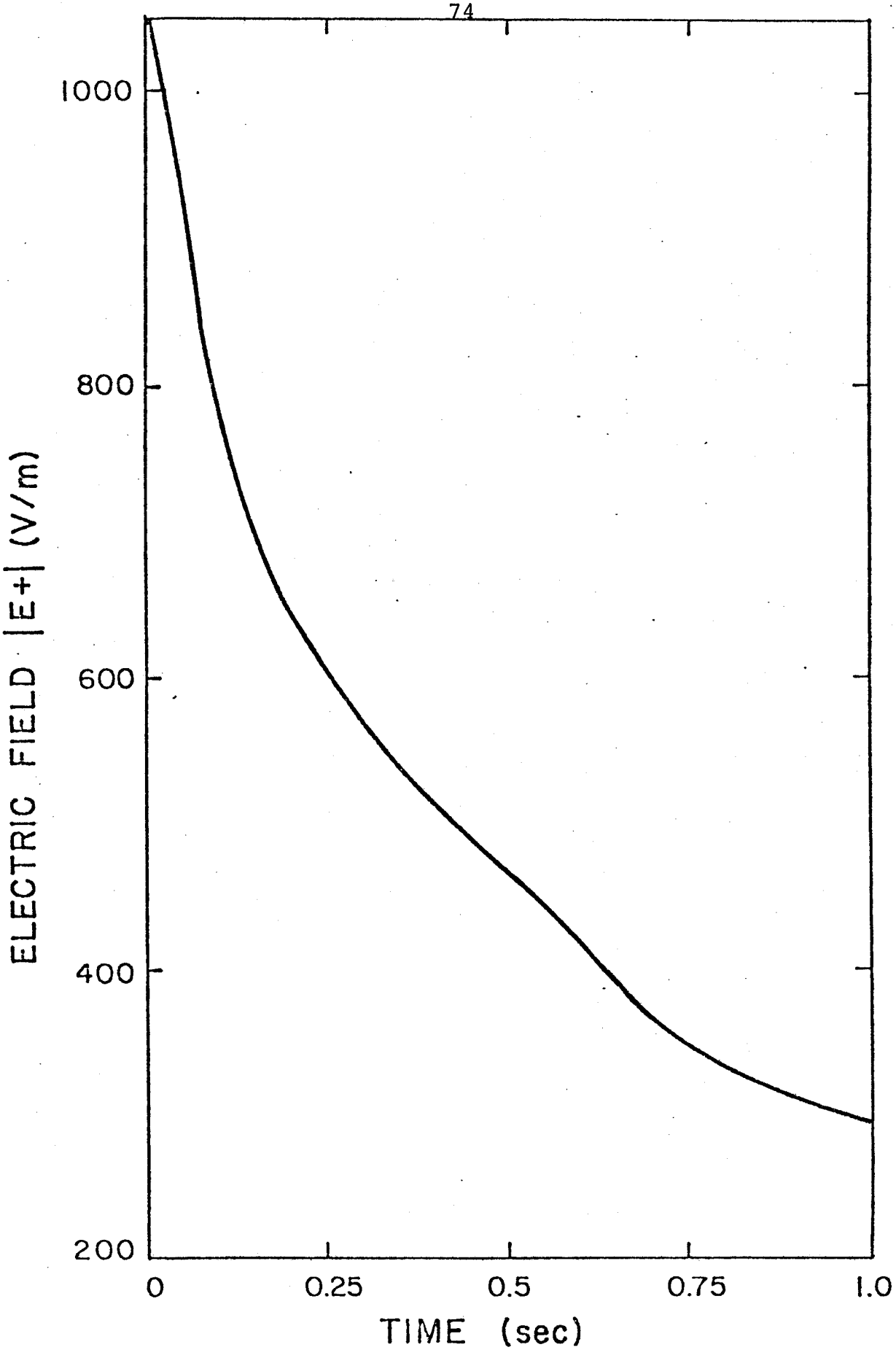

Fig. II-B-6 Magnetosonic wave electric field $|E_+|$ for an RF power level of 175 MW.

In Fig. II-B-7, we see the amount of RF power supplied to each species. Most of the power supplied goes to the ions though it does decrease from an initial high of 175 MW to 160 MW. As the plasma temperature increases, the power flow to deuterium decreases from 170 MW to 120 MW. This decrease is partially compensated by an increase of power flow to tritium, which rises from 7 MW to 40 MW. The remaining power is deposited in the electrons, reaching a peak before shut off of 15 MW. As the temperature increases, power flow to the electrons increases because the expression in the exponential factor of the electron heating term decreases. In addition we see more power going to the tritium at the expense of the deuterium because of the ratio $\frac{P_T}{P_D} \sim T_i$.

Figures II-B-8 and 9 show the terms in the electron and ion energy balance equations. Dashed lines indicate energy losses and solid lines indicate heating terms. In Fig. II-B-8, we see that at these high plasma temperatures the Ohmic heating term is quite small, decreasing from 7 MW to 1 MW. After 500 ms, the alpha heating term becomes so large that even if mode conversion processes were present causing most of the power to be deposited in the electrons, our results would still be the same. As Fig. II-B-3 shows, since $T_i \approx T_e$, the electron-ion equilibration time is quite short, indicating that heating of the electrons would drag the ion temperature along with it, thus not changing our results. Equilibrium is reached when the loss terms equal the heating terms. In the case of the electrons, at equilibrium as shown in Fig. II-B-8, the electrons lose 18 MW from synchrotron radiation, 28 MW from Bremsstrahlung, 235 MW through con-

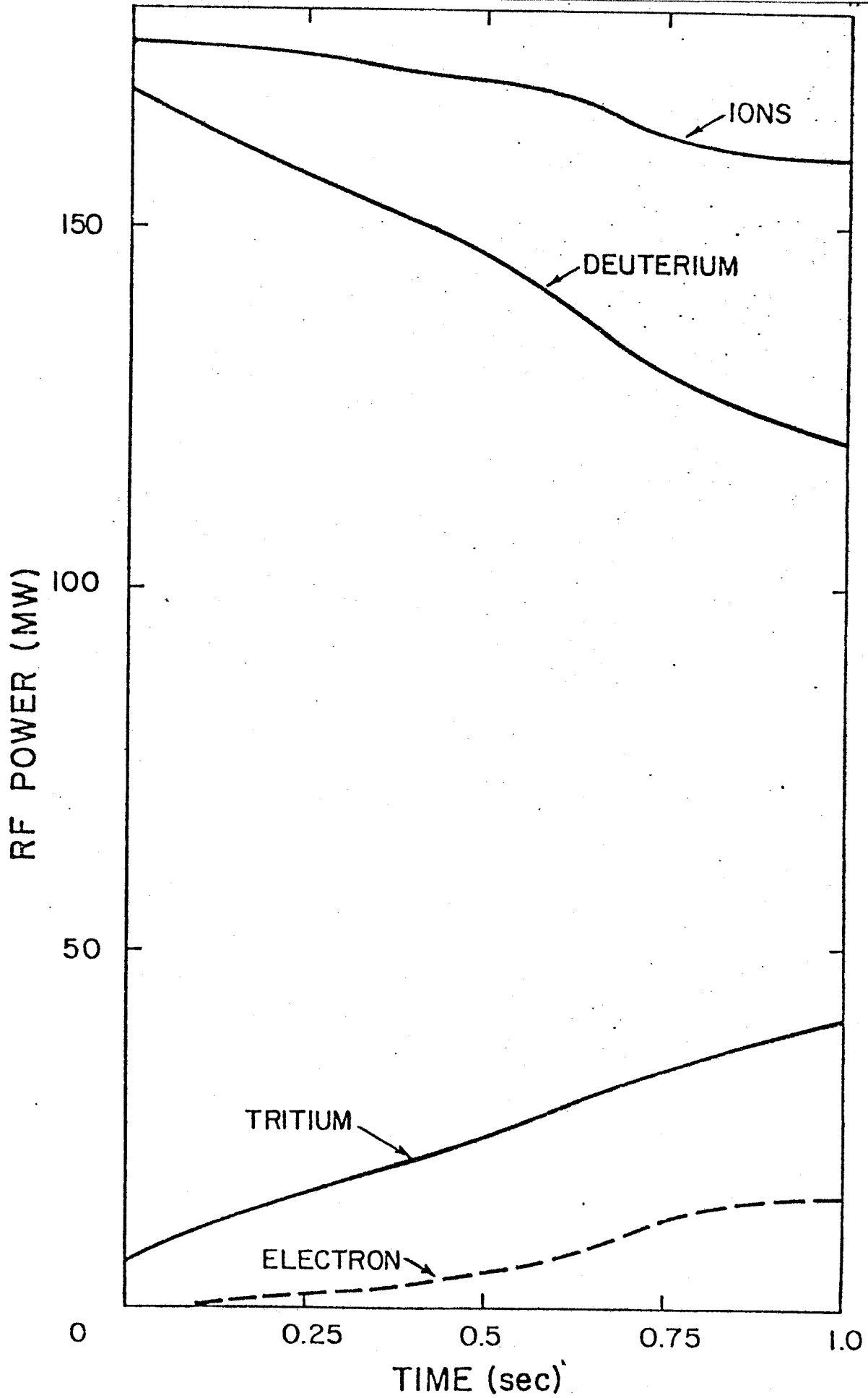

Fig. II-B-7 RF power absorbed by each species for a total input power of 175 MW.

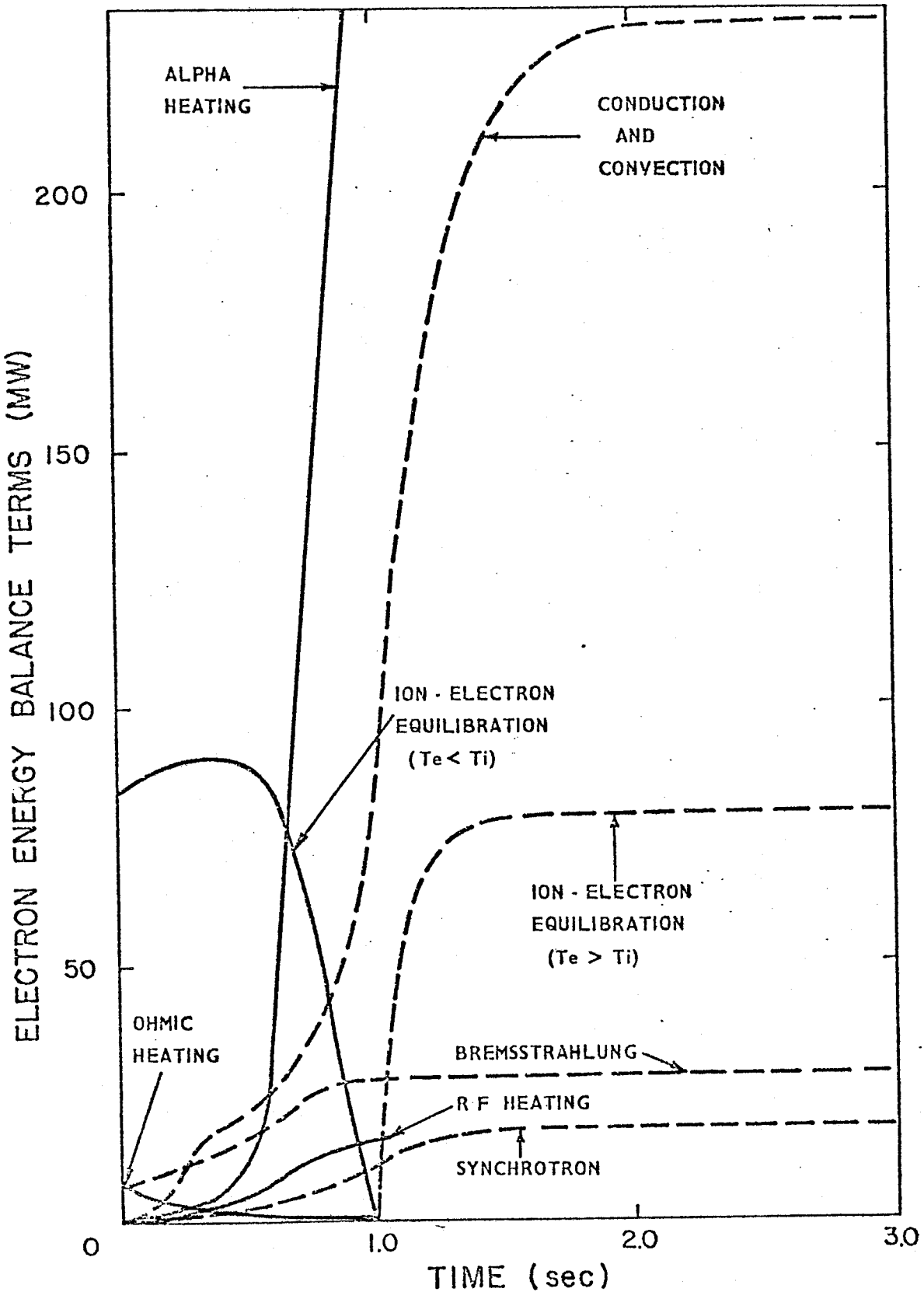

Fig. II-B-8 Electron energy balance terms for an RF power level of 175 MW for a 1 sec. pulse.

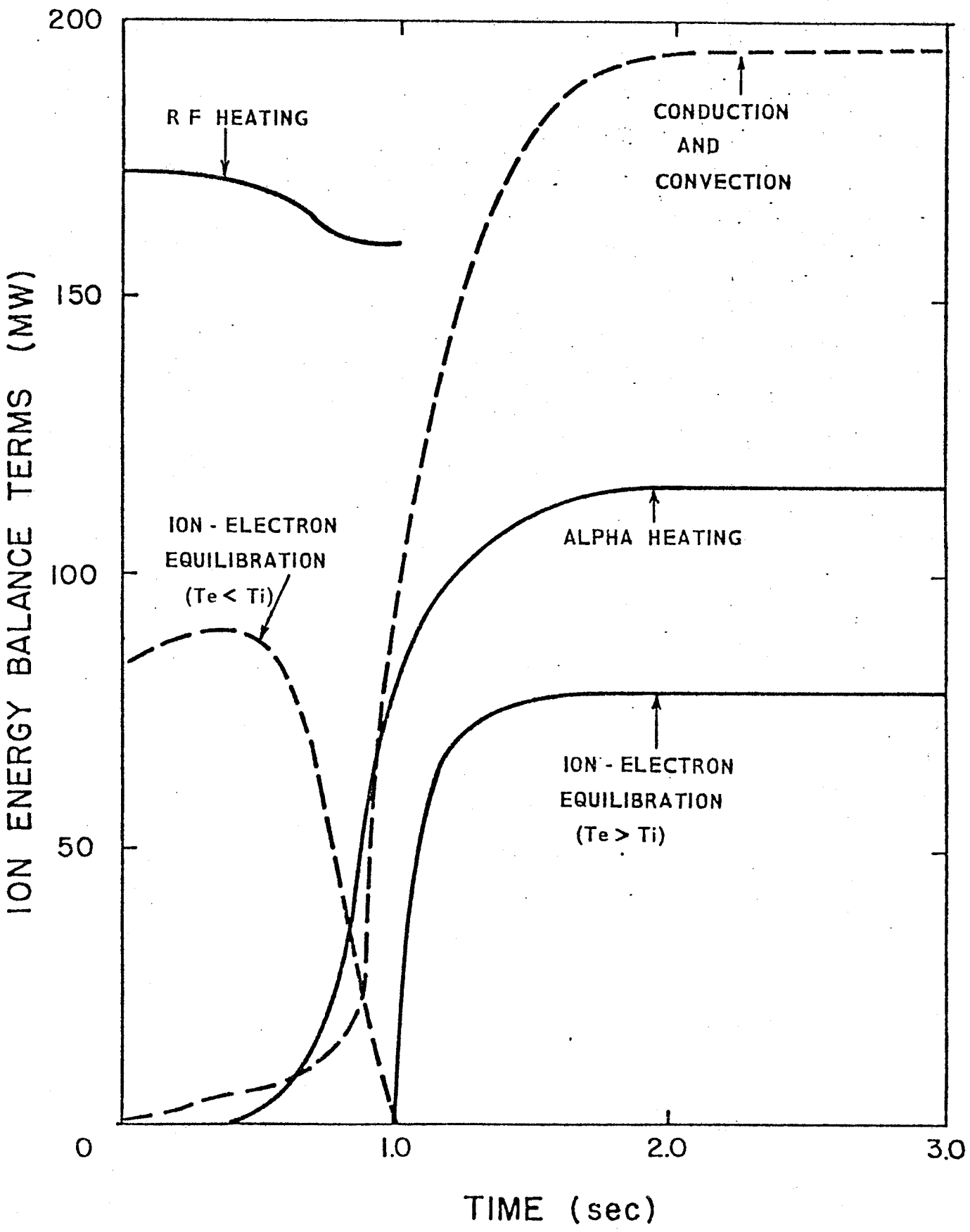

Fig. II-B-9 Ion energy balance terms for an RF power level of 175 MW for a 1 sec. pulse.

duction and convection, and since $T_e > T_i$ at equilibrium, the electrons lose 80 MW to the ions from the equilibration term. However, as shown in Fig. II-B-3, the electrons receive 360 MW from the thermalization the alphas. As for the ions at equilibrium, Fig. II-B-9 shows that the ions lose 195 MW through conduction and convection, but receives 80 MW from the electrons due to the equilibration term and also receives 115 MW from the thermalization of the alphas.

Finally,in order to increase the duty cycle of a reactor while at the same time use a lower level of RF power, it may be possible to heat during the Ohmic-heating current-rise phase of operation. Figure II-B-10 shows the amount of RF power to each species as well as the total amount. In this case, the RF power is ramped linearly up to 75 MW in 3 seconds and then kept at this power level for an additional .1 second after the current rise period. We see that the power to the ions reaches a peak value of 72 MW after 3 seconds and then decreases to a value of 68 MW. During this time the power to deuterium also peaks at 3 seconds with a value of 60 MW before it declines to the final value of 48 MW. Again we see a steady rise in power to tritium up to 20 MW as well as to the electrons, up to 7 MW. The drop in power to the deuterium while the rise in power to both tritium and electrons may be explained as before.

In Fig. II-B-11, we notice that during the Ohmic-heating current rise period, the plasma current is assumed to rise linearly in 3 seconds from 1 MA to its final value of 6.5 MA. During this period, by assuming that q, the safety factor, or consequently, the plasma current density remains constant, we obtain a plot of the increasing plasma minor

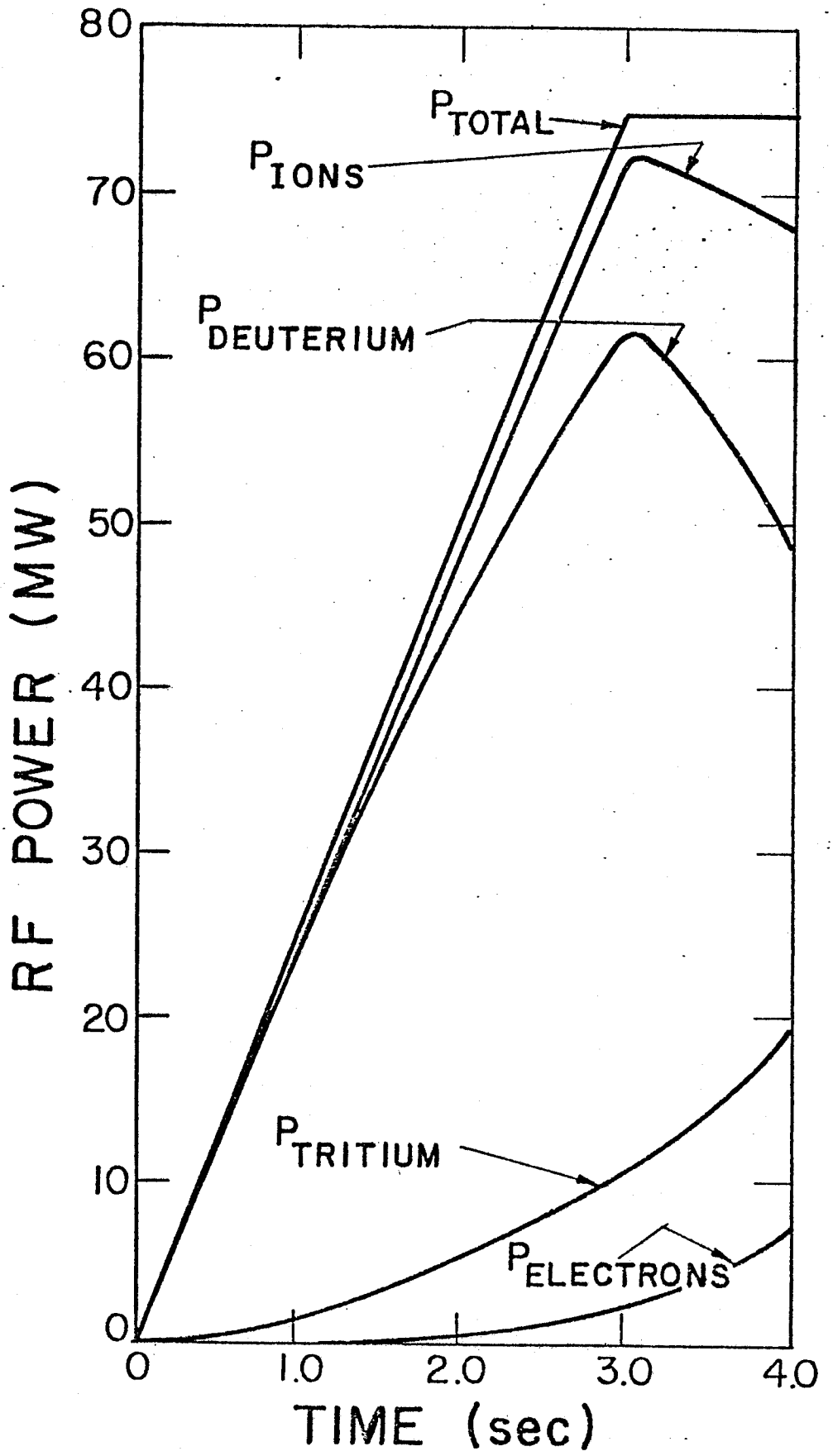

Fig. II-B-10 RF power absorption of each species for a pulse ramped linearly from 0 to 75 MW in 3 sec. and then constant 75 MW for 1 sec. During the first 3 secs, the plasma current rises linearly from 1 to 6.5 MA.

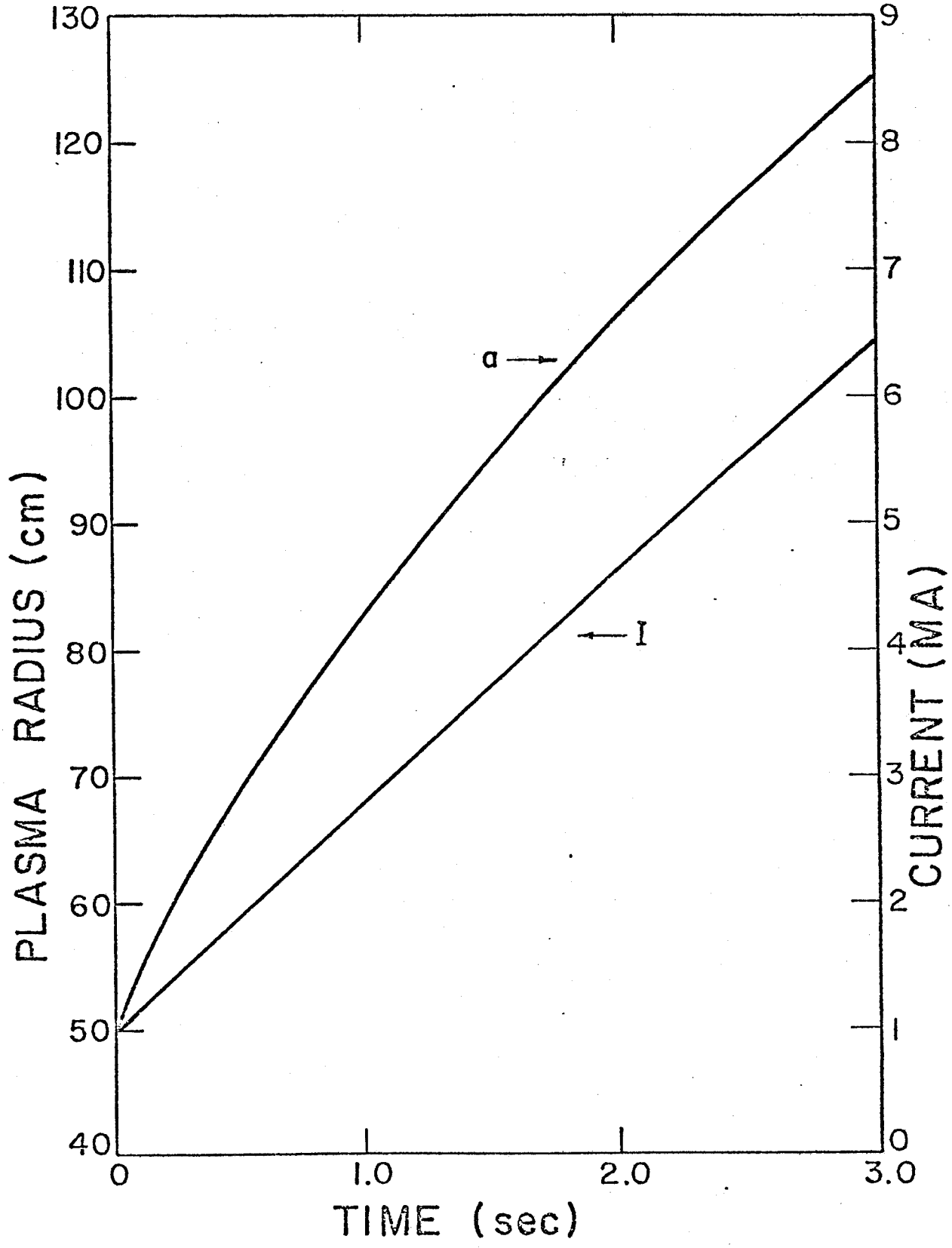

Fig. II-B-11 Evolution of plasma current and minor radius during the plasma current rise for a 3 sec. operation.

radius also displayed in Fig. II-B-11. At 1 MA we have a corresponding plasma minor radius of 50 cm while at the full current of 6.5 MA the corresponding final minor radius is 1.25 m.

In Fig. II-B-12, by looking at the plot of the ion and electron temperatures, we see that equilibrium is achieved after a total time of 4.4 seconds or 1.4 seconds after the Ohmic-heating current-rise period. This time is approximately 1.5 seconds sooner than that obtained in Fig. II-B-1. While this time is essentially identical to that obtained in Fig. II-B-3, lower power levels were used.

Figures II-B-13 to II-B-14 refer to the RF heating scheme derived for NUWMAK[15] when parameters are given in Table 1. Figure II-B-13 shows how the ion and electron temperatures as well as the amount of alpha power deposited in the electrons varies with time. From 0.0 to 4.0 seconds the plasma is ohmically heated while from 4.0 to 6.0 seconds 75 MW of RF power is assumed to be deposited in the plasma. As seen in Fig. II-B-13, the plasma reaches the equilibrium ion temperature of 13.2 keV and 15.4 keV for the electrons 500 to 1000 ms after the RF is shut off. As seen in Figs. II-B-13 and II-B-16, the alpha power to the electrons rises sharply 1500 ms after the RF is turned on reaching an equilibrium value of 310 MW.

Figure II-B-14 shows the plasma minor radius and current changes during the current rise-RF heating phase of operation. The plasma current rises linearly from 1.0 MA to 5.2 MA in 5.5 sec while the plasma minor radius increases from 38 cm to 112 cm in such a way as to keep the safety factor q at a value of 2.6 at the edge. When the RF is supplied the plasma radius is initially at a value of 92 cm which is 82% of its final value.

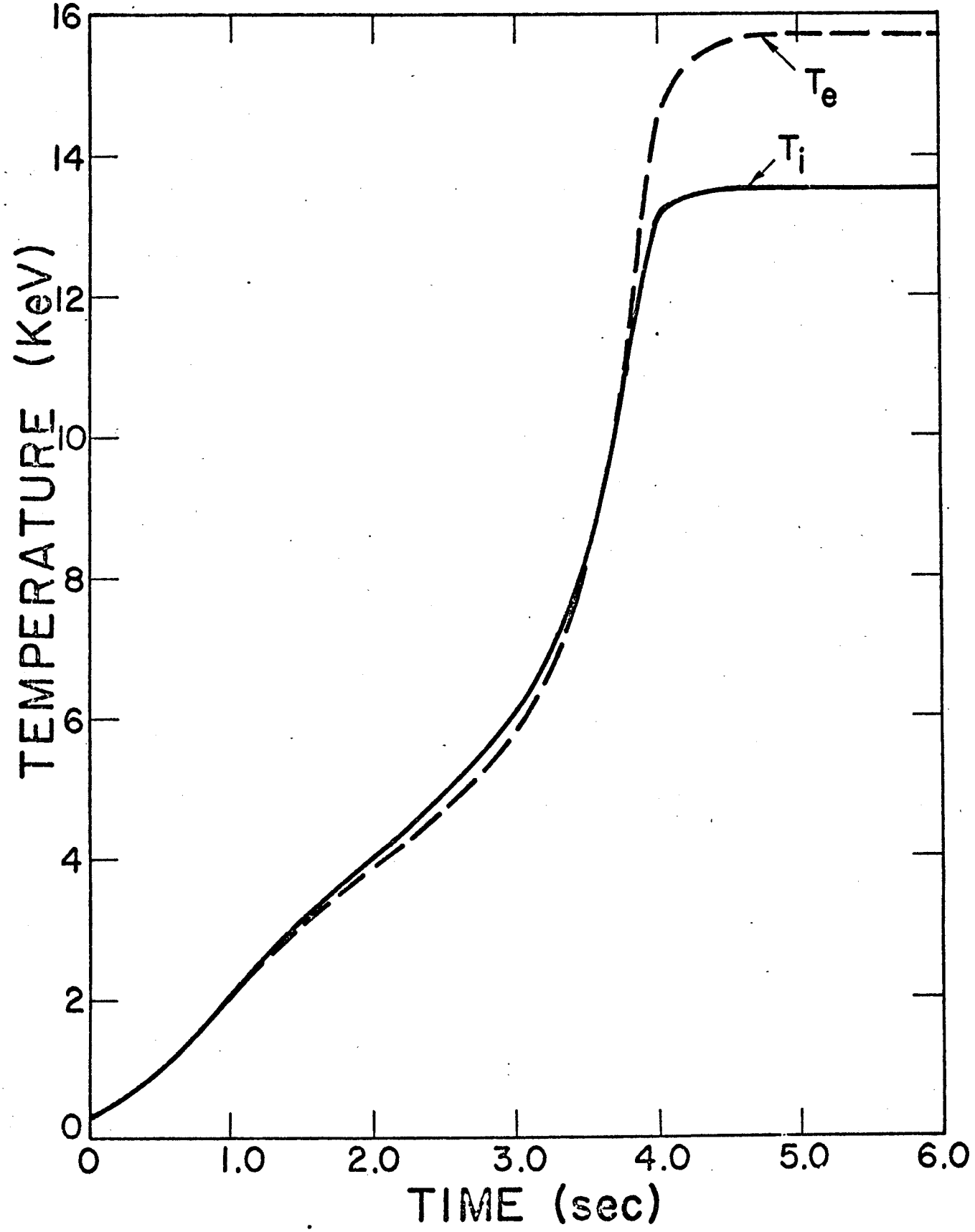

Fig. II-B-12 Magnetosonic wave heating to ignition for an RF pulse ramped from 0 to 75 MW during the 3 sec. plasma current rise and then constant 75 MW for an additional 1 sec.

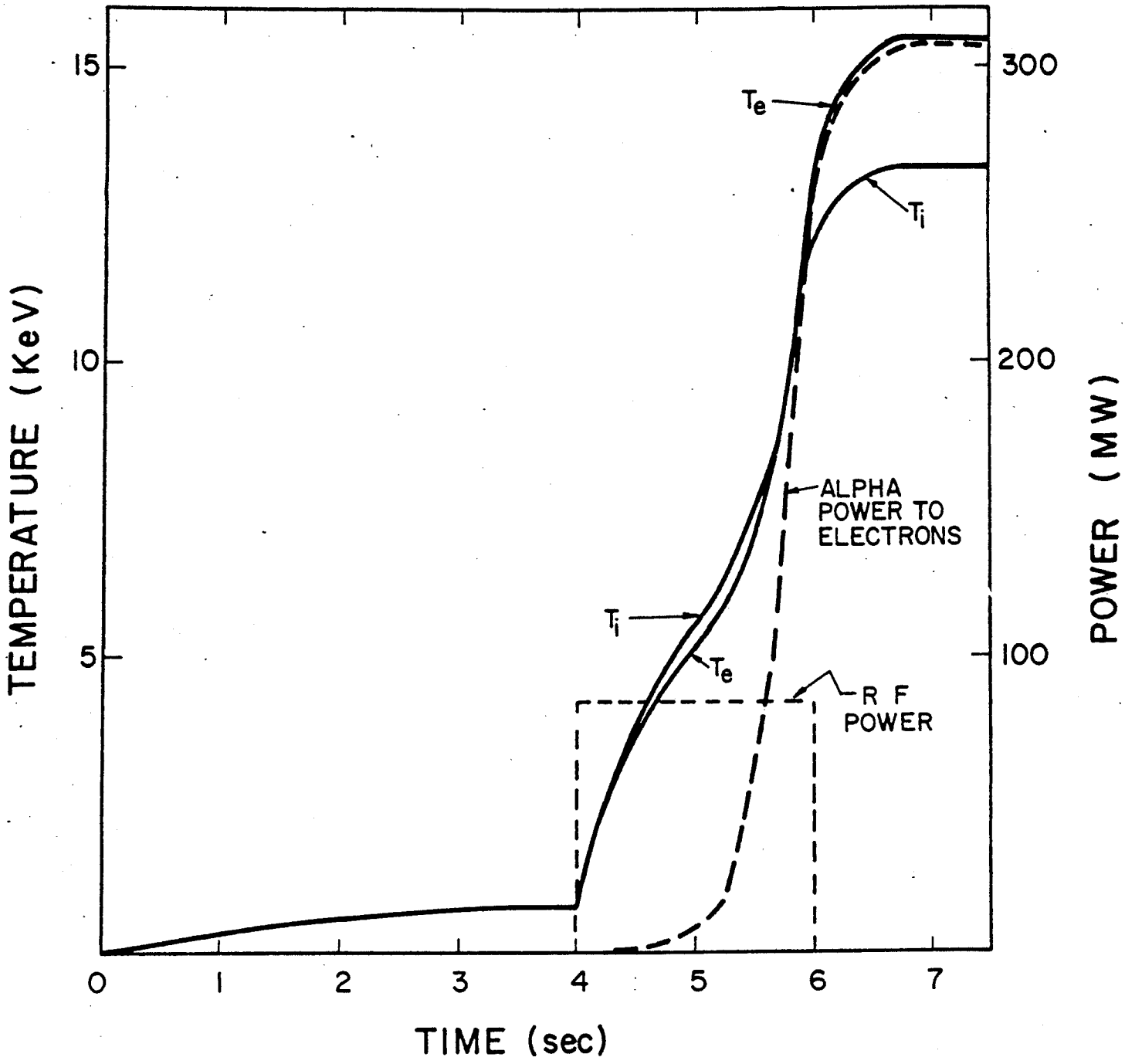

Fig. II-B-13 Startup scenario for NUWMAK. The plasma is ohmicly heated for 4.0sec and then heated with an RF pulse of 75 MW for 2.0 sec. Besides T_i and T_e, the amount of alpha power deposited in the electrons is shown.

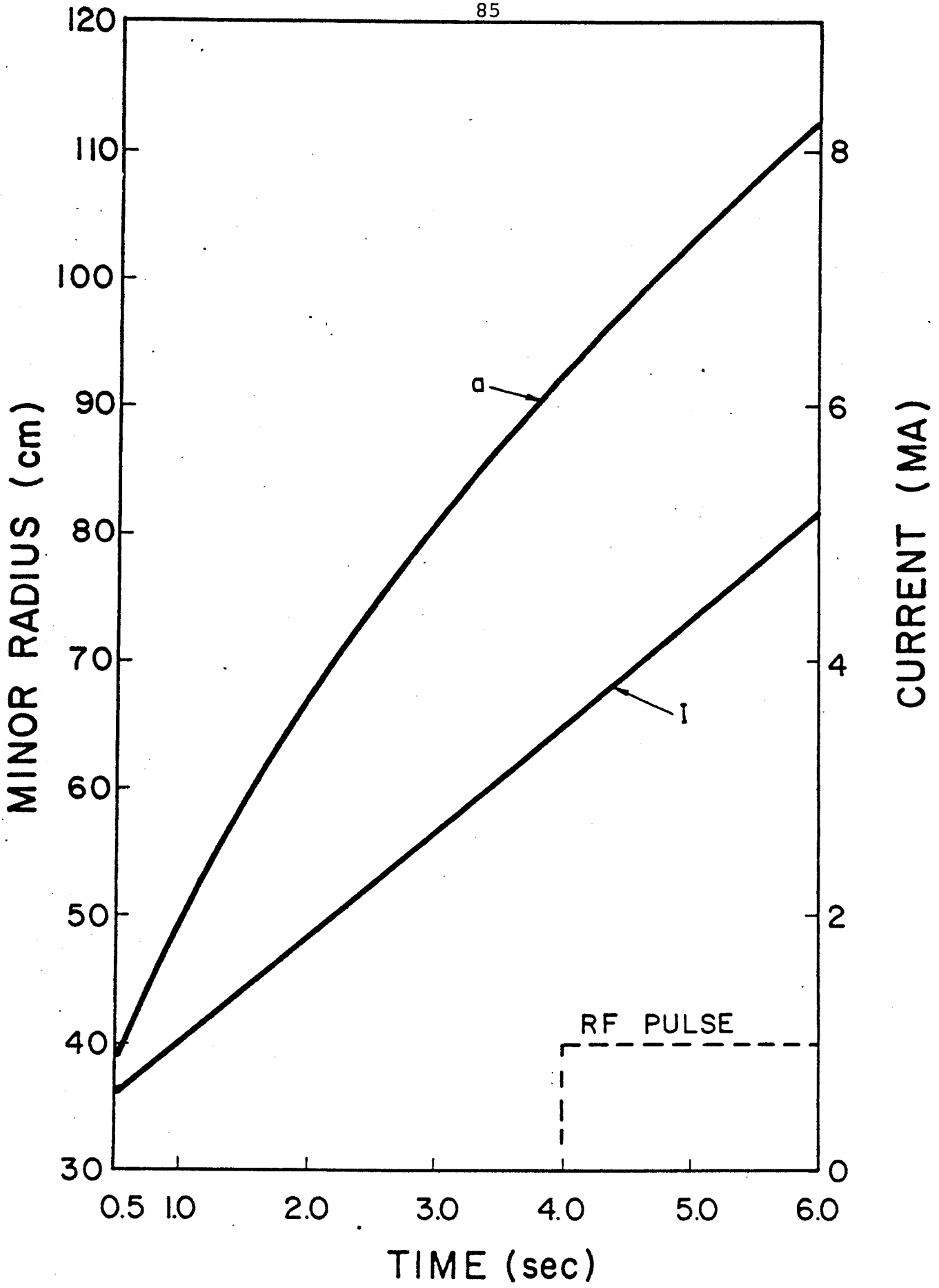

Fig. II-B-14 Evolution of the plasma current and minor radius during the startup phase for NUWMAK.

In Figure II-B-15, we see the amount of RF power deposited in each species. Most of the power supplied goes to the ions, decreasing slightly from 75 MW to 74 MW. As the plasma temperature increases the power flow to deuterium decreases from 73 MW to 56 MW while that to tritium increases from 1.6 MW to 18 MW. For the ions $\langle k_{\perp}^2 \rangle = 2.45\ cm^{-2}$ where $k_{\perp}^2$ is averaged over the resonant ion width while for the electrons $\langle k_{\perp}^2 \rangle = 1.5\ cm^{-2}$ and $k_{\perp}^2$ is averaged over the entire plasma cross section since electron heating occurs throughout the plasma. The electron heating term is again small because the exponential factor in Eq. 51 is larger, thus making PRFE small. The magnitude of the spatially averaged electric field $|E_+|$ drops steadily from a peak value of 980 V/m to 212 V/m.

Figures II-B-16 and II-B-17 show the terms in the electron and ion energy balance equations. Dashed lines indicate energy loss mechanisms while solid lines indicate heating terms. After 1700 ms, the alpha heating term becomes so large that even if mode conversion processes were present causing most of the power to be deposited in the electrons, our results would still be the same. As Fig. II-B-13 shows, $T_i \approx T_e$, the electron-ion equilibration time is quite short, indicating that heating of the electrons would drag the ion temperature along with it, thus not changing our results. In the case of the electrons, at equilibrium as shown in Fig. II-B-16, the electrons lose 15 MW from synchrotron radiation, 25 MW from Bremsstrahlung, 200 MW through conduction and convection, and since $T_e > T_i$ at equilibrium, the electrons lose 70 MW to the ions from the equilibrium term. However, as shown in Fig. II-B-13, the electrons

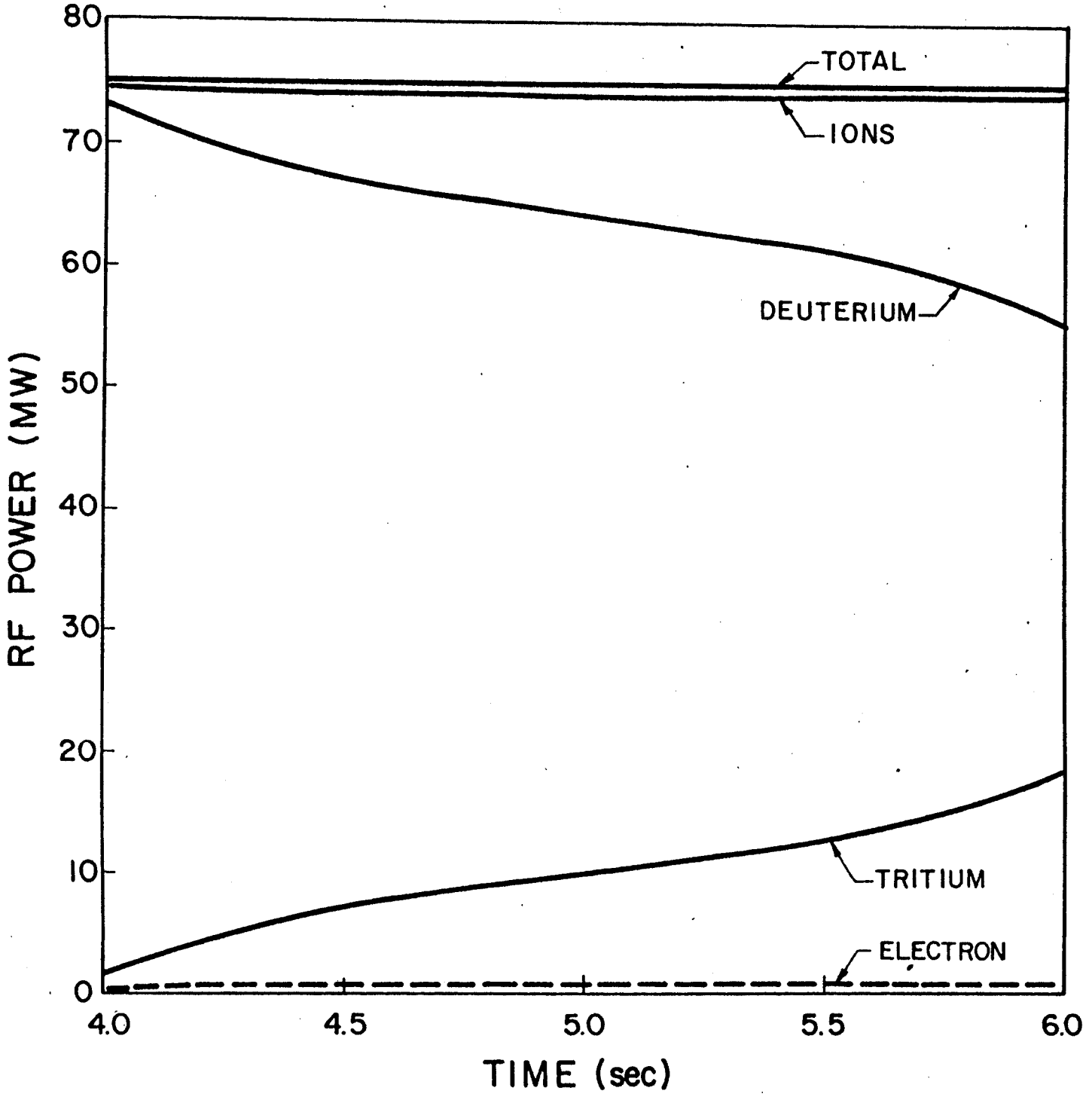

Fig. II-B-15 RF power absorbed by each species for an RF pulse of 75 MW for 2.0 sec.

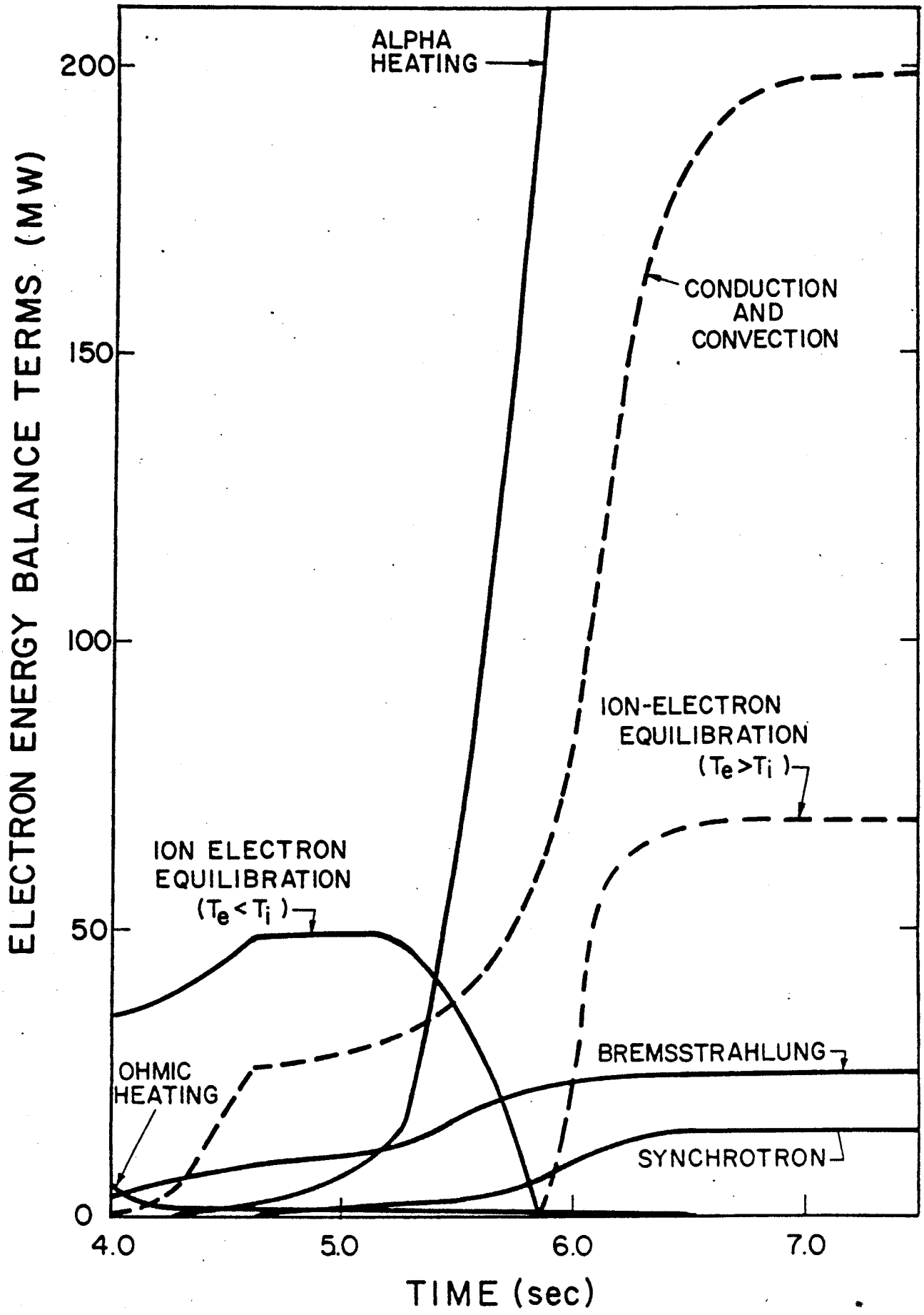

Fig. II-B-16 Electron energy balance terms for an RF pulse of 75 MW for 2.0 sec.

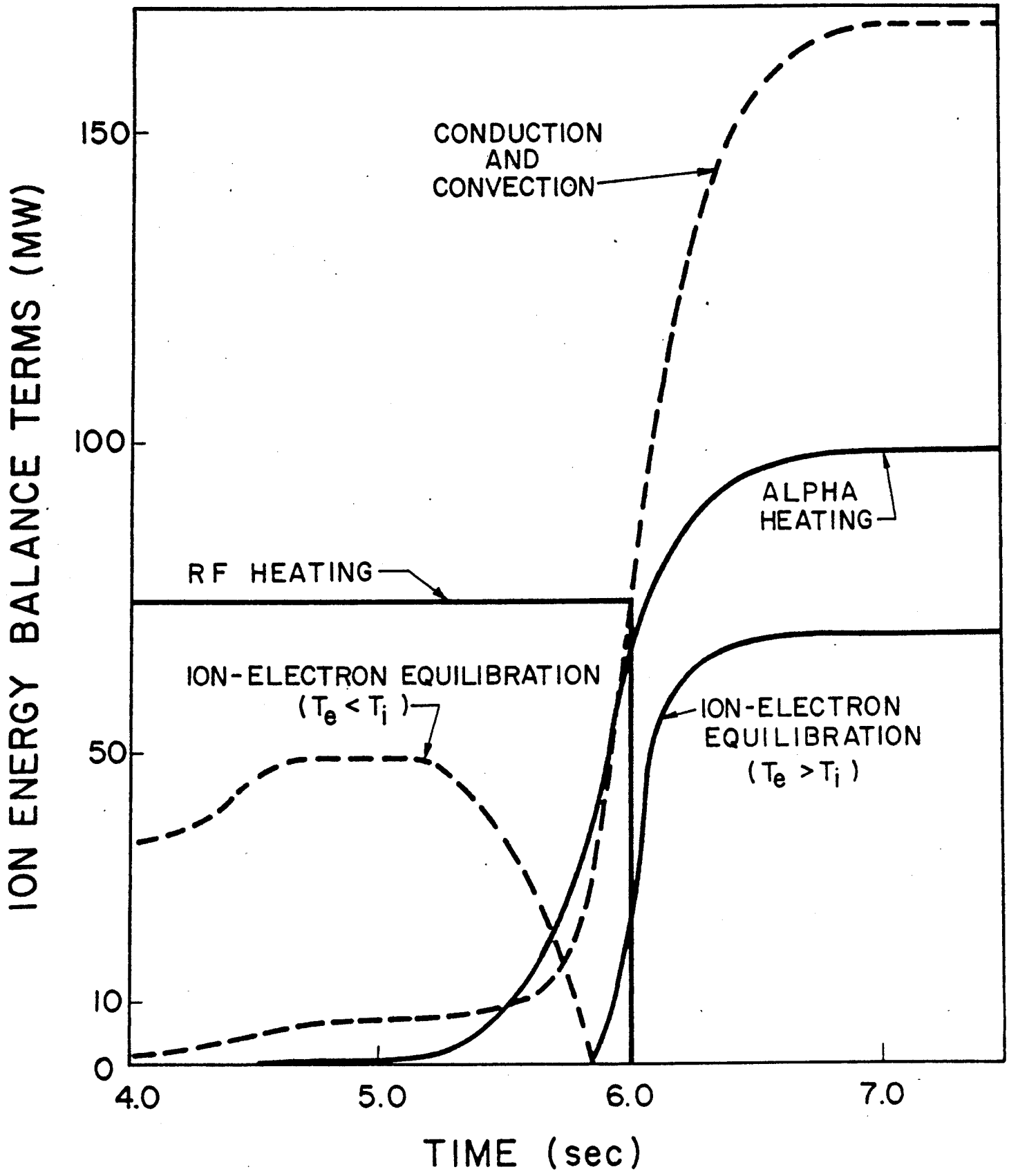

Fig. II-B-17 Ion energy balance terms for an RF pulse of 75 MW for 2.0 sec.

receive 310 MW from the thermalization of the alphas. As for the ions at equilibrium, Fig. II-B-17 shows that the ions lose 168 MW through conduction and convection, but receives 70 MW from the electrons due to the equilibration term and also receives 98 MW from the thermalization of the alphas.

Earlier NUWMAK studies showed that 75 MW of RF power was needed to heat the plasma ignition when the RF was supplied after the ohmic heating-current rise phase. By overlapping the RF heating phase with the current rise phase, we need only provide 75 MW for 2 seconds. Thus, less energy is needed to heat the plasma to ignition and the plasma reaches equilibrium 3 seconds sooner, thereby increasing the duty cycle.

References

1. W. Houlberg, Ph.D. Thesis, (1977) University of Wisconsin-Madison, Madison, Wisconsin.

2. S. I. Braginskii, Review of Plasma Physics, M. A. Leontovich, Ed., Plenum Publishing Co., New York, Vol. I, p. 205, (1965).

3. N. A. Krall and A. W. Trivelpiece, Principles of Plasma Physics McGraw-Hill Book Co., New York (1973).

4. F. L. Hinton and R. D. Hazeltine, "Theory of Plasma Transport in Toroidal Confinement Systems", Reviews of Modern Physics 48, 239 (1976).

5. R. W. Conn, "Plasma Equations and Energy Equilibria and Stability", Nuclear Engineering Department Report UWFDM-16, p. 4, (University of Wisconsin-Madison, July 1972).

6. Lyman Spitzer, Jr., Physics of Fully Ionized Gases, Interscience Publishers, New York (1962).

7. D. J. Rose and M. Clark, Jr., Plasmas and Controlled Fusion, MIT Press, p. 233, Cambridge (1961).

8. T. F. Yang, H. K. Forsen and G. A. Emmert, "The Calculation and Parametric Study of the Synchrotron Radiation Loss for Tokamak Reactors", Nuclear Engineering Department Report UWFDM-49 (University of Wisconsin-Madison, 1973).

9. J. E. Scharer, R. W. Conn and D. T. Blackfield, "Study of Fast Magnetosonic and Neutral Beam Heating of Large Tokamaks", EPRI Report ER-268 Project 237-3 Topical Report, Sept. 1976.

10. B. Badger, et al. "UWMAK-III, A Noncircular Tokamak Power Reactor Design", Nuclear Engineering Department Report UWFDM-150 (Univ. of Wisconsin-Madison, July 1976).

11. "Status and Objectives of Tokamak Systems for Fusion Research" U.S. Atomic Energy Commission Report WASH-1239 UC-20.

12. J. E. Scharer, J. Beyer and D. T. Blackfield, Proceedings of the Third Topical Conference on Radio Frequency Plasma Heating, paper D7-1 (1978).

13. J. E. Scharer and D. T. Blackfield, Bulletin of the American Physical Society, 21, 1158 (1976).

14. D. T. Blackfield and J. E. Scharer, Bulletin of the American Physical Society, 22, 1185 (1977).

15. B. Badger, et al., Nuclear Engineering Department Report UWFDM-330 (Univ. of Wisconsin-Madison, 1979).

III FOKKER-PLANCK THEORY AND RF HEATING

As shown earlier (Sec.I-B), second and third harmonic heating are inherently non-Maxwellian processes in the absence of a substantial number of ion-ion collisions. Ions with large $v_\perp$ are preferentially heated, resulting in the formation of a high energy tail which has been observed in several experiments (see Sec.I-E).

A Fokker-Planck calculation has two important functions. First, the point and space-time codes use the fluid equations and are, therefore, only valid for Maxwellian plasmas. A Fokker-Planck calculation can check the validity of this assumption. Secondly, it has been suggested that when a high energy ion tail is formed, more fusions will result. The amount of supplementary power needed by a plasma to reach ignition can therefore be reduced. Fokker-Planck calculations can give a better estimate on the amount of RF power needed if tails are produced than a fluid code.

In Sec.III-A the Fokker-Planck equation in the form used by the two spherical velocity dimensions (v,θ), [illegible] HYBRID II[3] is derived. In Sec.III-B, the quasi-linear RF diffusion operator[15,16] is calculated while in Sec.III-C, various RF startup scenarios using the RF code HYBRID III[21] are presented for NUWMAK.

III-A FOKKER-PLANCK THEORY

The Boltzman transport equation[1,2], which describes the statistical transport of particles in a plasma, is used to obtain the Fokker-Planck equation. This equation is

$$\frac{\partial f_\alpha}{\partial t} + \vec{v}\cdot\frac{\partial f_\alpha}{\partial \vec{r}} + \frac{\vec{F}}{m_\alpha}\cdot\frac{\partial f_\alpha}{\partial \vec{v}} = \left.\frac{\partial f_\alpha}{\partial t}\right)_c + S_\alpha \qquad (1)$$

where $f_\alpha(\vec{r},\vec{v},t)$ is the distribution function for species "α" in the six dimensional phase space $(\vec{r},\vec{v})$ and $\left.\frac{\partial f_\alpha}{\partial t}\right)_c$ is the Fokker-Planck collision operator[1,3-6,8-11] in spherical coordinates (see Appendix B), $S_\alpha(\vec{r},\vec{v},t)$ is a particle source term and $\vec{F}$ is the force acting on species "α".

Since HYBRID III is a spatially independent code,

$$\frac{\partial f_\alpha}{\partial \vec{r}} \equiv 0 \quad . \qquad (2)$$

The forces which act on species "α" are assumed to arise only from an external magnetic field about which f_α posses azimuthal symmetry. Therefore,

$$\frac{\vec{F}}{m_\alpha}\cdot\frac{\partial f_\alpha}{\partial \vec{v}} \equiv 0 \quad , \qquad (3)$$

and eq.(1) becomes

$$\frac{\partial f_\alpha}{\partial t} = \left.\frac{\partial f_\alpha}{\partial t}\right)_c + S_\alpha \quad . \qquad (4)$$

To eq.(4) may be added C_α: a charge-exchange term; T_α: a toroidal effect term representing finite particle and

energy confinement times; A_α an alpha particle heating term[6,11-14]. Eq. (4) then has the following form

$$\frac{\partial f_\alpha}{\partial t} = \left.\frac{\partial f_\alpha}{\partial t}\right)_c + S_\alpha + C_\alpha + T_\alpha + A_\alpha \ . \qquad (5)$$

To incorporate the RF heating term, the above equation is first written for each species, dropping the "α" subscript

$$\frac{\partial f}{\partial t} = n_o \Gamma \frac{1}{v^2}\frac{\partial}{\partial v}(\bar{A}f+\bar{B}\tilde{v}\frac{\partial f}{\partial \tilde{v}}+\bar{C}\frac{\partial f}{\partial \theta}) + \frac{1}{\tilde{v}v^2\sin^2\theta}\frac{\partial}{\partial \theta}(\bar{D}f+\bar{E}\tilde{v}\frac{\partial f}{\partial v}+\bar{F}\frac{\partial f}{\partial \theta}) + S - \frac{f}{\tau_p} \qquad (6)$$

where $\Gamma = 4\pi Z^4 e^4/m^2$, n_o is a normalizing density, $\tilde{v}$ is the normalizing velocity and the terms $\bar{A},\bar{B},..\bar{F}$ contain integrals of the distribution function and of the independent variables.

In a tokamak, losses occur due to cross field transport. Since the Fokker-Planck code assumes no spatial dependence, these losses, T_α, are modeled by specifying particle (τ_p) and energy (τ_E) confinement times. The convective losses are then given by the term $-f/\tau_p$ and the conductive losses by a term $\frac{\partial}{v^2\partial v}(\frac{v^3 f}{\tau_E})$ which is added to eq.(6). To obtain an expression for the RF heating term, D^α_{RF}, quasi-linear theory as developed by Kennel and Engelmann[15], and Stix[16] must be reviewed.

III-B QUASI-LINEAR THEORY

Quasi-linear theory describes the evolution of a distribution function under the action of a spectrum of uncorrelated waves, an inherently stochastic heating process. Stix[16] has argued that this formalism is applicable to the study of ICRF heating when the plasma is sufficiently collisional that the collisions destroy wave-particle coherence between successive transits of the particle through the resonant heating zone, shown in fig.(III-B-1). Reactor plasmas should be sufficiently collisional.

In deriving the RF heating terms, the following assumptions are made:

1) a nonrelativistic, collisionless, infinite spatially uniform plasma exists in the absence of wave excitation
2) the plasma is in a constant valued static B field oriented along the z axis with no curvature
3) no static electric field exists
4) direct nonlinear coupling between waves can be neglected
5) the spatially averaged distribution function changes slowly compared to a gyroperiod and the characteristic times of the wave motion
6) the constant B field is strong enough that the particles' gyration frequencies are larger than the frequencies and growth rates of the waves

The last assumption implies that there is no strong dependence of the spatially averaged distribution function on the azimuthal velocity about the constant magnetic field, i.e.

$$\frac{\partial f}{\partial \phi} = 0 \ . \qquad (7)$$

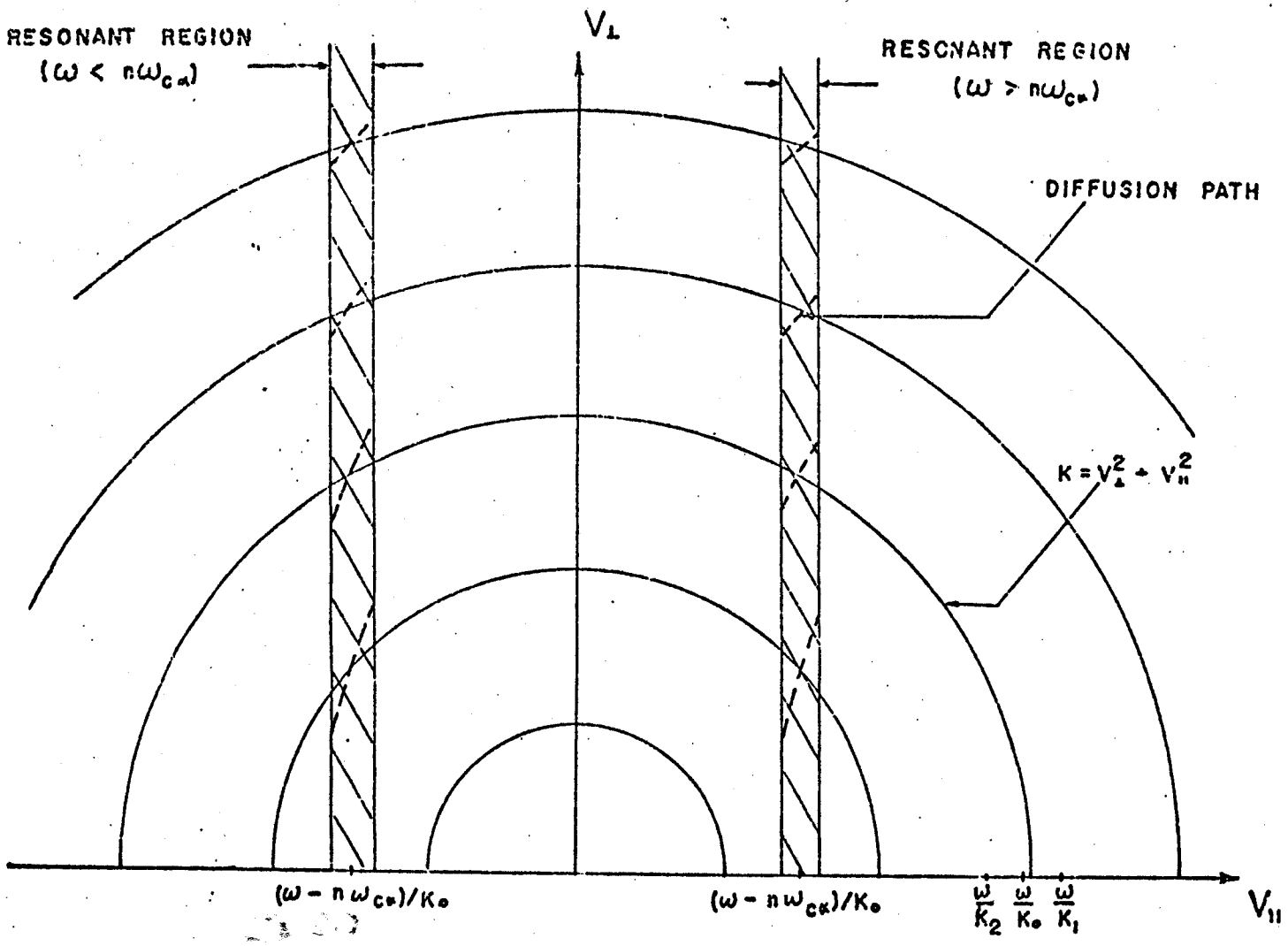

Fig. III-B-1 Quasi-linear velocity diffusion paths for a finite $k_{\parallel}$ spectrum at the nth harmonic cyclotron resonance, assuming $k_1 > k_o > k_2 > 0$. (reproduced from Ref.22)

This assumption also will allow the spectrum of excited modes to be approximately axially symmetric and allows for strongly anisotropic spectra providing that the time variation of the averaged particle distribution is small during one particle gyration.

Quasi-linear theory starts with the Vlasov equation[2]. Let $f^+(\vec{r},\vec{v},t)$ be the distribution function for singly charged ions, either deuterium and tritium, and let $f^-(\vec{r},\vec{v},t)$ be the corresponding function for electrons. The Vlasov equation is

$$\frac{\partial f^{\pm}}{\partial t} + \vec{v}\cdot\vec{\nabla} f^{\pm} \pm \frac{e}{m_{\pm}c}(c\vec{E} + \vec{v}\times\vec{B})\cdot\frac{\partial f^{\pm}}{\partial \vec{v}} = 0 \quad . \tag{8}$$

Assume now that $f^{\pm}$, $\vec{E}$ and $\vec{B}$ can be expressed as the sum of a spatially independent part and a small, rapidly fluctuating part due to the waves. Let $\delta f^{\pm}$ be the fluctuation part of the distribution function so that

$$\int d^3r \ \delta f^{\pm} = 0 \quad . \tag{9}$$

Then

$$f^{\pm}(\vec{r},\vec{v},t) = g^{\pm}(\vec{v},t) + \int \frac{d^3k}{(2\pi)^3} \delta f^{\pm}(\vec{v},t) e^{i\vec{k}\cdot\vec{x}} \tag{10}$$

with

$$g^{\pm} \equiv \lim_{V\to\infty} \frac{1}{V} \int d^3r \ f^{\pm}(\vec{r},\vec{v},t) \tag{11}$$

where V is the volume of integration after Fourier analyzing $f^{\pm}$ in space. The magnetic and electric fields may be written as

$$\begin{aligned} \vec{B}(\vec{r},t) &= B_o\hat{z} + \int \frac{d^3k}{(2\pi)^3} \vec{B}_k(t) e^{i\vec{k}\cdot\vec{x}} \\ \vec{E}(\vec{r},t) &= \int \frac{d^3k}{(2\pi)^3} \vec{E}_k(t) e^{i\vec{k}\cdot\vec{x}} \end{aligned} \tag{12}$$

To transform from Cartesian to cylindrical geometry

$$v_x = v_\perp \cos\phi \qquad v_y = v_\perp \sin\phi \qquad v_z = v_\parallel \tag{13}$$

$$k_x = k_\perp \cos\psi \qquad k_y = k_\perp \sin\psi \qquad k_z = k_\parallel \tag{14}$$

Defining

$$\varepsilon_k^L = \frac{(E_x+iE_y)_k}{2^{1/2}} \qquad \varepsilon_k^R = \frac{(E_x-iE_y)_k}{2^{1/2}} \qquad \varepsilon_k'' = (E_z)_k \tag{15}$$

$$\beta_k^L = \frac{(B_x+iB_y)_k}{2^{1/2}} \qquad \beta_k^R = \frac{(B_x-iB_y)_k}{2^{1/2}} \qquad \beta_k'' = (B_z)_k \tag{16}$$

where (R,L) stand for the right and left handed rotations of the electric and magnetic fields about B_o in the z direction. Eq.(8) can be written as

$$\hat{L}_k^{\pm}\delta f_k^{\pm} = \hat{P}_k^{\pm} g^{\pm} + \frac{1}{2}\int \frac{d^3k'}{(2\pi)^3}(\hat{P}_{k-k'}\delta f_{k'}^{\pm} + \hat{P}_{k'}^{\pm}\delta f_{k-k'}^{\pm}) \tag{17}$$

where

$$\hat{L}_k^{\pm} = \frac{\partial}{\partial t} + i(k_\parallel v_\parallel + k_\perp v_\perp \cos(\phi-\psi) - \Omega_\pm \frac{\partial}{\partial\phi}),$$

$$\hat{P}_k^{\pm} = \mp\frac{e}{m_\pm c}(c\vec{E}_k + \vec{v}\times\vec{B}_k)\cdot\frac{\partial}{\partial\vec{v}}$$

and

$$\left[E_x\right] = \begin{bmatrix} \varepsilon_k^L e^{-i\psi} \\ \varepsilon_k^R e^{+i\psi} \\ \varepsilon_k'' \end{bmatrix} \qquad \left[B_k\right] = \begin{bmatrix} \beta_k^L e^{-i\psi} \\ \beta_k^R e^{+i\psi} \\ \beta_k'' \end{bmatrix} \qquad \Omega_\pm = qB_o/m_\pm c$$

where due to the axial symmetry of the wave properties, ε_k^L, ε_k^R, β_k^L and β_k^R are rotated by the angle ψ.

The second term in eq.(17) represents nonlinear mode-mode coupling and can be neglected. Eq.(17) becomes

$$\hat{L}_k^{\pm}\delta f_k^{\pm} = P_k^{\pm} g^{\pm} \quad . \tag{18}$$

Assuming that $g^{\pm}$ is a constant in time and replacing $\frac{\partial}{\partial t}$ by $-i\nu_k$ where ν_k is the complex wave frequency

$$\nu_k = \omega_k + i\gamma_k \tag{19}$$

to lowest order

$$\hat{L}^{\pm}_{k,\nu,t} = -i\left\{\lambda_k - k_\perp v_\perp \cos(\phi-\psi) - \Omega_\pm \frac{\partial}{\partial\phi}\right\}$$

$$= \Omega_\pm \exp\left[-\frac{\lambda_k\phi - k_\perp v_\perp \sin(\phi-\psi)}{\Omega_\pm}\right]\frac{\partial}{\partial\phi}\cdot\left\{\exp\left[\frac{i\lambda_k\phi - k_\perp v_\perp \sin(\phi-\psi)}{\Omega_\pm}\right]\right\} \tag{20}$$

with $\lambda_k = \nu_k - k_\parallel v_\parallel$.

On inverting eq.(20)

$$\hat{\delta}^{\pm} = (\hat{L}^{\pm}_{k,k'})^{-1}\hat{P}^{\pm}_k g^{\pm} \ , \tag{21}$$

where, to lowest order

$$(\hat{L}^{\pm}_{k,k'})^{-1} = \sum_{n,m}\frac{J_n J_m}{\Omega_\pm}\exp(i(n-m)\psi - i\frac{(\lambda_k - m\Omega_\pm)\phi}{\Omega_\pm}\cdot\int d\phi'\left[\exp(i\frac{(\lambda_k - m\Omega_\pm)\phi'}{\Omega_\pm})\right] \tag{22}$$

where $J_n = J_n(\frac{k_\perp v_\perp}{\Omega_\pm})$.

Using Faraday's law

$$\vec{\nabla}\times E_k = -\frac{1}{c}\frac{\partial B_k}{\partial t} \ , \tag{23}$$

and considering only the fast time scale where $\frac{\partial}{\partial t} \to -i\nu_k$,

$$\hat{P}^{\pm}_k = \mp\frac{e}{M_\pm}e^{i(\phi-\psi)}\left\{\frac{\varepsilon^R_k e^{i\psi}}{\sqrt{2}}(\hat{G}_k + \frac{i\lambda_k}{\nu_k v_\perp}\frac{\partial}{\partial\phi}) + \frac{k_\perp\varepsilon''_k}{2\nu_k}(\hat{H} - \frac{iv_\parallel}{v_\perp}\frac{\partial}{\partial\phi})\right\}$$

$$\mp\frac{e}{M_\pm}e^{-i(\phi-\psi)}\left\{\frac{\varepsilon^L_k e^{-i\psi}}{\sqrt{2}}(\hat{G}_k - \frac{i\lambda_k}{\nu_k v_\perp}\frac{\partial}{\partial\phi}) + \frac{k_\perp\varepsilon''_k}{2\nu_k}(H - \frac{iv_\parallel}{v_\perp}\frac{\partial}{\partial\phi})\right\} \tag{24}$$

$$\mp\frac{e}{M_\pm}\left\{\frac{ik_\perp}{\nu_k}\left(\frac{\varepsilon^L_k e^{-i\psi} - \varepsilon^R_k e^{i\psi}}{\sqrt{2}}\right)\frac{\partial}{\partial\phi} + \varepsilon''_k\frac{\partial}{\partial v_\parallel}\right\}$$

where $$\hat{G}_k \equiv \frac{\partial}{\partial v_\perp} - \frac{k_\parallel}{\nu_k}\hat{H} \tag{25}$$

and $$\hat{H} \equiv v_\parallel \frac{\partial}{\partial v_\perp} - v_\perp \frac{\partial}{\partial v_\parallel} \quad . \tag{26}$$

The spatially averaged Vlasov equation using Fourier transforms is then

$$\frac{\partial g^\pm}{\partial t} - \Omega_\pm \frac{\partial g^\pm}{\partial \phi} = \lim_{V\to\infty} \frac{1}{2V} \int \frac{d^3k}{(2\pi)^3} \left[\hat{P}^\pm_{-k}(\hat{L}^\pm_{k,\nu_k})^{-1}\hat{P}^\pm_k + \hat{P}^\pm_k(\hat{L}^\pm_{-k,\nu_k})^{-1}\hat{P}^\pm_{-k}\right] g^\pm$$

$$= \frac{1}{2}\int \frac{d^3k}{(2\pi)^3}(\hat{D}^\pm_k + \hat{D}^\pm_{-k})g^\pm \quad . \tag{27}$$

The space-averaged distribution functions $g^\pm$ have been assumed be effectively constant over times on the order of gyroperiods and the characteristic wave periods. Expanding $g^\pm$ in powers of $1/\Omega_\pm$, i.e.

$$g^\pm = g^\pm_o + \frac{g^\pm_1}{\Omega_\pm} + O(1/\Omega^2_\pm) + \ldots , \tag{28}$$

to lowest order, using eq.(7)

$$\frac{\partial g^\pm_o}{\partial \phi} = 0 \quad . \tag{29}$$

Eq.(29) shows that to lowest order, the spatially averaged distribution function is independent of the Larmour phase ϕ. To expand $g^\pm$ using eq.(28), the mean diffusion time for the particles must be long compared to the particles' gyroperiod. To first order

$$\frac{1}{\Omega_\pm}\frac{\partial g^\pm_o}{\partial t} + \frac{\partial g^\pm_1}{\partial \phi} = \frac{1}{2\Omega_\pm}\int \frac{d^3k}{(2\pi)^3}(\hat{D}^\pm_k + \hat{D}^\pm_{-k})g^\pm_o \quad . \tag{30}$$

Since $\int_0^{2\pi} \frac{\partial g_1}{\partial \phi}\, d\phi = 0$,

$$\frac{\partial g^{\pm}}{\partial t} = \frac{1}{4\pi} \int_0^{2\pi} d\phi \int \frac{d^3k}{(2\pi)^3} (\hat{D}^{\pm}_{+k} + \hat{D}^{\pm}_{-k}) g^{\pm} \quad , \tag{31}$$

where the zero subsript has been dropped. Since

$$\int_0^{2\pi} e^{i(n-m)\phi} d\phi = 2\pi\delta(n-m) \quad , \tag{32}$$

$$\frac{\partial g^{\pm}}{\partial t} = \lim_{V\to\infty} \sum \frac{e^2}{nM_{\pm}^2} \int \frac{d^3k}{V(2\pi)^3} \Big| \{ (\hat{G}_k + \frac{\lambda_k}{\nu_n v_{\perp}})^* (\varepsilon^{\pm}_{n,k})^* +$$

$$\hat{K}^{\pm}_{n,k} J_n (\varepsilon^{"}_k)^* \} \frac{(\varepsilon^{\pm}_{n,k} \hat{G}_k + \varepsilon^{"}_k J_n \hat{K}^{\pm}_{n,k}) g^{\pm}}{(\nu_k - k_{"} v_{"} - n\Omega_{\pm})} \Big| \tag{33}$$

where $\varepsilon^{\pm}_{n,k} \equiv \frac{\varepsilon^{R}_k e^{i\psi} J_{n+1} + \varepsilon^{R}_k e^{-i\psi} J_{n-1}}{\sqrt{2}}$ (34)

and $\hat{K}_{n,k} \equiv \frac{v_{"}}{v_{\perp}} \hat{G}_k - \frac{(\lambda_k - n\Omega_{\pm})}{\nu_k v_{\perp}} \hat{H}$. (35)

In the limit of $\gamma_k \to 0$

$$\frac{\partial g^{\pm}}{\partial t} = \lim_{V\to\infty} \sum_n \frac{\pi e^2}{M^2} \int \frac{d^3k}{V(2\pi)^3} \{ (\hat{G}_k + \frac{\lambda_k}{\nu_k v_{\perp}})^* \delta(\omega_k - k_{"} v_{"} - n\Omega_{\pm}) |\zeta^{\pm}_{n,k}|^2 \hat{G}_k \} g^{\pm} \tag{36}$$

where $\zeta^{\pm}_{n,k} \equiv \varepsilon^{\pm}_{n,k} + \frac{v_{"}}{v_{\perp}} J_n \varepsilon^{"}_k$ and $\lim_{\gamma_k \to 0} \hat{K}_{n,k} = \frac{v_{"}}{v_{\perp}} \hat{G}_k$. Setting $f_{\alpha} = g^{\pm}$

$$\frac{\partial f_{\alpha}}{\partial t} = \lim_{V\to\infty} \sum_n \frac{\pi e^2}{m_{\alpha}^2} \int \frac{d^3k}{V(2\pi)^3} L v_{\perp} \delta(\omega - k_{"} v_{"} - n\omega_{c\alpha}) |\Theta_{n,k}|^2 L f_{\alpha} \tag{38}$$

where $L \equiv (1 - \frac{k_{"} v_{"}}{\omega}) \frac{1}{v_{\perp}} \frac{\partial}{\partial v_{\perp}} + \frac{k_{"}}{\omega} \frac{\partial}{\partial v_{"}}$ (39)

and

$$\Theta_{n,k} \equiv \frac{e^{i\psi}}{2}(E_x - iE_y)_k J_{n+1} + \frac{e^{-i\psi}}{2}(E_x + iE_y)_k J_{n-1} + \frac{v_\parallel}{v_\perp}(E_z)_k J_n \tag{40}$$

with $J_n \equiv J_n(k_\perp v_\perp/\omega_{c\alpha})$.

Setting $\psi=0$, assuming a monochromatic spectrum of waves and transforming to spherical velocity coordinates

$$\frac{\partial f_\alpha}{\partial t} = \frac{\pi e^2}{8m_\alpha^2}|E_x+iE_y|^2\{\frac{1}{v^2}\frac{\partial}{\partial v}J_{n-1}^2\delta(n\omega_{c\alpha}-\omega+k_\parallel v_\parallel)(v^2\sin^2\theta)\frac{\partial f_\alpha}{\partial v} -$$

$$v\sin\theta(\frac{k_\parallel v}{\omega}-\cos\theta)\frac{\partial f_\alpha}{\partial\theta}) + \frac{1}{v^2\sin\theta}\frac{\partial}{\partial\theta}(J_{n-1}\delta(n\omega_{c\alpha}-\omega+k_\parallel v_\parallel)$$

$$(-v\sin^2\theta(\frac{k_\parallel v}{\omega}-\cos\theta)\frac{\partial f_\alpha}{\partial v} + \sin\theta(\frac{k_\parallel v}{\omega}-\cos\theta)^2\frac{\partial f_\alpha}{\partial\theta})\}$$

$$+ \frac{\pi e^2}{8m_\alpha^2}|E_x-iE_y|^2\{\frac{1}{v^2}\frac{\partial}{\partial v}J_{n+1}^2\delta(n\omega_{c\alpha}-\omega+k_\parallel v_\parallel)(v^2\sin^2\theta)\frac{\partial f_\alpha}{\partial v} -$$

$$v\sin\theta(\frac{k_\parallel v}{\omega}-\cos\theta)\frac{\partial f_\alpha}{\partial\theta}) + \frac{1}{v^2\sin\theta}\frac{\partial}{\partial\theta}(J_{n+1}\delta(n\omega_{c\alpha}-\omega+k_\parallel v_\parallel) \tag{41}$$

$$(-v\sin^2\theta(\frac{k_\parallel v}{\omega}-\cos\theta)\frac{\partial f_\alpha}{\partial v} + \sin\theta(\frac{k_\parallel v}{\omega}-\cos\theta)^2\frac{\partial f_\alpha}{\partial\theta})\}$$

$$+ \frac{\pi e^2}{8m_\alpha^2}|E_\parallel|^2\{\frac{1}{v^2}J_n^2\,\mathrm{ctn}^2\theta\delta(n\omega_{c\alpha}-\omega+k_\parallel v_\parallel)(v^2\sin^2\theta)\frac{\partial f_\alpha}{\partial v} -$$

$$v\sin\theta(\frac{k_\parallel v}{\omega}-\cos\theta)\frac{\partial f_\alpha}{\partial\theta}) + \frac{1}{v^2\sin\theta}\frac{\partial}{\partial\theta}(J_n^2\mathrm{ctn}^2\theta\delta(n\omega_{c\alpha}-\omega+k_\parallel v_\parallel)$$

$$(-v\sin^2\theta(\frac{k_\parallel v}{\omega}-\cos\theta)\frac{\partial f_\alpha}{\partial v} + \sin\theta(\frac{k_\parallel v}{\omega}-\cos\theta)^2\frac{\partial f_\alpha}{\partial\theta})\} .$$

Kennel and Engelmann have assumed that a spectrum of randomly phased modes exists in order to justify the concept of particle diffusion caused by several random velocity displacements. A monochromatic rather than a spectrum of waves can be used if a plasma ion, having passed through the resonant heating zone, encounters many collisions so as to forget the phase of the cyclotron heating field before it passes through the heating zone again. The time between passes through this zone is[16]

$$\Delta\tau_p \simeq \pi R q / v_\parallel \tag{42}$$

and the variation in τ_p is given by[16,17]

$$\Delta\tau_p \simeq \pi R q \Delta v_\parallel / v_\parallel^2 \quad . \tag{43}$$

After half a poloidal rotation, Coulomb scattering causes an RMS deviation, $\Delta v_\parallel$, on the order of $(\langle \Delta v_\parallel \rangle^2 \tau_p)^{1/2}$, where $\langle \Delta v_\parallel \rangle^2$ is the diffusion coefficient[17,18]. Ions "forget" the cyclotron phase between transits when $\omega_{ci}\Delta\tau_p >> 1$ or

$$\frac{\langle (\Delta v_\parallel)^2 \rangle}{v_\parallel^2} >> \frac{1}{(\omega_{ci}\tau_p)^2}\,\frac{1}{\tau_p} \quad , \tag{44}$$

where the diffusion coefficient is[16,17]

$$\langle (\Delta v_\parallel)^2 \rangle = \sum_f \frac{C_f}{v}\, G(\ell_f v)$$

$$C_f \equiv \frac{8\pi n_f Z_f^2 Z^2 e^4 \ln\Lambda}{m_f^2} \quad , \quad \ell_f^2 \equiv m_f / 2kT_f \tag{45}$$

$$G(x) \equiv \frac{\Phi(x) - x\Phi'(x)}{2x^2} \quad , \quad \Phi(x) \equiv \frac{2}{\pi^{1/2}} \int_0^x \exp(-y^2)\, dy$$

and f denotes the background plasma field particles. For NUWMAK, with $T_f \simeq 10keV$, $\ell_f v \simeq 1$, $v_\parallel \simeq v_{thi}$, and $G(x)^{(18)} \simeq .1$, $\tau_p \simeq 2.6\times10^{-6}sec$ and the inequality in eq.(44) yields $140sec^{-1} >> .7sec^{-1}$.

Using eq.(41), the following RF diffusion terms may then be added to the general diffusion terms derived in eq.(6),

$$A_{RF} = 0 \qquad B_{RF} = Cv\tilde{B}\sin^2\theta/\tilde{v} \qquad C_{RF} = -Cv\sin\theta(k_\parallel v/\omega-\cos\theta)$$

$$D_{RF} = 0 \qquad E_{RF} = -Cv\sin^2\theta(k_\parallel v/\omega-\cos\theta)\cos\theta) \qquad (46)$$

$$F_{RF} = C\tilde{v}\sin\theta(k_\parallel v/\omega-\cos\theta)^2$$

where

$$C = \frac{|E_x+iE_y|^2J_{n-1}^2+|E_x-iE_y|^2J_{n+1}^2+|E_\parallel|^2J_n^2ctn^2\theta \quad \delta(n\omega_{ci}-\omega+k_\parallel v_\parallel)}{32Z^2e^2n_o} \qquad (47)$$

and $J_n \equiv J_n(k_\perp v_\perp/\omega_{ci})$.

To eliminate the delta function the diffusion equation can be integrated around the minor radius in a manner similar to Stix to obtain the following expression for C[17] (see Appendix C)

$$C \to |E_+|^2J_{n-1}^2R/(32\pi aZ^2e^2n_on\omega_{cio}\xi) \qquad (48)$$

with $\xi = (1-(\frac{R}{a})^2(\frac{n\omega_{cio}}{\omega+k_\parallel v_\parallel}-1)^2)^{1/2}$, where ω_{cio} is the cyclotron frequency at the major radius ,R, and a is the minor radius at which the ions are heated. Similar equations may be derived for E_- (J_{n-1} is replaced by J_{n+1}) and the $E_\parallel$ (J_{n-1} is replaced by $J_nctn\theta$) terms. In the next section, numerical results for the RF heating of NUWMAK using quasi-linear theory are presented.

III-C NUMERICAL RESULTS FOR NUWMAK USING HYBRID III

In this section the time evolution of both the ion and electron distribution functions are examined during reactor startup[21]. Again, the dispersion relation for a fast magnetosonic wave propagating in a D-T plasma is solved for complex $k_\perp$ given a real ω and $k_\parallel$ which can be established by an array of launching structures distributed toroidally around the torus. Every 5 or 10 time steps, $k_\perp$ and D^{α}_{RF} are recalculated using the new densities and temperatures. The wave equation is also solved to obtain both the magnitude of the RF electric field locally in the plasma and the relative phases between E_+, E_- and $E_\parallel$.

As before, the possible effects which might occur if mode conversion proceeses were present are neglected. In addition, a suitable launching structure which excites only a single eigenmode is assumed to exist. Though alpha particles are also resonant at the second harmonic, in the 100 MW case, the alpha density is less than 1% of the total ion density as shown in fig.(III-C-1). Since RF absorption is proportional to density, the alphas absorb a small amount of power which is ignored.

Figs.(III-C-1-6) use the NUWMAK sized tokamak parameters given in Table 5. Figures (III-C-3-5) show the assumption that the ion distribution remains Maxwellian during the reactor startup underestimates the reactor $Q = \frac{\text{Fusion Power Out}}{\text{Auxiliary Heating Power}}$ by 11%. A large hot ion tail is not observed in Fig.(III-C-6a). For NUWMAK, both the ion isotropization time as well as the ion slowing down time are on the order of 20-30 ms. Since the plasma

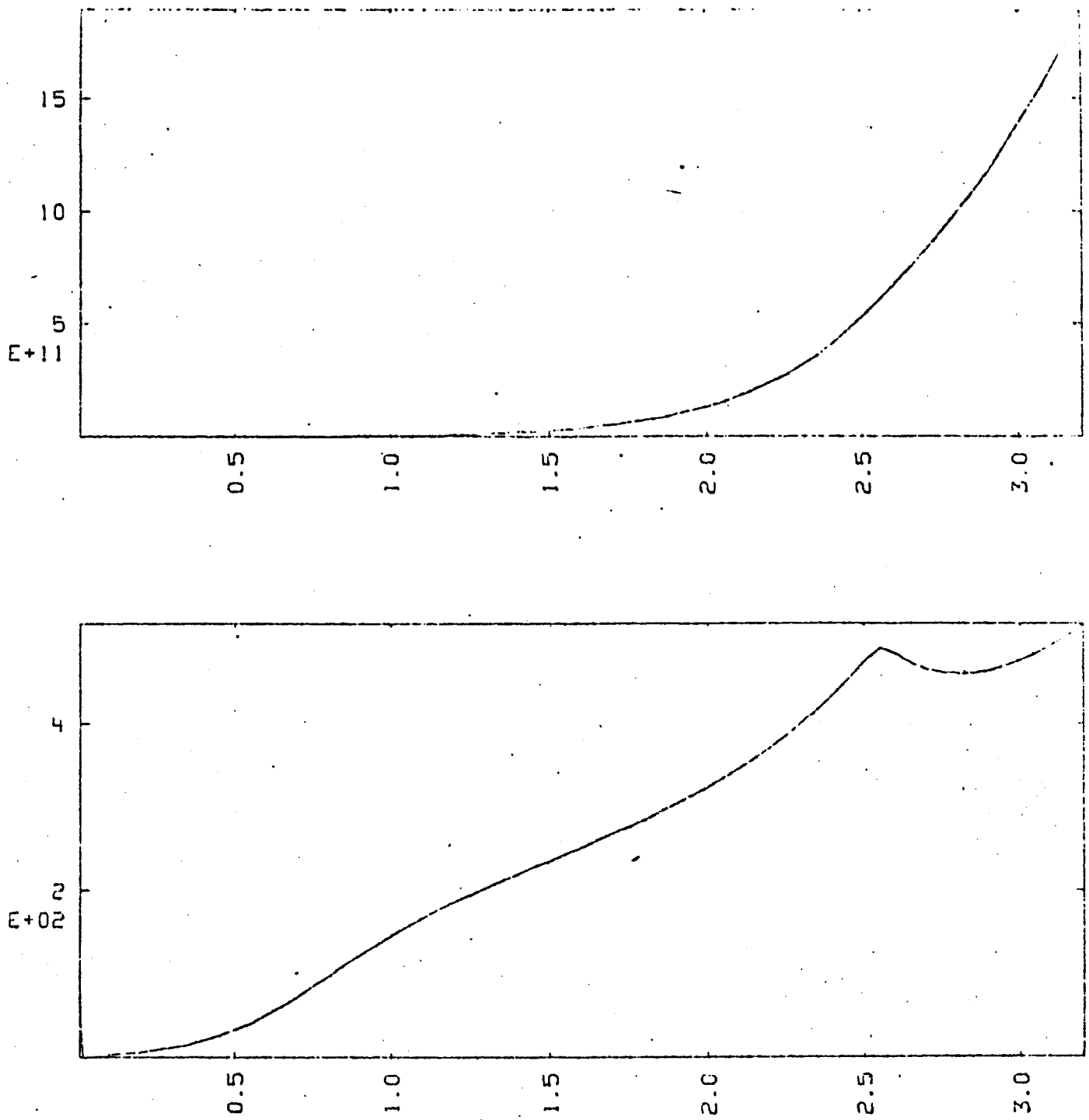

Time evolution of the alpha density and energy for a 100 MW 2.5 sec RF pulse reactor startup.

Fig. III-C-1

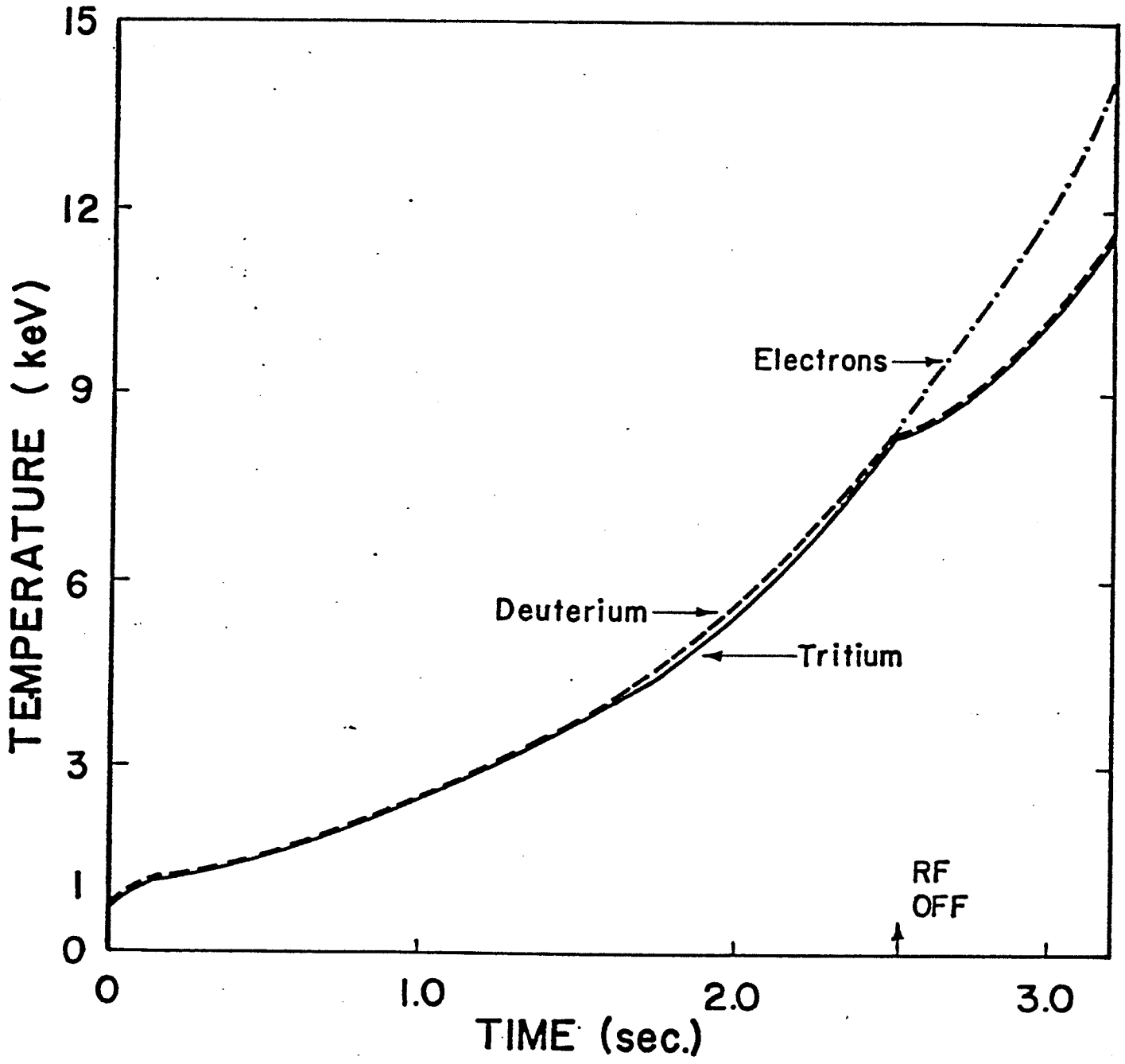

Fig. III-C-2 Ion and electron temperatures for a fusion reactor ignited with a 2.5 sec 100 MW RF pulse.

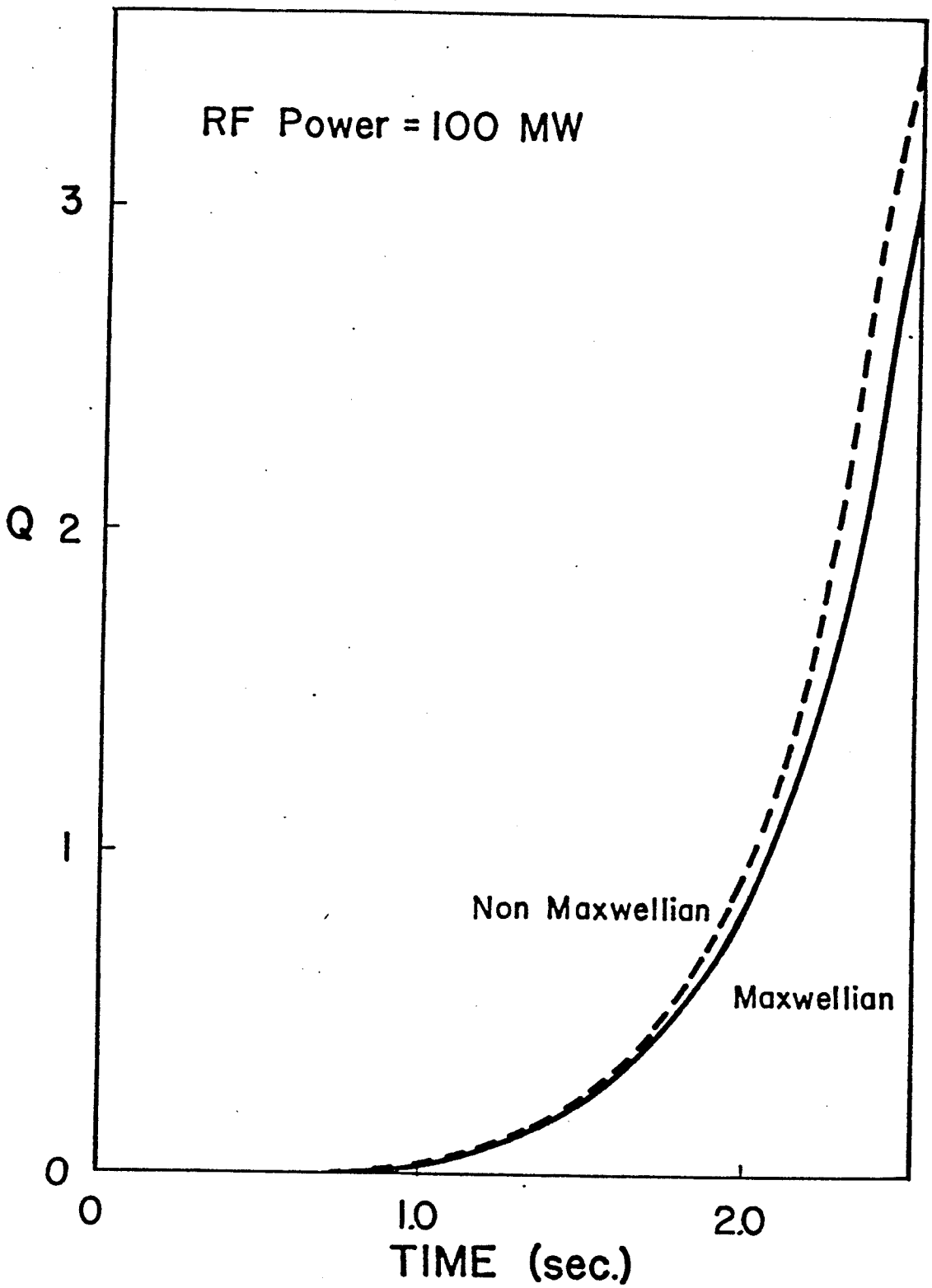

Fig. III-C-3 Fusion reactor Q = Fusion power/Auxiliary heating power for the nonmaxwellian case as compared with the maxwellian assumption for a 2.5 sec 100 MW RF pulse.

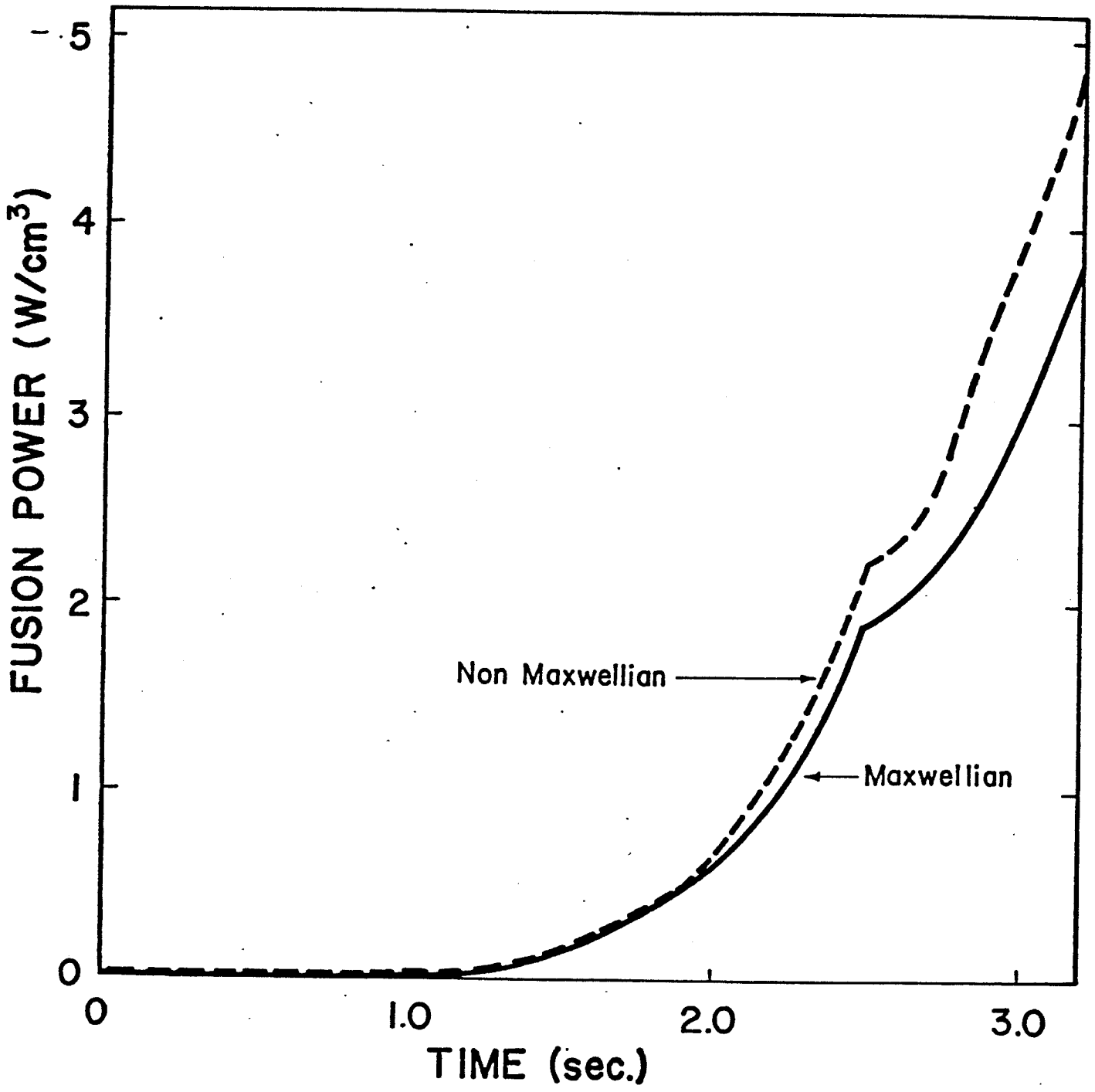

Fig. III-C-4 Fusion power for the nonmaxwellian case as compared with the maxwellian assumption for a 2.5 sec 100 MW RF pulse.

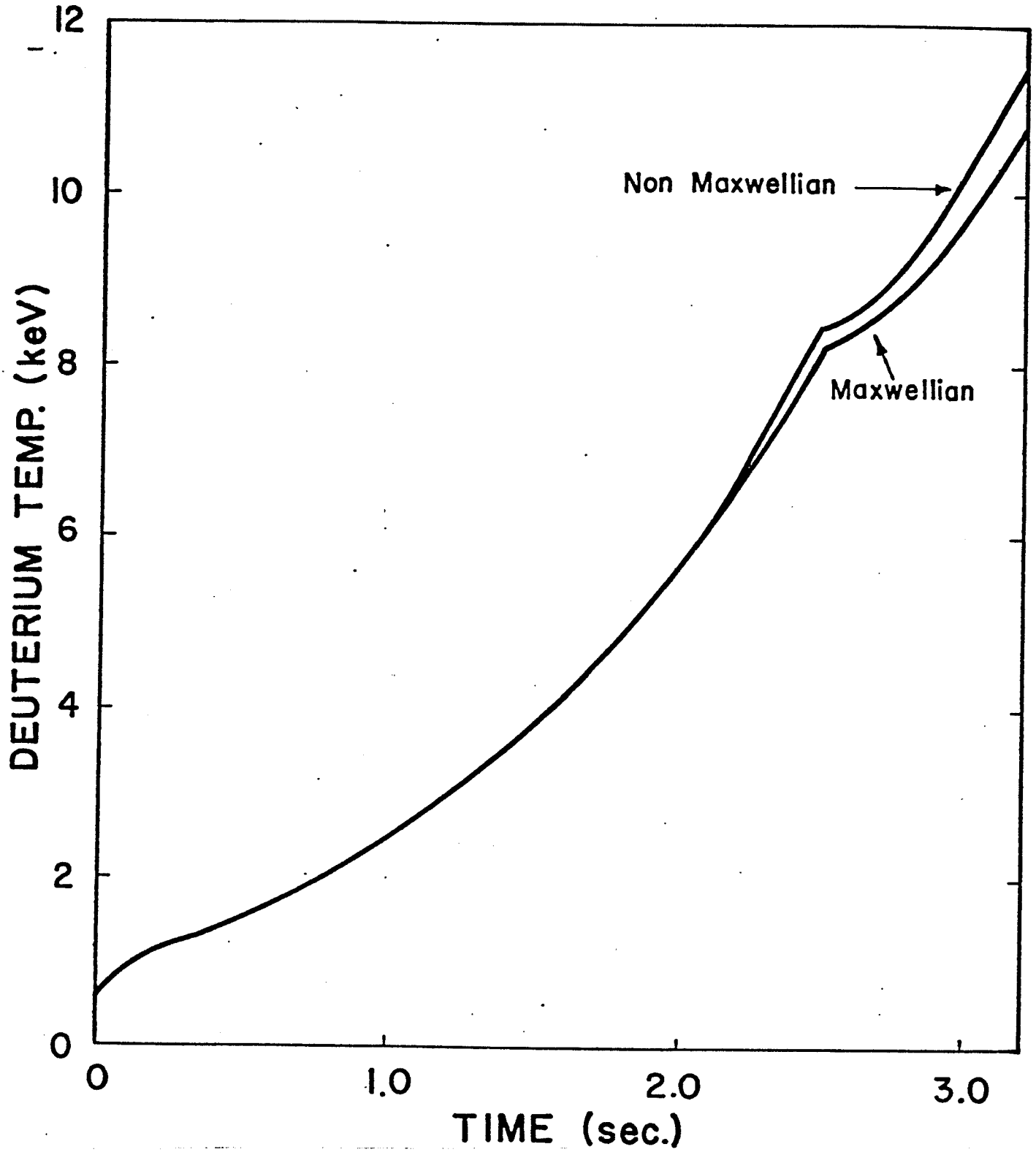

Fig. III-C-5 Deuterium temperature for the nonmaxwellian case as compared with the maxwellian assumption for a 2.5 sec 100 MW RF pulse.

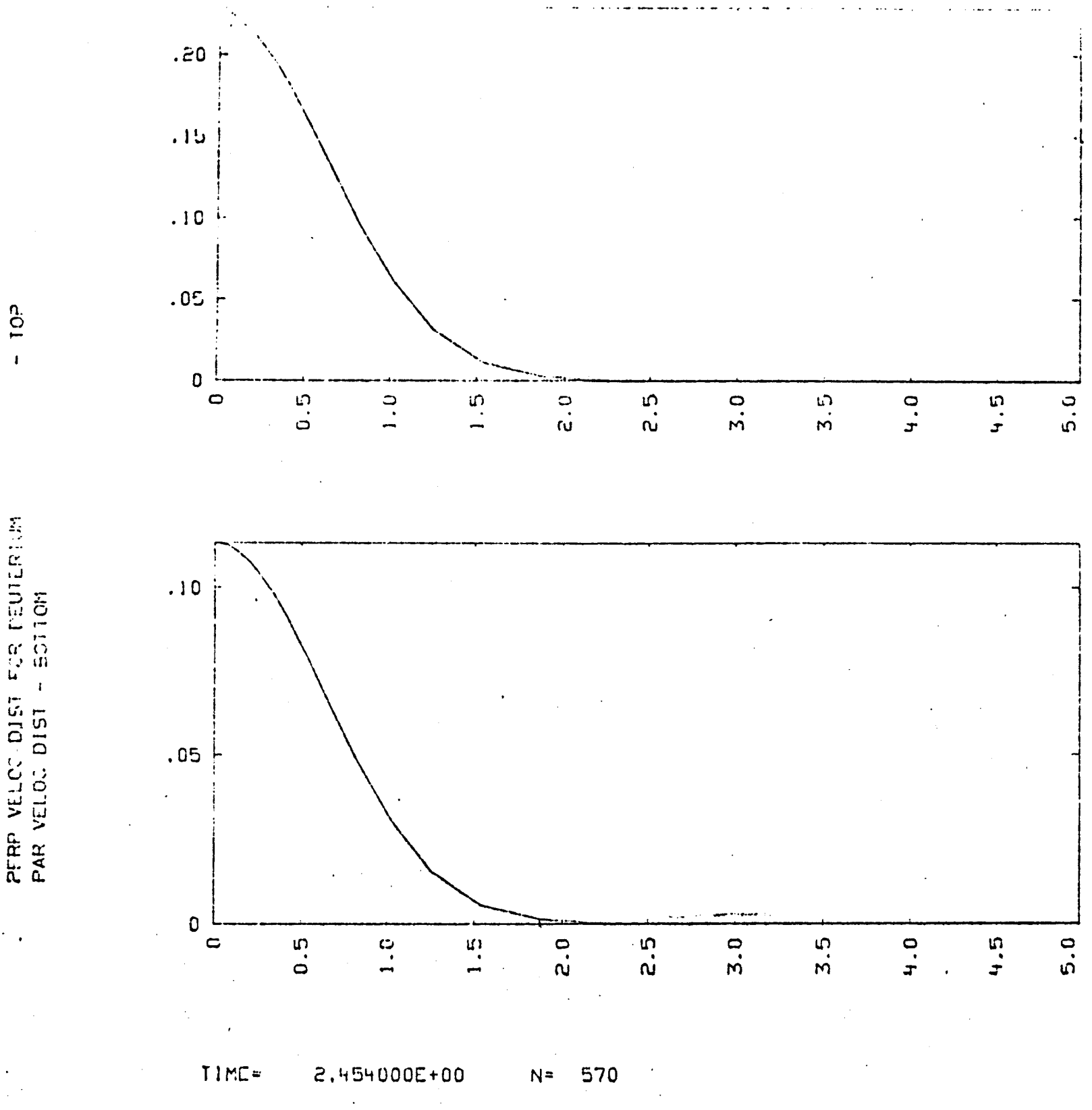

Fig. III-C-6a Deuterium velocity distribution function in the parallel and perpendicular directions at time t = 2.45 sec for a 2.5 sec 150 MW RF pulse.

CONTOURS

4.266580E-04
5.928394E-04
8.237477E-04
1.144594E-03
1.590408E-03
2.209865E-03
3.070597E-03
4.266580E-03
5.928394E-03
8.237477E-03
1.144594E-02
1.590408E-02
2.209865E-02
3.070597E-02
4.266580E-02
5.928394E-02
8.237477E-02
1.144594E-01
1.590408E-01
2.209865E-01
3.070597E-01

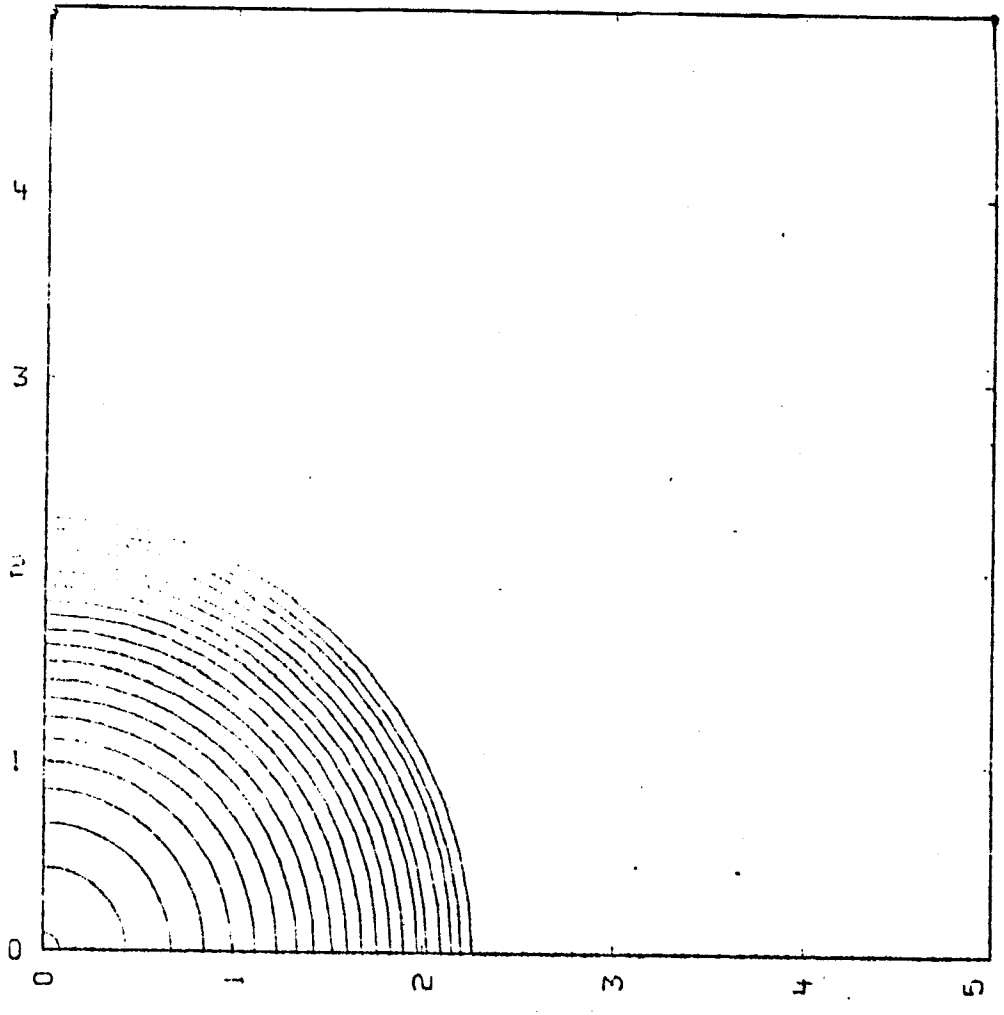

CONTOUR PLOT FOR DEUTERIUM TIME= 2.454000E+00 N= 570

Fig. III-C-6b

is heated for 3000ms, tail formation may be supressed by the collisions. Figure(III-C-6b) shows that the RF heats the ions isotropically.

In Figs.(III-C-7-10), the parameters in Table 6 are used to examine the feasibility of using NUWMAK in a TCT mode. Contrary to the results obtained in an earlier study by Kesner[17], the reactor Q is lowered when neutral beams are replaced by RF. In the earlier study, the effect of resonant tritium ions was ignored. On including this effect, up to 80% of the RF power goes to heating the background tritons. The RF clamping effect on the deuterium beams is much lower than previously computed. Keeping the total input power constant requires that the beam current decrease with increasing RF power. This results in fewer TCT fusions with a corresponding decrease in reactor Q. Figure III-C-7 shows how Q scales with the total amount of injected power as well as the percentage of RF power supplied. Figure III-C-8 shows this scaling for the total fusion power. In Figs.(III-C-9-10), how Q evolves with time as the fraction of RF power is changed is shown. In fig.(III-C-10), Q drops in the 100% and 75% neutral beam cases after 1.4sec. This decrease in Q occurs because of the pollution of the tritium target caused by the high current deuterium beams. The buildup of deuterons in the plasma lowers the probability of a fast deuteron colliding with a triton; hence, the number of TCT fusions is lowered.

Figures(III-C-11-12) show the RF electric field and complex $k_{\perp}^2$ for a 100MW RF pulse for 2.5sec. In the hot plasma case, there is a sizeable percentage of the electric field rotating

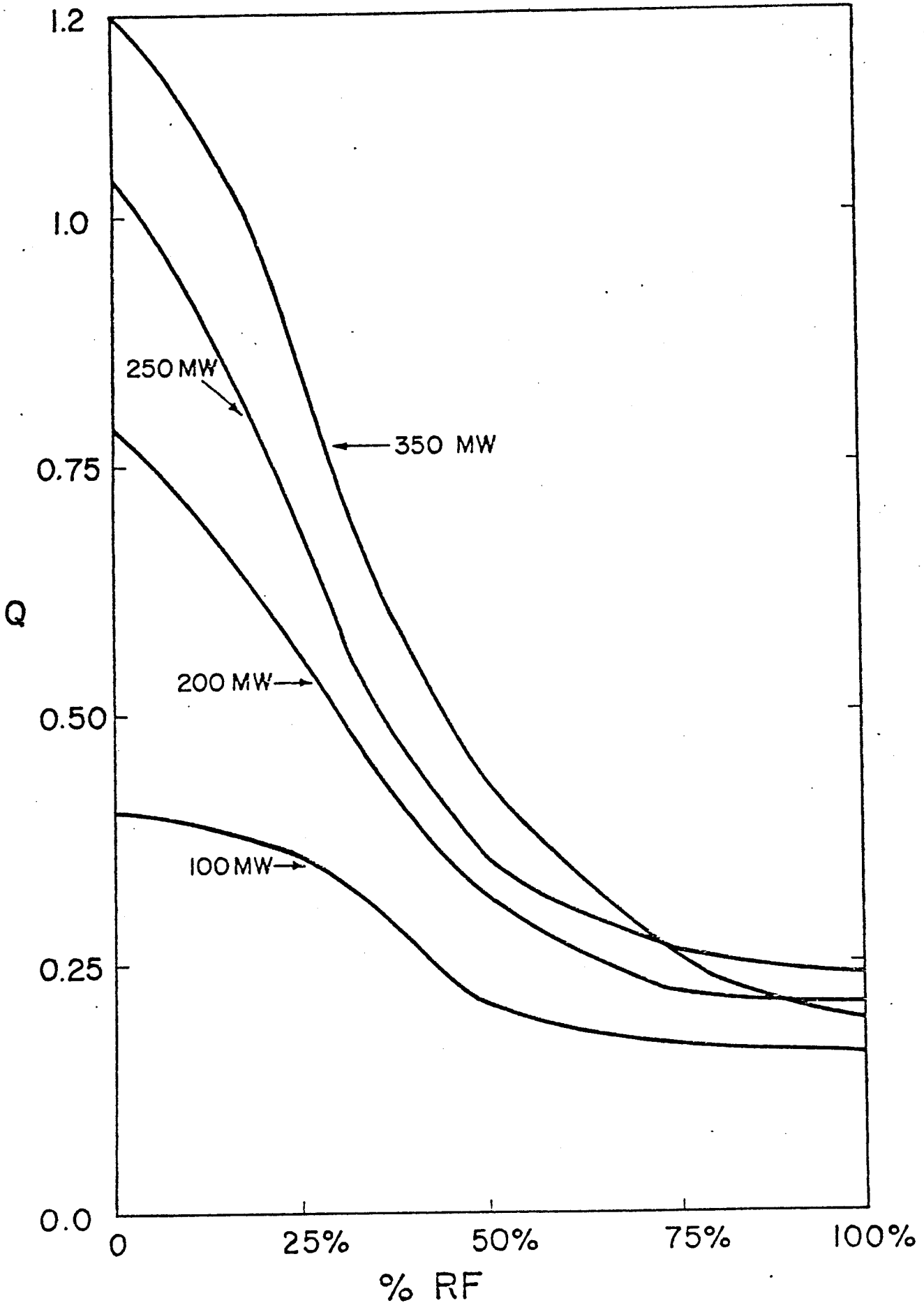

Fig. III-C-7 TCT reactor Q using 200 keV neutral beams as a function of the percentage of RF power for various amounts of total injected power.

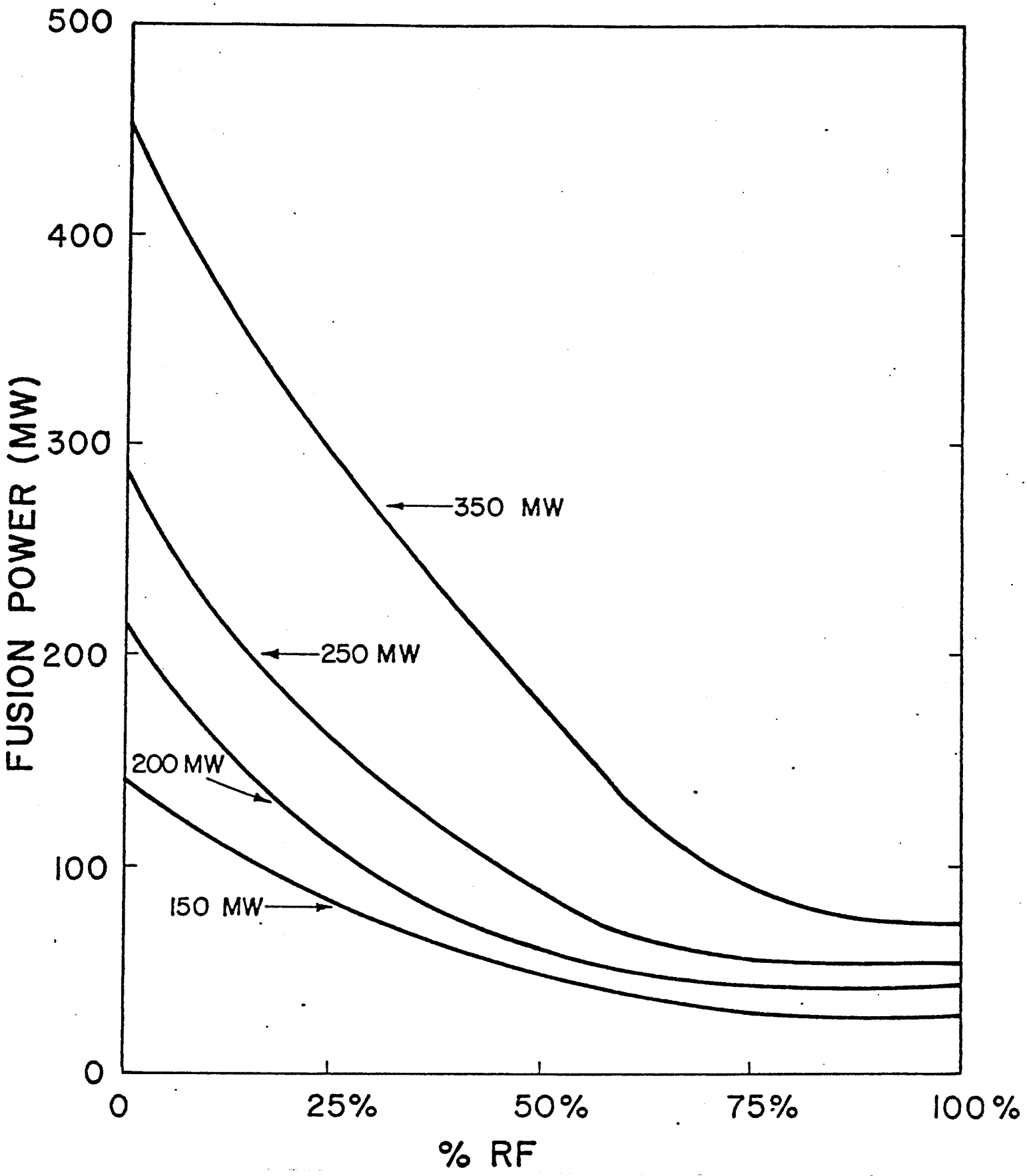

Fig. III-C-8 TCT fusion power using 200 keV neutral beams as a function of the percentage of RF power for various amounts of total injected power.

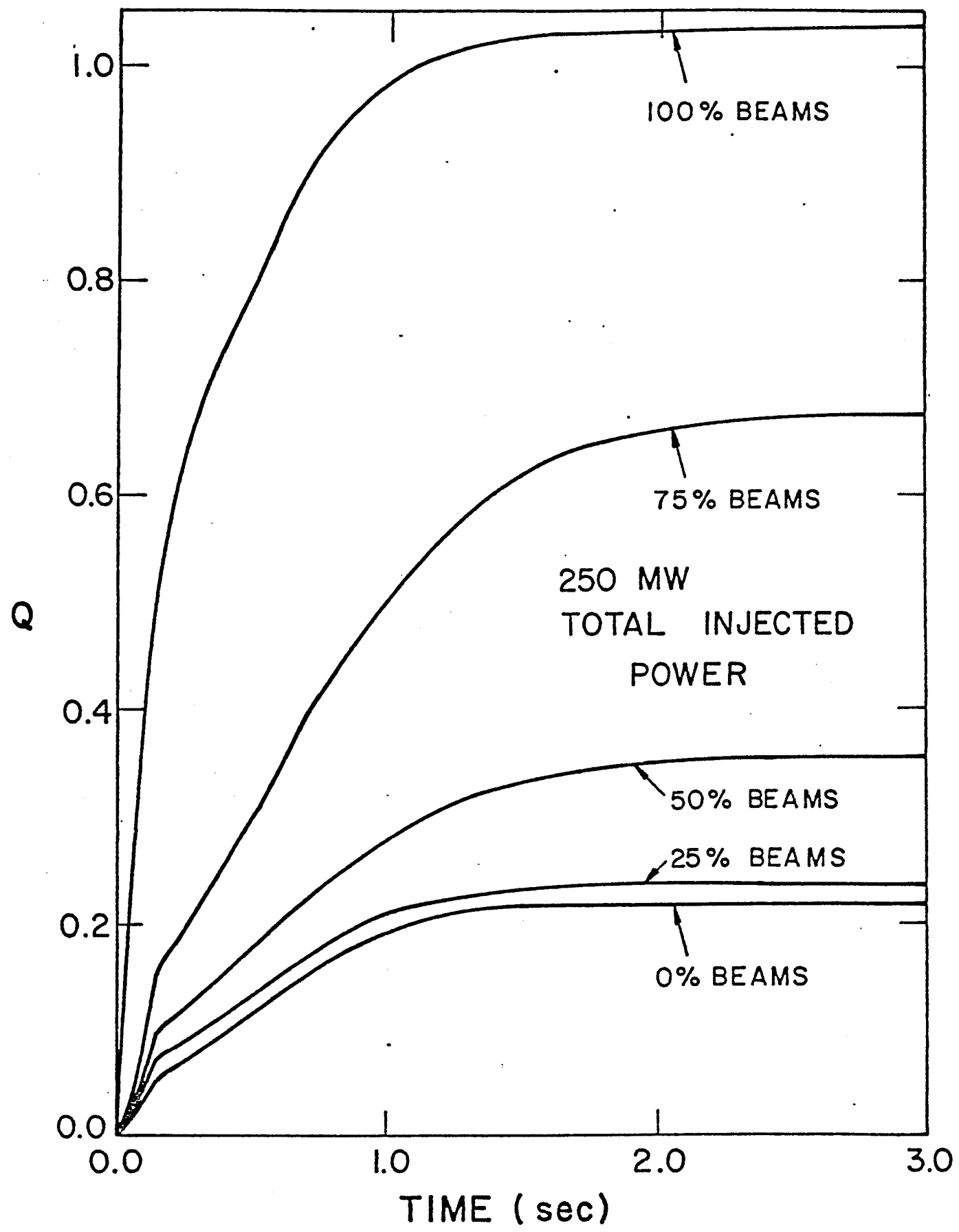

Fig. III-C-9 TCT reactor Q using 200 keV neutral beams as a function of the percentage of RF power with a total injected heating power of 250 MW.

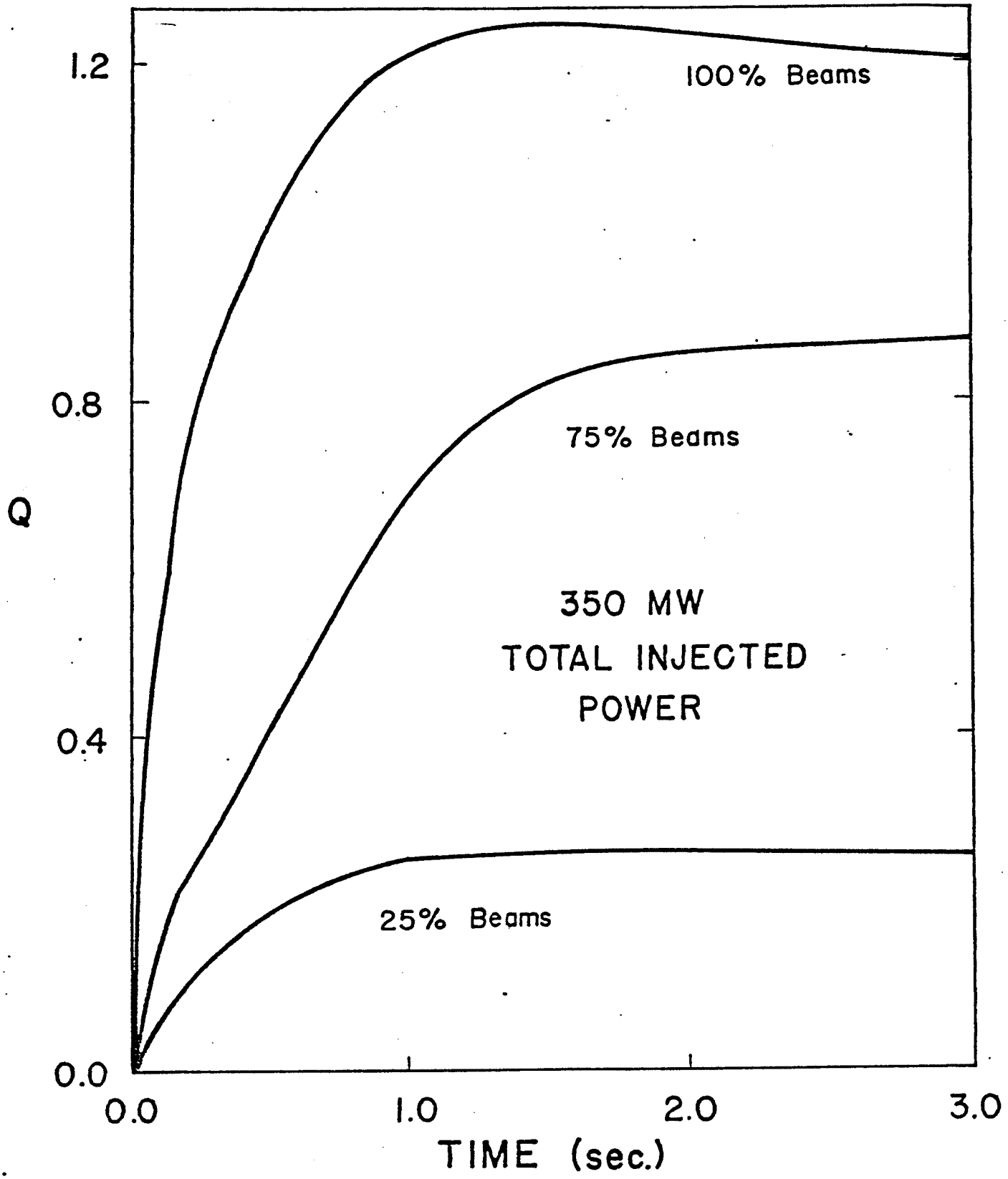

Fig. III-C-10 TCT reactor Q using 200 keV neutral beams as a function of the percentage of RF power with a total injected heating power of 350 MW.

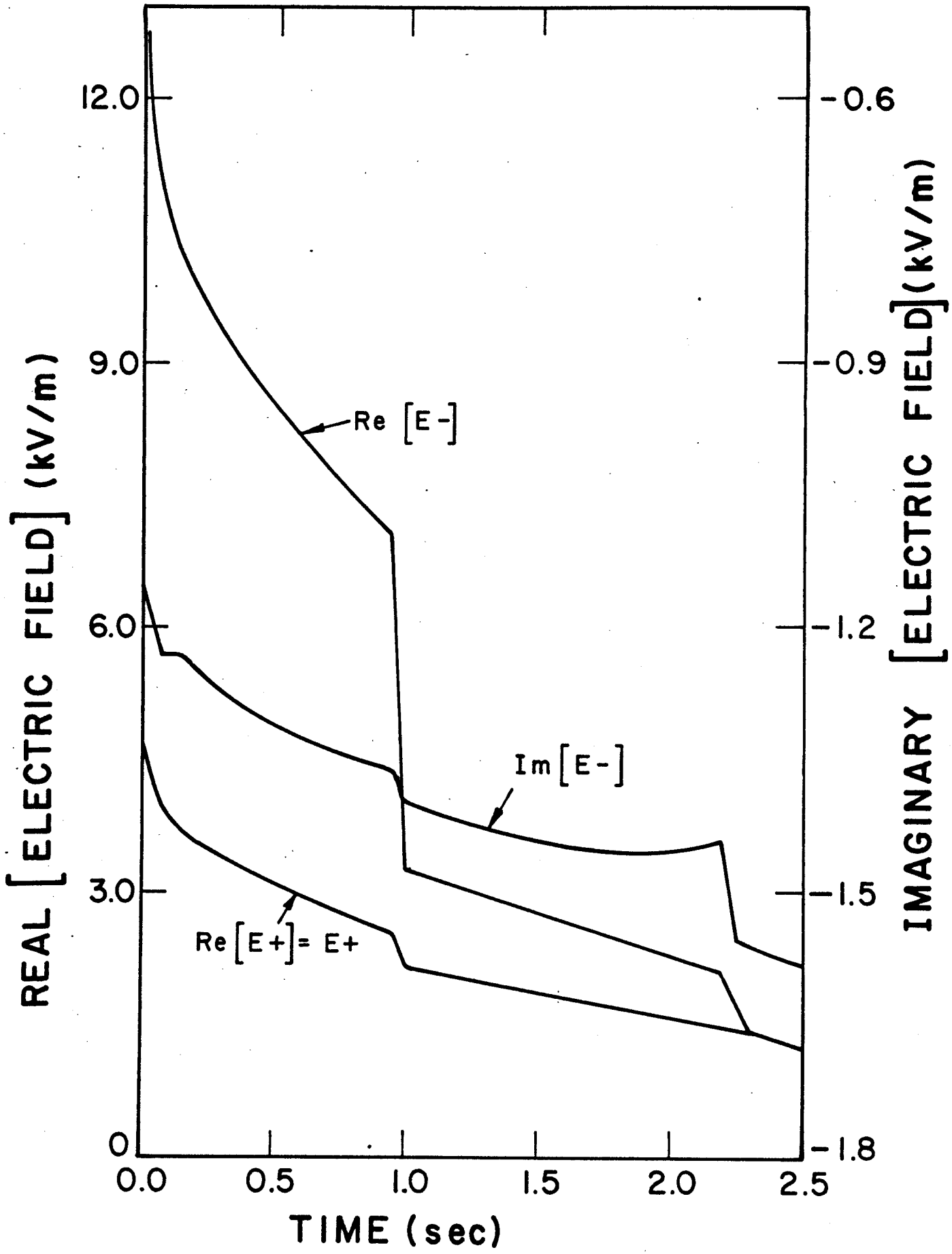

Fig. III-C-11 RF electric fields for a 2.5 sec 100 MW RF pulse and the parameters in Table 5.

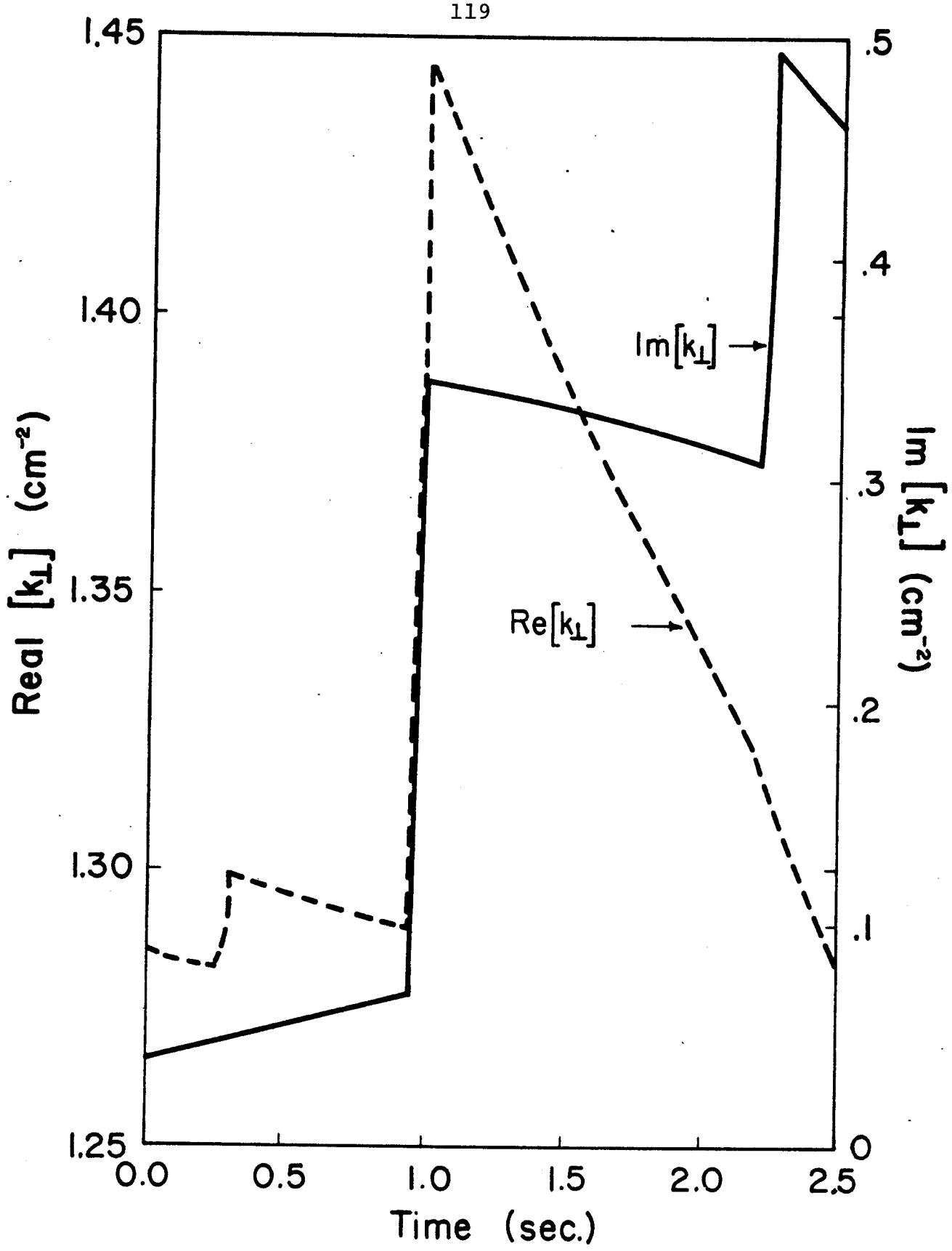

Fig. III-C-12 Complex $k_\perp^2$ for a 2.5 sec 100 MW RF pulse and the parameters in Table 5.

in the same sense as the ions

$$\left|\frac{E_+}{E_-}\right| \simeq \frac{1}{3} \quad . \tag{49}$$

The jump in the electric field at 1.0sec corresponds to a jump in $k_\perp^2$. In HYBRID III, unlike either the point or space-time calculations, $k_\perp^2$ is evaluated at a single point (r=0) rather than averaged over the entire heating zone. There is a sharp bend in $k_\perp^2(r)$ near r=0 (see fig.(I-B-5)). Though relatively insensitive to temperature ($Rek_\perp^2$ changes from $1.25cm^{-2}$ to $1.45cm^{-2}$) there is enough of a dependence to cause this bend to shift in position causing this small jump in $k_\perp^2$. As shown in figs.(III-C-3-5), there is no corresponding discontinuity in the plasma heating.

In conclusion, it has been shown that the Maxwellian assumption used in fluid codes is fairly accurate though Q is underestimated by 11%. A sizeable percentage of the RF electric field rotates in the same sense as the ions which leads to cyclotron damping of the ions. Finally the reactor Q drops when NUWMAK is operated in the TCT mode when beams are replaced by RF due to a decrease in the number of TCT fusions.

References

(1) John Killeen and Kenneth D. Marx, "The Solution of the Fokker-Planck Equation for a Mirror-Confined Plasma", Methods in Computational Physics, Vol. 9, pp. 421-489, Academic Press, Inc. (New York, 1970).

(2) Nicholas A. Krall and Alvin W. Trivelpiece, Principles of Plasma Physics, McGraw-Hill, Inc. (New York) (1973), p. 312.

(3) Arthur A. Mirin, "Hybrid-II, A Two-Dimensional Multi-species Fokker-Planck Computer Code", LLL Report UCRL-51615 Rev. 1 (Feb. 3, 1975).

(4) M.N. Rosenbluth, W.M. MacDonald, and D.L. Judd, Phys. Rev. 107, 1 (1957).

(5) D.C. Montgomery and D.A. Tidman, Plasma Kinetic Theory, pp. 19-20, McGraw-Hill, New York.

(6) J. Killeen, T.H. Jonnson, A.A. Mirin, and M.E. Rensink, "Computational Studies of the Two-Component Toroidal Fusion Test Reactor", LLL Report UCID-16530 (June 1974).
J. Killeen, A.A. Mirin, and M.E. Rensink, "The Solution of the Kinetic Equations for a Multi-species Plasma", Methods Computational Physics 16 (1975), pp. 387-431.

(7) John D. Jackson, Classical Electrodynamics, John Wiley & Sons, Inc., New York (1962), p. 490.

(8) J.P. Shkarofsky, T.W. Johnson, and M.P. Bachynski, The Particle Kinetics of Plasmas, Addison-Wosley Publ. Co., Reading, Massachusetts (1966), pp. 242-272.

(9) S.S. Chern, "Introduction to Differntial Geometry Math 140 Notes", Dept. of Mathematics, Univ. of California, Berkeley, (Aug. 1971).

(10) Eugene Butkov, Mathematical Physics, Addison-Worely Publ. Co., Reading, Mass. (1968).

(11) A.H. Futch, Jr., J.P. Holdren, J. Killeen, and A.A. Mirin, "Multi-species Fokker-Planck Calculations for D-T and D-^{3}He Mirror Reactors", Plasma Physics 14, pp. 211-244 (1972).

(12) M.R. Gordinier, "Evaluation of the Reaction Rate for the Arbitrary Maxwellian Distributions", IFDM-12.

(13) M.R. Gordinier, "Numerical Evaluation of the Reaction Rate and Amplification Factor for an Arbitrary Beam-Plasma System", IFDM-13.

(14) L.G. Kuo-Petravic, M. Petravic, and C.J.H. Watson, Proc. Intl Con. on Nucl. Fusion Reactors, Culham, England Paper 2.4 (1969).

(15) C.I. Kennel and F. Engelmann, "Velocity Space Diffusion From Weak Plasma Turbulence in a Magnetic Field", Physics of Fluids 9 (1966), 2377-2388.

(16) T.H. Stix, "Fast-Wave Heating of a Two-Component Plasma", Nuclear Fusion 15 (1975).

(17) J. Kesner, "Quasi-Linear Model for Ion Cyclotron Heating of Tokamaks and Mirrors", Nuclear Fusion.

(18) L. Spitzer, Physics of Fully Ionized Gases, Interscience Publishers (1962).

(19) C. Hastings, Jr., Approximation for Digital Computers, p. 175, Princeton University Press, Princeton, New Jersey.

(20) D.W. Peaceman and H.H. Rackford, Jr., J. Soc. Ind. Appl. Math. 3, 28, p. 15.

(21) D.T. Blackfield, et al., Bull. Am. Phys. Soc. 23, (1978) 821.

(22) T.K. Mau, University of Wisconsin PhD. Thesis (1977).

Appendix A

Ion-Ion Hybrid Resonance and Fundamental Minority Species Heating in Reactor Tokamaks

The alternative schemes of ion-ion hybrid resonance and fundamental minority species heating[22,27,37,107,108]* involve the presence of the ion-ion (two ion) hybrid resonance layer within the plasma. This surface is located at[27]

$$\omega^2 = \frac{\chi_t f_d + \chi_d f_t}{\chi_d f_d + \chi_t f_t} \omega_{cd} \omega_{ct} \qquad \text{(A-1)}$$

where χ_d = concentration of deuterium, $f_d = m_e/M_d$

χ_t = concentration of deuterium, $f_t = m_e/M_t$.

At this resonance surface, where the ions oscillate 180° out of phase with each other, an incoming fast wave may either be reflected or mode converted into an I.B. wave and then damped by Landau damping.

In the following analysis, $k_\parallel$ is assumed to be small enough so ion cyclotron resonance width ΔR (Eq. (45), Sec. I) does not overlap the ion-ion resonance surface. Any electron absorption which is small for small $k_\parallel$ is also neglected. In addition, the concentration of minority species is assumed to be greater than 10%.

With $k_\parallel$ small, cold plasma theory may be used to obtain the following dispersion relation[37]

$$k_\perp^2 = \frac{\omega^2}{c^2} \frac{(R-n_\parallel^2)(L-n_\parallel^2)}{S-n_\parallel^2} \qquad (2)$$

* All Refs. refer to those listed at the end of Sec. I.

where $R = 1 - \sum_{\alpha} \frac{\omega_{p\alpha}^2}{\omega(\omega+\omega_{c\alpha})}$ $\qquad L = 1 - \sum_{\alpha} \frac{\omega_{p\alpha}^2}{\omega(\omega-\omega_{c\alpha})}$

$$S = (R + L)/2 \ .$$

Using Sec. I, Eq. (50) the following differential equation describing the mode coupling at the resonance surface is obtained:

$$\frac{d^2E(x)}{dx^2} + \frac{\omega^2}{c^2} \frac{(R(x)-n_{\parallel}^2)(L(x)-n_{\parallel}^2)}{S(x)-n_{\parallel}^2} E(x) = 0 \ . \qquad (3)$$

$R(x)$, $L(x)$ and $S(x)$ are expanded about $n_{\parallel}^2 = S(x)$ in a Taylor series to find that

$$\frac{d^2E_y(x)}{dx^2} + k_{\infty}^2 \left(1-\frac{w}{x}\right) E_y(x) = 0 \qquad (4)$$

where $$k_{\infty}^2 = \frac{\omega^2}{c^2} \frac{d}{dx} \left((L-n_{\parallel}^2)(R-n_{\parallel}^2)\right) / \frac{d}{dx} (S-n_{\parallel}^2)$$

$$W = \frac{-(L-n_{\parallel}^2)(R-n_{\parallel}^2)}{\frac{d}{dx}\left((L-n_{\parallel}^2)(R-n_{\parallel}^2)\right)} \ .$$

The derivatives are calculated at that value of x where $S(x) = n_{\parallel}^2$. McVey[37] again obtains transmission and reflection coefficients of the form of Sec. I, Eqs. (54) and (55) where

$$\eta = k_{\infty} W \ . \qquad (5)$$

In a fusion reactor, the resonance layer appears as a reflecting barrier for a fast wave approaching from the LFS and

as an absorbing layer from the HFS.

For two ion resonance heating, a fast wave is launched from the HFS and propagates to the plasma center where the two ion resonance layer is located. There, it mode converts into an I.B. wave which is rapidly Landau damped and heats the electrons.

For fundamental minority species heating, a fast wave is launched from the LFS with frequency $f = f_{cd}$, with deuterium being the minority species. The deuterium cyclotron resonance is then located between the launching structure and the two-ion resonance surface. As the fast wave propagates inwards, energy is first absorbed in the cyclotron resonance layer. The remaining transmitted fast wave energy is reflected at the two-ion resonance surface and is again absorbed in the deuterium cyclotron layer, thereby enhancing the fundamental ion heating.

Unfortunately, Perkins[22] finds that for a fusion reactor, these heating processes are less efficient than second harmonic heating. They both tend to suppress the toroidal eigenmodes, which results in a lowering of the RF antenna loading resistance. A high loading resistance is desirable since RF power can be more easily coupled to the plasma. In addition, two-ion resonance heating has the undesirable feature of requiring the wave to be launched from the HFS where space is limited and cooling of the launching structure is more difficult.

Appendix B

The Fokker-Planck Collision Operator

In HYBRID III, the Fokker-Planck collision operator[8]* is used for $\left.\frac{\partial f_\alpha}{\partial t}\right)_c$. From Appendix A and Refs.(3-6)

$$\frac{1}{\Gamma_\alpha}\left.\frac{\partial f_\alpha}{\partial t}\right)_c = -\frac{\partial}{\partial \vec{v}} \cdot f_\alpha \frac{\partial \vec{h}_\alpha}{\partial \vec{v}} + \frac{1}{2}\frac{\partial^2}{\partial \vec{v}\partial \vec{v}} : f_\alpha \frac{\partial^2 g_\alpha}{\partial \vec{v}\partial \vec{v}} \qquad (1)$$

where g_α and h_α are the Rosenbluth potentials[4]

$$g_\alpha = \sum_\beta \left(\frac{Z_\beta}{Z_\alpha}\right)^2 \ln\Lambda_{\alpha\beta} \int f_\beta(\vec{v}') \left|\vec{v}-\vec{v}'\right| d^3\vec{v}' \qquad (2)$$

$$h_\alpha = \sum_\beta \left(1+\frac{m_\alpha}{m_\beta}\right)\left(\frac{Z_\beta}{Z_\alpha}\right)^2 \ln\Lambda_{\alpha\beta} \int \frac{f_\beta(\vec{v}')}{\left|\vec{v}-\vec{v}'\right|} d^3\vec{v}' \qquad (3)$$

$$\text{and } \Lambda_{\alpha\beta} = \left(\frac{m_\alpha m_\beta}{m_\alpha+m_\beta}\right)\frac{2\alpha'\lambda_D}{r_e m_e c} \max\left(\frac{2\bar{E}}{m}_{\alpha,\beta}\right)^{1/2} - 1/2 \qquad (4)$$

α' is the fine structure constant $\simeq 1/137$

λ_D is the electron Debeye length $= (T_e/4\pi n_e e^2)^{1/2}$

$n_e \equiv \int d\vec{v} f_e(\vec{v})$

$\bar{E}$ is the mean energy of the particles of species "α" or "β"

r_e is the classical electron radius[7] $= e^2/m_e c^2$ (5)

and $\Gamma_\alpha = 4\pi Z_\alpha^4 e^4/m_\alpha^2$. (6)

In eqs.(1-6) f_α is normalized so that

$$n_\alpha = \int f_\alpha(\vec{v}) d\vec{v} \quad . \qquad (7)$$

* All Refs. refer to those listed at the end of Sec.III

Eq.(6) has the following form , dropping the "α" subscript

$$\frac{1}{\Gamma}\left(\frac{\partial f}{\partial t}\right)_c = -\nabla\cdot(f\nabla h)+\frac{1}{2}\nabla\nabla\dot{:}(f\nabla\nabla g) \tag{8}$$

which may be written as[8]

$$\frac{1}{\Gamma}\left(\frac{\partial f}{\partial t}\right)_c = \left(\frac{\nabla\nabla\dot{:}\nabla\nabla g}{2} - \nabla\cdot\nabla h\right)f + (\nabla\cdot\nabla\nabla g-\nabla h)\cdot\nabla f + \frac{\nabla\nabla g\dot{:}\nabla\nabla f}{2} \tag{9}$$

$$= \left(\frac{1}{2}\nabla^4 g-\nabla^2 h\right)f + (\nabla(\nabla^2 g)-\nabla h)\cdot\nabla f + \frac{1}{2}(\nabla\nabla g)\dot{:}(\nabla\nabla f) \tag{10}$$

where $\nabla^4 \equiv \nabla\nabla\dot{:}\nabla\nabla = \nabla^2(\nabla^2$.

To express Eq.(5) in the two dimensional spherical coordinates (v,θ) used in HYBRID III, $\nabla\nabla g\dot{:}\nabla\nabla f$ must first be transformed from cartesian to spherical coordinates (see fig.B-1). Defining the partial derivative of a vector, A_i by

$$\frac{\partial A_i}{\partial v_k} \equiv A_{i,k} \tag{11}$$

the covariant derivative of a vector A_i may be written as[9,10]

$$A_{i;k} = A_{i,k} - \Gamma^m_{ik}A_m \tag{12}$$

where Γ^m_{ik} is the Christoffel symbol of the second kind[9,10]

$$\Gamma^m_{ik} = \frac{1}{2}r^{nk}\left(\frac{\partial r_{ki}}{\partial v_j} + \frac{\partial r_{jk}}{\partial v_i} + \frac{\partial r_{ij}}{\partial v_k}\right) \tag{13}$$

where r_{ij} is the metric tensor and r^{jk} the associate metric tensor such that

$$r_{ij}r^{ik} = r^{kj}r_{ji} = \delta^k_i \ . \tag{14}$$

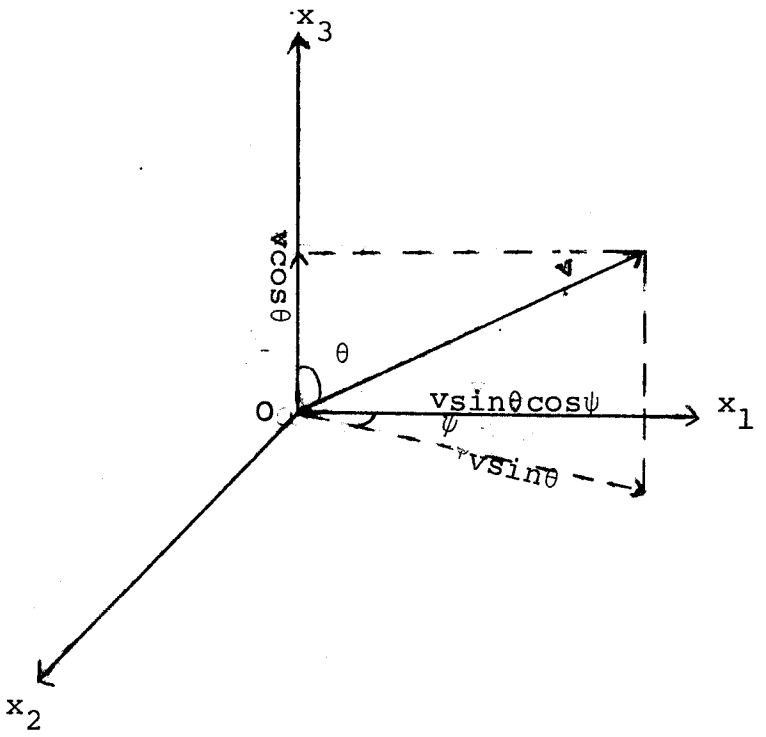

$$x_1 = \tilde{v}\sin\theta\cos\psi$$

$$x_2 = \tilde{v}\sin\theta\sin\psi \qquad \tilde{v} = \frac{v}{|v|}$$

$$x_3 = \tilde{v}\cos\theta$$

Fig. B-1 Cartesian and spherical coordinate systems.

Defining

$$(u_1,u_2,u_3) \equiv (v,\theta,\psi) \quad , \tag{15}$$

then[10]

$$r_{jk} = \frac{\partial x_i}{\partial u_j}\frac{\partial x_i}{\partial u_k} \quad , \tag{16}$$

and

$$\left[g\right]_{ij} = \begin{bmatrix} 1 & 0 & 0 \\ 0 & v^2 & 0 \\ 0 & 0 & v^2\sin^2\theta \end{bmatrix} \quad , \tag{17}$$

since

$$\left[\frac{\partial x}{\partial u}\right]_{ij} = \begin{bmatrix} \sin\theta\cos\psi & \sin\theta\cos\psi & \cos\theta \\ v\cos\theta\cos\psi & v\cos\theta\sin\psi & v\sin\theta\cos\psi \\ -v\sin\theta\sin\psi & -v\sin\theta & 0 \end{bmatrix} . \tag{18}$$

From Eq.(14)

$$\left[g\right]^{jk} = \begin{bmatrix} 1 & 0 & 0 \\ 0 & 1/v^2 & 0 \\ 0 & 0 & 1/v^2\sin\theta \end{bmatrix} . \tag{19}$$

Combining eqs.(17),(18), and (13) the Christoffel symbols of the second kind are[9,10]

$$\Gamma^1_{ij} = \begin{bmatrix} 0 & 0 & 0 \\ 0 & -v & 0 \\ 0 & 0 & -v^2\sin^2\theta \end{bmatrix} \quad \Gamma^2_{ij} = \begin{bmatrix} 0 & 1/v & 0 \\ 1/v & 0 & 0 \\ 0 & 0 & -\sin\theta\cos\theta \end{bmatrix} \quad \Gamma^3_{ij} = \begin{bmatrix} 0 & 0 & 1/v \\ 0 & 0 & \cos\theta \\ 1/v & \cos\theta & 0 \end{bmatrix} . \tag{20}$$

Let $\nabla f \equiv A_i$ in eq.(12), then

$$\nabla(\nabla f)_{i;k} = \frac{\partial(\partial f/\partial u_i)}{\partial u_k} - \Gamma^m_{ik}\frac{\partial f}{\partial u_m} \quad , \tag{21}$$

so that

$$\nabla\nabla f \equiv \nabla(\nabla f)_{i;k} = \begin{bmatrix} \frac{\partial^2 f}{\partial v^2} & \frac{\partial^2 f}{\partial v\partial\theta} - \frac{1}{v}\frac{\partial f}{\partial\theta} & 0 \\ \frac{\partial^2 f}{\partial v\partial\theta} - \frac{1}{v}\frac{\partial f}{\partial\theta} & \frac{\partial^2 f}{\partial\theta^2} + v\frac{\partial f}{\partial v} & 0 \\ 0 & 0 & v^2\sin^2\theta\frac{\partial f}{\partial v} + \sin\theta\cos\theta\frac{\partial f}{\partial\theta} \\ \frac{\partial f}{\partial\psi} \equiv 0 \quad . & & \end{bmatrix} \tag{22}$$

where

(23)

To find $\nabla(\nabla g)_{i;k} \equiv \nabla\nabla g$, simply replace f by g in eq.(22).

Since $\nabla\nabla f$ and $\nabla\nabla g$ are both second rank tensors, they may be contracted through the use of the metric tensor r^{ij} [10,11]

$$\nabla\nabla g : \nabla\nabla f \equiv r^{ik}r^{jl}g_{,kl}f_{,ij} = \tag{24}$$

$$\frac{1}{2}\frac{\partial^2 g}{\partial v^2}\frac{\partial^2 f}{\partial v^2} + (\frac{1}{v^2}\frac{\partial^2 g}{\partial v\partial\theta} - \frac{1}{v^3}\frac{\partial g}{\partial\theta})\frac{\partial^2 f}{\partial v\partial\theta} + (\frac{1}{2v^4}\frac{\partial^2 g}{\partial\theta^2} + \frac{1}{2v^3}\frac{\partial g}{\partial\theta})\frac{\partial^2 f}{\partial\theta^2}$$

$$+ (\frac{1}{2v^3}\frac{\partial^2 g}{\partial\theta^2} + \frac{1}{v^2}\frac{\partial g}{\partial\theta} - \frac{1}{v^3}\frac{\partial^2 g}{\partial v\partial\theta})\frac{\partial f}{\partial v} + (\frac{1}{v^4\sin\theta}(1 - \frac{\cos^2\theta}{2})\frac{\partial g}{\partial\theta} \tag{25}$$

$$- \frac{1}{v^3}\frac{\partial^2 g}{\partial v\partial\theta} + \frac{\cot\theta}{2v^3}\frac{\partial g}{\partial v})\frac{\partial f}{\partial\theta} \quad .$$

Since $\nabla^4 \equiv \nabla\nabla : \nabla\nabla$, in a similar manner

$$f\nabla^4 g = \frac{f}{2}\frac{\partial^4 g}{\partial v^4} + \frac{f}{v^2}\frac{\partial^4 g}{\partial v^2\partial\theta^2} + \frac{f}{2v^4}\frac{\partial^4 g}{\partial\theta^4} + \frac{f}{2v^3}\frac{\partial^3 g}{\partial\theta^3} - \frac{3f}{2v^3}\frac{\partial^3 g}{\partial\theta^2\partial v}$$
$$+ \frac{f}{v^2}\frac{\partial^2 g}{\partial v^2} + \frac{f\cot\theta}{v^3}\frac{\partial^2 g}{\partial\theta\partial v} + \frac{f}{v^4\sin\theta}(1 - \frac{\cos^2\theta}{2})\frac{\partial^2 g}{\partial\theta^2} \quad . \tag{26}$$

Referring to eq.(10)

$$-(\nabla^2 h)f = -\frac{f}{v^2}\frac{\partial}{\partial v}\left(v^2\frac{\partial h}{\partial v}\right) - \frac{f}{v^2\sin\theta}\frac{\partial}{\partial\theta}\left(\sin\theta\frac{\partial h}{\partial\theta}\right) \quad , \tag{27}$$

while

$$\nabla(\nabla^2 g)\cdot\nabla f = \frac{\partial}{\partial v}\left(\frac{1}{v^2}\frac{\partial}{\partial v}\left(v^2\frac{\partial g}{\partial v}\right)\right) + \frac{1}{\sin\theta}\frac{\partial}{\partial v}\left(\frac{1}{v^2}\frac{\partial}{\partial\theta}\sin\theta\frac{\partial g}{\partial\theta}\right)\cdot\frac{\partial f}{\partial v} +$$

$$\frac{1}{v^3}\frac{\partial}{\partial v}v^2\frac{\partial^2 g}{\partial v\partial\theta} + \frac{1}{v^2}\frac{\partial}{\partial\theta}\left(\frac{1}{\sin\theta}\frac{\partial}{\partial\theta}\left(\sin\theta\frac{\partial g}{\partial\theta}\right)\right)\frac{1}{v}\frac{\partial f}{\partial\theta} \quad . \tag{28}$$

Finally

$$-\nabla h\cdot\nabla f = -\frac{\partial h}{\partial v}\frac{\partial f}{\partial v} - \frac{1}{v^2}\frac{\partial h}{\partial\theta}\frac{\partial f}{\partial\theta} \quad . \tag{29}$$

By inserting eqs.(25-29) into eq.(10), eq.(1) becomes

$$\frac{1}{\Gamma}\left(\frac{\partial f}{\partial t}\right)_c = \frac{1}{v^2}\frac{\partial G}{\partial v} + \frac{1}{v^2\sin\theta}\frac{\partial H}{\partial\theta} \tag{30}$$

where

$$G \equiv Af + B\frac{\partial f}{\partial v} + C\frac{\partial f}{\partial\theta} \quad , \tag{31}$$

$$H \equiv Df + E\frac{\partial f}{\partial v} + F\frac{\partial f}{\partial\theta} \quad , \tag{32}$$

and

$$A = \frac{v^2}{2}\frac{\partial^3 g}{\partial v^3} + v\frac{\partial^2 g}{\partial v^2} - \frac{\partial g}{\partial v} - v^2\frac{\partial h}{\partial v} - \frac{1}{v}\frac{\partial^2 g}{\partial\theta^2} + \frac{1}{2}\frac{\partial^3 g}{\partial v\partial\theta^2}$$

$$- \frac{\cot\theta\,\partial g}{v\,\partial v} + \frac{\cot\theta}{2}\frac{\partial^2 g}{\partial\theta\partial v} \tag{33}$$

$$B = \frac{v^2}{2}\frac{\partial^2 g}{\partial v^2} \tag{34}$$

$$C = -\frac{1}{2v}\frac{\partial g}{\partial \theta} + \frac{1}{2}\frac{\partial^2 g}{\partial v \partial \theta} \tag{35}$$

$$D = \frac{\sin\theta \partial^2 g}{2v^2 \partial \theta^3} + \frac{\sin\theta}{2}\frac{\partial^2 g}{\partial v^2 \partial \theta} + \frac{\sin\theta}{v}\frac{\partial^2 g}{\partial v \partial \theta} - \frac{1}{2v^3 \sin\theta}\frac{\partial g}{\partial \theta}$$

$$+ \frac{\cos\theta \partial^2 g}{2v^2 \partial \theta^2} - \sin\theta \frac{\partial h}{\partial \theta} \tag{36}$$

$$E = \sin\theta \left[-\frac{1}{2v}\frac{\partial g}{\partial \theta} + \frac{1}{2}\frac{\partial^2 g}{\partial v \partial \theta} \right] \tag{37}$$

$$F = \frac{\sin\theta \partial^2 g}{2v^2 \partial \theta^2} + \frac{\sin\theta}{2v}\frac{\partial g}{\partial v} \quad . \tag{38}$$

In HYBRID III, θ is the angle between $\vec{v}$ and the magnetic or $\hat{z}$ axis. A normalizing velocity x may be defined as

$$v = \tilde{v}x \tag{39}$$

where $\tilde{v}$ is a constant. The particle distribution functions may then be normalized by

$$\bar{F}_\alpha \equiv \frac{v^3}{K_\alpha} f_\alpha(v,\theta,t) \text{ where } K_\alpha = n_\alpha(t=0), \tag{40}$$

so that eq.(27) becomes, again dropping the "α" subscript

$$\left(\frac{\partial F}{\partial t}\right)_C = \frac{K}{\tilde{v}^3}\left(\frac{1}{x^2}\frac{\partial \bar{G}}{\partial x} + \frac{1}{x^2 \sin\theta}\frac{\partial \bar{H}}{\partial \theta} \right) \tag{41}$$

where

$$\bar{G} = \bar{A}F + \bar{B}\frac{\partial F}{\partial x} + \bar{C}\frac{\partial F}{\partial \theta} , \tag{42}$$

$$\bar{H} = \bar{D}F + \bar{E}\frac{\partial F}{\partial x} + \bar{F}\frac{\partial F}{\partial \theta} , \tag{43}$$

and eqs.(28-38) are the same with $v \to x$, $g \to G$, $h \to H$, where

$$G_\alpha = \sum_\beta \ln\Lambda_{\alpha\beta} \frac{Z_\beta^2}{Z_\alpha^2} \frac{K_\beta}{K_\alpha} g_\beta \tag{44}$$

$$H_\alpha = \sum_\beta \ln\Lambda_{\alpha\beta} \frac{Z_\beta^2}{Z_\alpha^2} \frac{K_\beta}{K_\alpha} \left(1+ \frac{m_\alpha}{m_\beta}\right) h_\beta \quad . \tag{45}$$

The Rosenbluth potentials are defined[3,8]

$$\nabla^4 g = -8\pi F \tag{46}$$

and

$$\nabla^2 h = -4\pi F \quad . \tag{47}$$

To solve eqs.(46) and (47), F, g, and h are expanded using Legendre polynomials[10]

$$F(x,\theta) = \sum_{j=0}^{M} v_j(x) P_j(\cos\theta) \quad , \tag{48}$$

$$g(x,\theta) = \sum_{j=0}^{M} \hat{G}_j(x) P_j(\cos\theta) \quad , \tag{49}$$

$$h(x,\theta) = \sum_{j=0}^{M} \hat{H}_j(x) P_j(\cos\theta) \quad , \tag{50}$$

where

$$P_0 = 1 \ , \qquad P_1(\mu) = \mu \ , \qquad P_2(\mu) = \tfrac{1}{2}(3\mu^2-1) \ ,$$
$$P_3(\mu) = \tfrac{1}{2}(5\mu^2-3\mu) \ , \quad jP_j(\mu) - (2j-1)\mu P_{j-1}(\mu) + (j-1)P_{j-2}(\mu) = 0 \tag{51}$$
$$\mu = \cos\theta \qquad\qquad j = 2,3, \ldots$$

Using eqs.(48-50)

$$\hat{H}_j(x) = \frac{4\pi}{2j+1}\int_0^x dx' V_j(x')\frac{x'^{j+2}}{x^{j+1}} + \frac{4\pi}{2j+1}\int^{\infty} dx' V_j(x')\frac{x^j}{x'^{j+1}} \quad (52)$$

$$\hat{\hat{G}}_j(x) = -\frac{4\pi}{(4j^2-1)}\int_0^x dx'\frac{x'^{j+2}}{x^{j-1}}\left(1-\frac{j-1/2}{j+3/2}\frac{x'^2}{x^2}\right)V_j(x')dx'$$

$$-\frac{4\pi}{(4j^2-1)}\int_x^{\infty} dx'\frac{x^j}{x'^{j-3}}\left(1-\frac{j-1/2}{j+1/3}\frac{x^2}{x'^2}\right)V_j(x') \quad . \quad (53)$$

Defining the functionals

$$M_j(f(x)) = \int_x^{\infty} f(y)y^{1-j}dy \quad (54)$$

$$N_j(f(x)) = \int_0^x f(y)y^{2+j}dy \quad (55)$$

$$R_j(f(x)) = \int_x^{\infty} f(y)y^{3-j}dy \quad (56)$$

$$E_j(f(x)) = \int_0^x f(y)y^{4+j}dy \quad (57)$$

eqs. (52) and (53) become

$$\hat{\hat{H}}_j = \frac{4\pi}{(2j+1)}\left(x^{-j-1}N_j(V_j) + x^jM_j(V_j)\right) \quad (58)$$

$$\hat{\hat{G}}_j = \frac{4\pi}{(2j+1)}\frac{1}{(2j+3)}\left(x^{-j-1}E_j(V_j) + x^{j+2}M_j(V_j)\right)$$

$$-\frac{1}{(2j-1)}\left(x^{1-j}N_j(V_j) + x^jR_j(V_j)\right) \quad . \quad (59)$$

In a similar fashion, the electron collision operator may be calculated. Since the electrons in HYBRID III are [illegible] in velocity space, all the angular

assumed to be isotropic in velocity space, all angular derivatives in eqs.(33)-(38) are set to zero and the angle dependent components in the Rosenbluth potentials are dropped. The angle dependent terms in eqs.(33)-(59) are retained for α=d,t. At each time step, the functionals eqs.(56)-(59) are evaluated. These determine the Rosenbluth potentials which in turn are used to evaluate the collision operators.

APPENDIX C

From Sec.III-B eq.(47), one term of C may be written as

$$C = \frac{|E_+^2|^2}{32Z^2e^2n_o}\,\delta(n\omega_{c\alpha}-\omega-k_\parallel v_\parallel)J_{n-1}^2 \tag{1}$$

where $J_n \equiv J_n(k_\perp v_\perp/\omega_{c\alpha})$.

With

$$k_\parallel = (m-l)q/qR \tag{2}$$

and with m=0, l=50 and $R\simeq R_o$=500 cm,

$$k_\parallel = -.1\ \text{cm}^{-1} \equiv -k_\parallel' \tag{3}$$

so that

$$C = \frac{|E_+|^2}{32Z^2e^2n_o}\,\delta(n\omega_{c\alpha}-\omega-k_\parallel' v_\parallel)J_{n-1}^2 \quad . \tag{4}$$

On averaging over θ

$$\langle C\rangle_\theta \simeq \frac{|E_+|^2}{32\pi Z^2e^2n_o}\,J_{n-1}^2\int_0^\pi \delta(n\omega_{c\alpha}-\omega-k_\parallel' v_\parallel)d\theta \quad . \tag{5}$$

Letting

$$x \equiv \frac{\omega}{n\omega_{c\alpha}} = \frac{n\omega_{c\alpha o}R_o}{R_o+a\sin\theta} \tag{6}$$

then

$$dx = -\frac{n\omega_{c\alpha o}R_o a\cos\theta}{(R_o+a\sin\theta)^2}\,d\theta = -\frac{a\cos\theta x^2}{R_o n\omega_{c\alpha o}}\,d\theta \quad . \tag{7}$$

Therefore

$$d\theta = - \frac{n\omega_{c\alpha o} R_o}{ax^2 \sin\theta} dx \quad . \tag{8}$$

Since $\sin\theta = (R/a)(n\omega_{c\alpha o}/x - 1)$

$$\cos\theta = (1 - (R/a)^2 (n\omega_{c\alpha o}/x - 1)^2)^{1/2} \equiv \xi(x) \quad . \tag{9}$$

Therefore

$$d\theta = - \frac{n\omega_{c\alpha o} R_o}{ax^2 \xi(x)} dx \tag{10}$$

and

$$\langle C \rangle_\theta = - \frac{|E_+|^2 J_{n-1}^2 R_o n\omega_{c\alpha o}}{32\pi Z^2 e^2 n_o a} \int_o^\pi \frac{\delta(x - k_\parallel' v_\parallel - \omega)}{x^2 \xi(x)} dx \tag{11}$$

$$= \frac{|E_+|^2 J_{n-1}^2 R_o n\omega_{c\alpha o}}{32\pi Z^2 e^2 n_o a (\omega + k_\parallel' v_\parallel)^2 \xi(x_o)} \tag{12}$$

where

$$\xi(x_o) \equiv \{1 - (\frac{R}{a})^2 (\frac{n\omega_{c\alpha o}}{\omega + k_\parallel' v_\parallel} - 1)^2\}^{1/2} \quad . \tag{13}$$

Since $\omega + k_\parallel' v_\parallel = n\omega_{c\alpha o}$,

$$\langle C \rangle_\theta = \frac{|E_+|^2 J_{n-1}^2 \omega_{c\alpha o} R_o}{32 Z^2 e^2 n_o a \pi n^2 \omega_{c\alpha}^2 \xi(x_o)} \simeq \frac{|E_+|^2 J_{n-1}^2 R}{32\pi Z^2 e^2 n_o a n \omega_{c\alpha o} \xi(x_o)} \tag{14}$$

with $\omega_{c\alpha} \simeq \omega_{c\alpha o}$.

A similar procedure may be used to derive the other two terms of the expression for C given in Sec.III eq.(48).

Appendix D

Low Frequency Alfven Wave Heating

D-1. Theory of Alfven Wave Heating

In this section the feasibility of heating a fusion test reactor is examined. Due to the assumed near term time frame of the TETR[2] machine, with its TCT mode of operation, an RF heating technique which complements the primary neutral beam supplementary heating is considered. The concept of RF clamping of neutral beam heated plasmas seems attractive but the analysis is complex and no theoretical work on this subject has been published. The initial rationale was that by heating the electrons to sufficiently high temperatures, one could improve the efficiency of producing beam-plasma fusions. The beam would have a higher probability of slowing down on the tritons rather than the electrons. In Appendix D-2, the results of heating TETR by electron Landau damping of the low frequency fast Alfven wave are examined.

However, a test reactor need not operate in a TCT mode. Perkins[1] has investigated the feasibility of heating TFTR (see Tables (1-2)) using 50 MW of RF power at 50 MHz at the second harmonic of tritium. Since TFTR is a mixture of 50-50 D-T, one does not need to rely on neutral beam produced TCT fusions for heating. By heating at the second harmonic of tritium, the deuterons do not see a resonant frequency, consequently, mode conversion processes should not occur.

Since TETR must use neutral beams we now investigate a possible heating scheme first proposed by Stix.[3] Stix suggested that the heating of electrons would be possible using the low frequency fast magnetosonic or compressional Alfven wave where $\omega<\omega_{ci}$. Through the resonant excitation of this mode, the plasma would be heated by both electron Landau and transit time magnetic damping.

Both Landau damping and transit time damping involve energy absorption by electrons travelling along $\vec{B}$ with the phase velocity of the excited RF wave ($\omega - k_{\parallel} v_{\parallel_e} = 0$). In Landau damping, the force accelerating the particle is $q\vec{E}$ while the transit time force is $-\mu\nabla\vec{B}$. From the weak damping formula (Sec. I, Eq. (3)), the K_{yy}, K_{zy}, K_{yz} and K_{zz} dielectric terms with the electron resonance condition satisfied lead to energy absorption by the electrons.

There are several advantages to heating at this low frequency.[3] First of all, from the general dispersion relation of Eq. (30) in Sec. I, lowering the frequency tends to increase the wavelength of the excited wave and thereby reduces the mode density. This effect enables mode tracking to be more easily accomplished with a resultant better coupling between the RF and the plasma. Secondly, the electron heating processes are well known, both theoretically as well as experimentally verified. Thirdly, the driving frequency is well below the cyclotron frequencies of most of the possible impurity ions which may be prevalent in reactors (O,Fe and C) so that RF induced sputtering should be reduced. In addition, no nonlinear processes which might lead to plasma surface heating have been seen at this low frequency. Finally, at this low frequency regime (.1-1. MHz) RF power supplies in the MW range are already available and the coupling of the RF to the plasma may be done with simple coils.

An alternative low frequency heating scheme proposed by others[3-8] makes use of the continuous spectrum modes which are strongly coupled to the critical layer where the shear Alfven wave dispersion relation is satisfied

$$\omega^2 = k_{\parallel}^2 v_A^2 = \frac{k_{\parallel}^2 B^2}{4\pi\rho(r)} \quad . \qquad (1)$$

This heating scheme, called resonant Alfven wave heating, makes use of the nonuniformity of the plasma. The RF power is coupled to a surface wave which is a cutoff electromagnetic wave rather than a surface eigenmode in the fast wave case. To couple to a surface wave one must choose $k_{\perp}$, the wavenumber perpendicular to both the density gradient and B_0, larger than $k_{\parallel}$ so that the driving frequency $\omega_0 < k_{\perp} v_A$ for the minimum Alfven speed. For TETR parameters (see Table (1)), the driving frequency would have to be between 56 kHz and 184 kHz which is far below our proposed frequency. Therefore, this heating process should not compete with proposed fast wave heating. In addition to using slow wave heating, one would need $k_{\perp} < \rho_i^{-1}$ so as to prevent finite Larmor radius coupling between the shear and compressional waves.[14]

The plasma nonuniformity allows the shear Alfven, magnetosonic and ion acoustic waves to all be coupled together. A singularity arises in the MHD equations where

$$\omega = k_{\parallel} v_A(r=r_o) \quad . \qquad (2)$$

This singularity causes wave phase mixing which dissipates the excited wave energy. This dissipated energy flows to other waves with continuous spectrums such as Landau damping. Ohmic and viscous dissipation destroys the reversibility of this process and the dissipated energy is converted to thermal energy.

The externally applied oscillating magnetic field resonantly mode converts to a kinetic Alfven wave which propagates in the higher density side of the conversion zone. The kinetic Alfven wave may then decay into another Alfven wave and an ion acoustic wave. For ($T_e \leq 5T_i$) the ions are heated through nonlinear ion Landau damping. In addition, Landau damping of the mode converted kinetic wave leads to electron heating.[8] For low β machines the ratio of ion heating to electron heating is given by[8]

$$\left(\frac{dT_i/dt}{dT_e/dt}\right) \sim \left(\frac{2M_i}{m_e}\right)^{1/2} \left(\frac{T_e}{T_i}\right)^{3/2} e^{-\beta_i^{-1}} \ll 1 \qquad (3)$$

so that most of the power flows to the electrons. Since these heating processes occur after mode conversion, undesirable surface heating can be avoided. Unfortunately, Stix[3] has stated that this heating process is inherently low Q (Q~3). Therefore, coupling to the plasma may be difficult. For this reason as well as the fact that the frequency needed is well below the frequency we propose to heat TETR with, we do not examine resonant Alfven wave heating further.

For a given density and machine size, Eq. (2) in Sec. I can be viewed as a low frequency cutoff, below which no toroidal eigenmodes may be excited. For the proposed heating frequency of $\omega = .01\omega_{cd}$, we cannot satisfy this equation since Eq. (2) yields

$$n_e a^2 \geq 1.5 \times 10^{20} \; . \qquad (4)$$

Since we have chosen this frequency so as to avoid coupling to the shear wave, as well as to insure having significant electron heating

($\omega/k_{\parallel}v_{\parallel_e} \sim 1$), we cannot expect to have eigenmode enhancement. However, as we show in the next section, fast wave heating still obtains high Q's, even without the presence of toroidal modes.

D-2. Fast Alfven Wave Electron Heating of TETR Plasma

In this section we investigate the heating of TETR with the low frequency fast Alfven wave, $\omega = 0.01\omega_{cd}$, corresponding to a frequency of 300 kHz in a 40 kG toroidal field. Mode conversion effects can be neglected since no hydrogen resonance occurs within the device. In the limit of weak damping, the power absorbed is given by

$$P_e = \frac{\omega_{pe}^2\omega^2 v_e |B_z|^2 e^{-(\omega/k_{\parallel}v_e)^2}}{8\pi^{1/2}\omega_{ce}^2 c^2 k_{\parallel}} \quad (\text{watts/cm}^3) \qquad (1)$$

with

$$v_e = \left(\frac{2kT_e}{m_e}\right)^{1/2} \qquad \omega_{ce} = \frac{-eB_o}{m_e c} \qquad \omega_{pe} = \left(\frac{4\pi n_e e^2}{m_e}\right)^{1/2}$$

with $\nabla \times \bar{B} = \frac{4\pi\bar{J}}{c}$ neglecting the displacement current.

In order for an appreciable amount of power to be absorbed by the electrons, $k_{\parallel}$ was chosen to be 0.001 cm^{-1}. Since $k_{\parallel}$ is small, hot plasma

effects can be neglected and one may use cold plasma theory in calculating $k_\perp$. For fast magnetosonic waves in an unbounded plasma we can write

$$k_\perp = [k_\parallel^4 - 2k_o^2 k_\parallel^2 + k_o^4 RL/S]^{1/2}/[k_o^2 - k_\parallel^2/S]^{1/2} \qquad (2)$$

with $k_o^2 = \omega^2/c^2$ and R, L, S defined by Stix.[5] We obtain $k_\perp = 0.003\ cm^{-1}$ for TETR with an average density of $7.5 \times 10^{13}\ cm^{-3}$.

The quality factor Q may be calculated in order to obtain an estimate of the absorption of the RF power in the walls. The Q of the walls is approximately given by

$$Q_w = a/\delta \qquad \text{where } \delta = (\pi f \mu \sigma)^{-1/2}$$

δ is the skin depth and σ is the electrical conductivity. At room temperature for 316 stainless steel $\sigma = 3.33 \times 10^6\ (\Omega m)^{-1}$ and $Q_w = 1600$ while at 500°C $\sigma = 9.5 \times 10^5\ (ohm\text{-}m)^{-1}$ and the resultant $Q_w = 850$.

The Q of the plasma may be defined as

$$Q_p = \frac{\omega U}{P_e} = \frac{k_\parallel \omega_{ce}^2\, c^2 e\, (\omega/k_\parallel\, v_e)^2}{\pi^{1/2}\, v_e\, \omega \omega_{pe}^2}$$

where $U = |B_z|^2/8\pi$

At $T_e = 1$ keV, $Q_p = 3660$ while at 10 keV, Q_p drops to a value of 160. Q_p approaches a minimum value when $k_\parallel = .001\ cm^{-1}$ and $\omega = .01\ \omega_{cd}$. This minimum value does not change as long as $k_\parallel/\omega$ is constant. Q_p increases when either $k_\parallel$ or ω is changed. Q_p is relatively sensitive to changes in T_e as can be seen from the two values given above. On the other hand, Q_w

may be raised to an acceptable value by raising both the frequency and $k_{\parallel}$. Thus, due to the plasma volume to surface area and magnetic field intensities in TETR the use of low frequency fast Alfvén wave heating does not seem attractive. However, for larger devices and higher toroidal magnetic field strengths, this technique is more attractive.

The electron power absorption density given by Equation (3) was included in an explicit fluid model space-time code which solves both ion and electron energy balance equations as well as the particle balance equation used in the point code. The ion and electron equations are again given by Sec. (II-A)[10]

$$\frac{\partial n_i T_i}{\partial t} = -4.28 \times 10^{-11} n_i n_e \frac{(T_i - T_e)}{3/2} + \frac{1}{1.5r}\frac{\partial}{\partial r}(r n_i \chi_i \frac{\partial T_i}{\partial r}) - \frac{1}{r}\frac{\partial}{\partial r}(r n_i V_i T_i)$$

$$+4.17 \times 10^{15} \{n_D n_T \langle\sigma v\rangle_{DT} U_{\alpha i} + P_{inj}(U_{bi} + f(\frac{E_\alpha}{E_B})U_{\alpha i})\} \qquad (3)$$

and

$$\frac{\partial n_e T_e}{\partial t} = 4.28 \times 10^{-11} n_e n_i \frac{(T_i - T_e)}{T_e\ 3/2} + \frac{1}{1.5r}\frac{\partial}{\partial r}(r n_e \chi_e \frac{\partial T_e}{\partial r}) - \frac{1}{r}\frac{\partial}{\partial r}(r n_e V_e T_e)$$

$$+4.17 \times 10^{15} \{n_D n_T \langle\sigma v\rangle U_{\alpha e} + \underline{E} \cdot \underline{J} + P_{inj}(U_{be} + f(\frac{E_\alpha}{E_b})U_{\alpha e}) \qquad (4)$$

$$- P_{RF} - P_B - P_S\} .$$

T_i,(e) is the ion (electron) temperature (eV), n_i,(e) is the ion (electron) density (cm^{-3}), V_i,(e) is the ion (electron) velocity (cm/ms), J is the toroidal current density (amp/cm^2), E is the toroidal electric field (volt/cm), r is the radius (cm), t_2 is time (ms), χ_i,(e) is the ion (electron) thermal diffusivity (cm^2/ms), U_{bi},(e) is the fraction of alpha energy going to ions

(electrons), and f is the fraction of deuterons in the neutral beam which undergo fusion as they slow down in a tritium target plasma. P_B and P_S represent bremsstrahlung and synchrotron radiation, respectively (watts), (given in Sec. (II-A)) and P_{RF} is the injected RF power (watts).

In Equation (3), B_z was normalized so that $B_z = B_{zo}J_m(k_\perp r)$ (3) where B_{zo} is a constant such that $B_{zo}^2 = P_{RF}/2\pi^2 R_o \int_o^a J_m^2(k_\perp r)rdr$ where R_o is the major radius, a is the minor radius and P_{RF} is the amount of injected RF power.

The initial temperature and density profiles were assumed parabolic with $T_e=T_i$ and taken to be 500 eV and 2×10^{14} cm^{-3} at the center and 135 eV and 1.9×10^{13} cm^{-3} at the edge. The diffusion coefficients were optimistically taken to be one-tenth the value of that obtained using trapped particle modes scaling (see Sec. (II-A)).

We decided to first examine the m=1 mode which peaks the electron temperature and RF injected power near the edge as shown in Figures D-1 and D-2. It was thought that by heating the electrons near the edge, the neutral beam particles would impart their kinetic energy more efficiently to the ions resulting in more beam plasma fusions. Figures D-2 and D-3 display the electron and ion temperature profiles as they evolve in time when 50 MW of RF power was used to preheat the plasma for 500 ms before 150 MW of neutral beams were turned on. The electrons reached an average value of 5 keV with a peak near the edge of 12.5 keV after 500 ms. The ions, after the 500 ms, reached an average value of 2 keV with a peak near the center of 2.4 keV. However, as seen in Figures D-2 and D-3, within 300 ms after the neutral beams are turned on, the plasma reaches the same operating conditions as those obtained with neutral beams without an RF preheat. Similar results were obtained when 150 MW of RF was used to preheat the electrons for 500 ms. In this case the electrons reached a peak of 29.8 keV with an average value of 24.0 keV while the ion temperatures were 2.4 keV and 4.0 keV respectively.

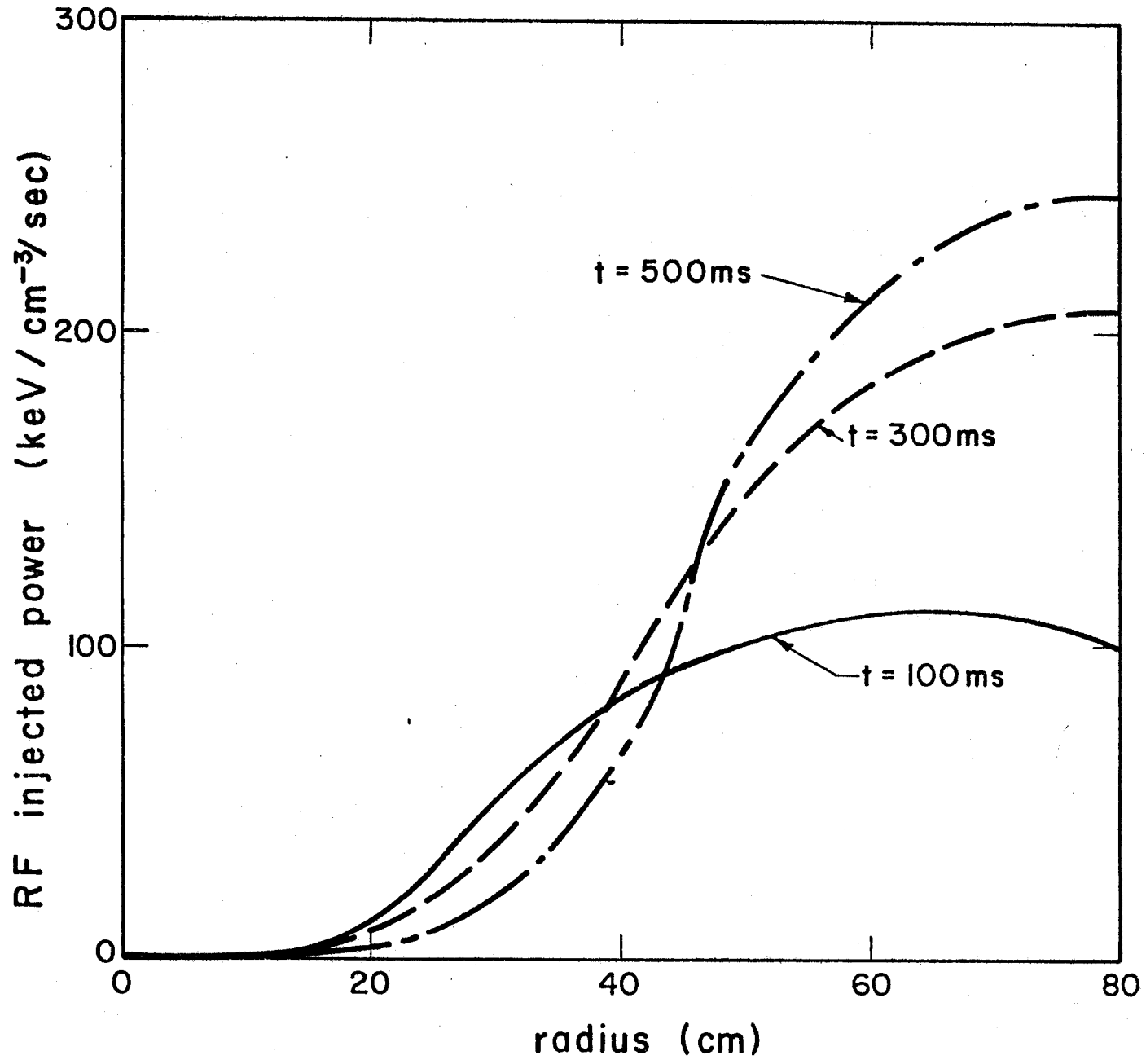

RF heating profile as a function of time with 50 MW supplied. In this case, $k_{||} = 10^{-3}cm^{-1}$, $\omega = 10^{-2}\omega_{CD}$ and the m=1 mode was assumed.

Figure D-1

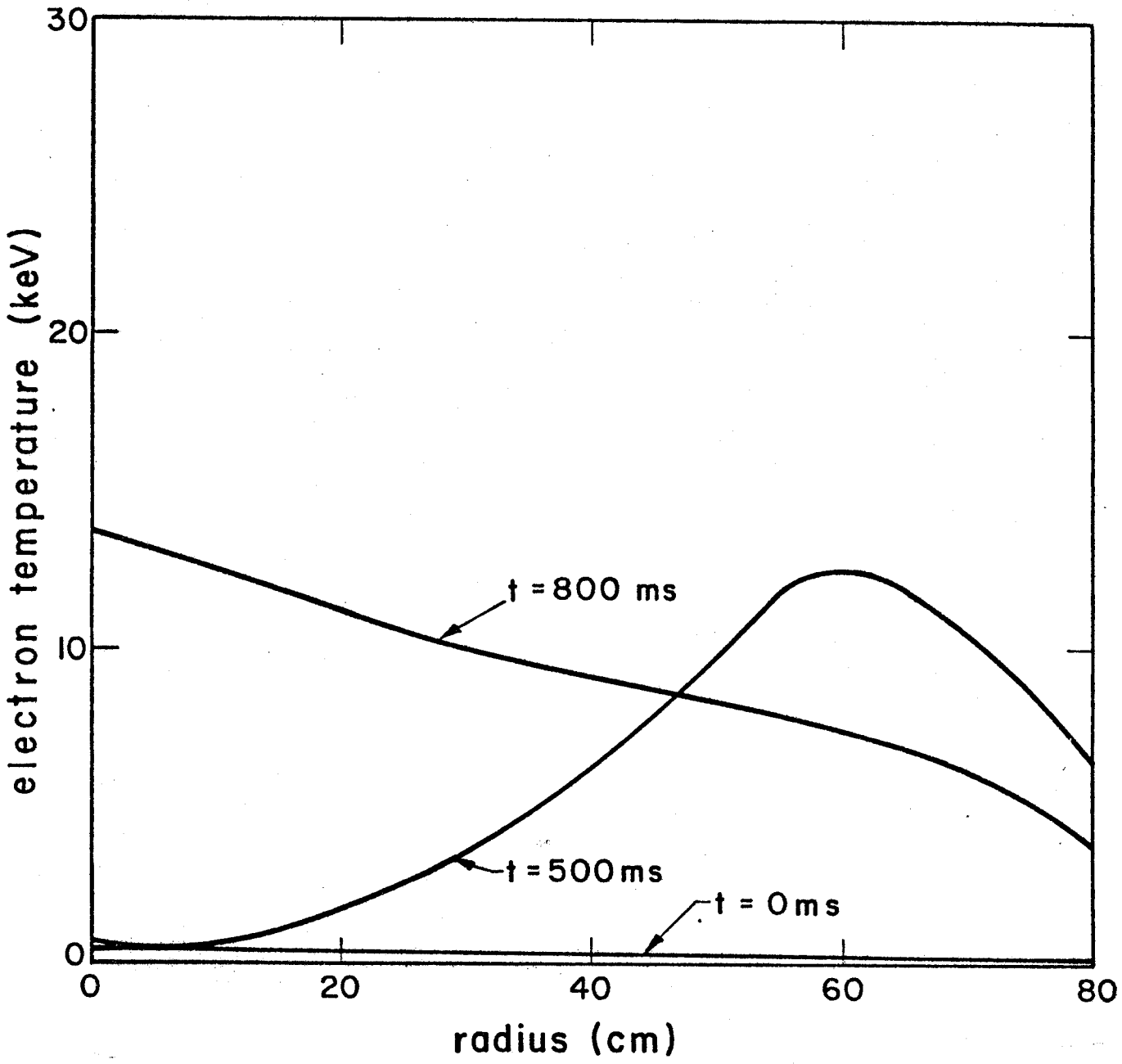

Electron temperature profile when 50 MW of RF power is supplied in the initial 500 ms of heating. After 500 ms, the RF is turned off and 150 MW of neutral beams are injected. In the RF phase $k_{\parallel} = 10^{-3}cm^{-1}$, $\omega = 10^{-2}\omega_{CD}$ and the m=1 mode was assumed.

Figure D-2

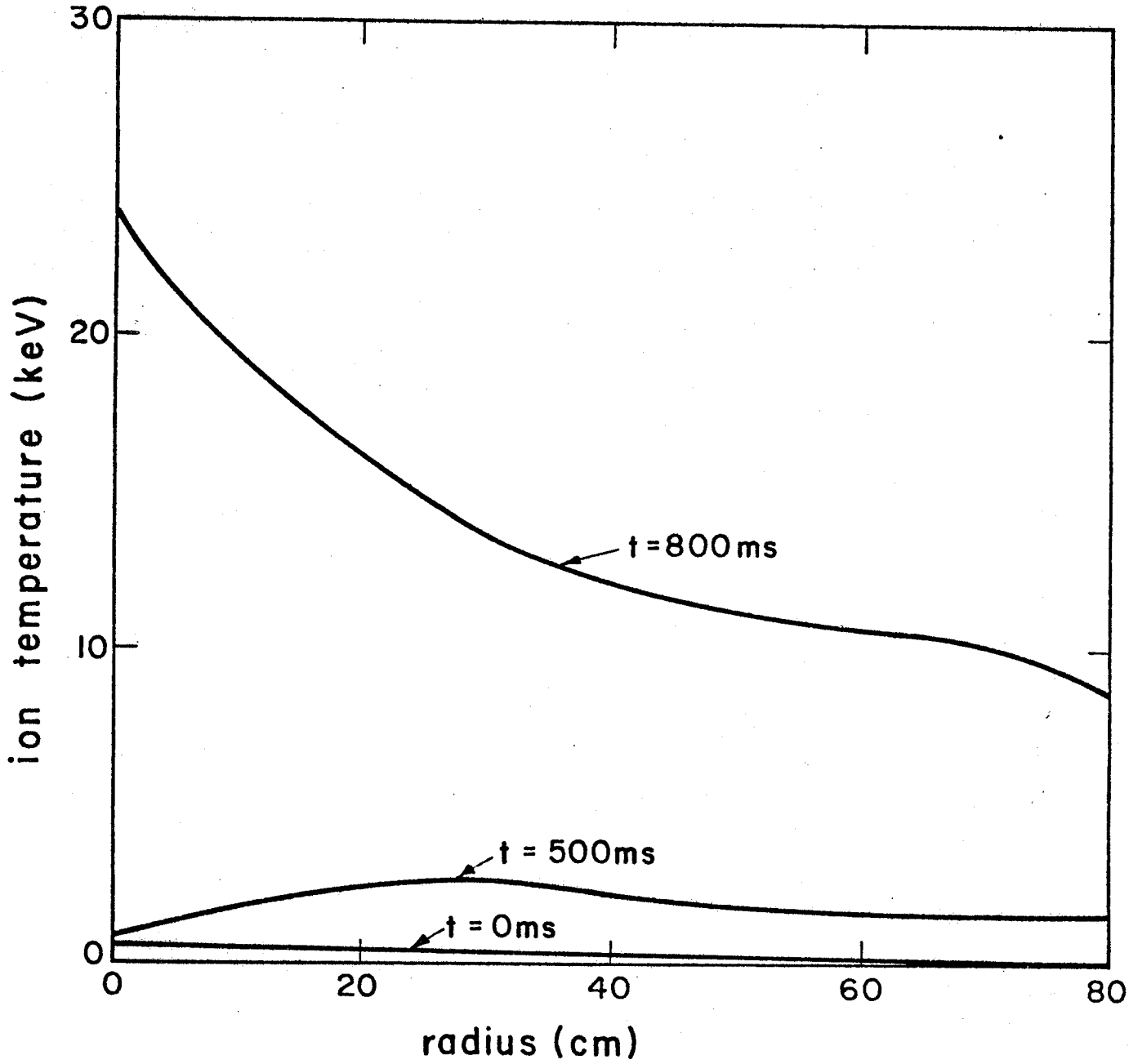

Ion temperature profile when 50 MW of RF power is supplied in the initial 500 ms of heating. After 500 ms, the RF is turned off and 150 MW of neutral beams are injected. In the RF phase, $k_{\parallel} = 10^{-3}cm^{-1}$, $\omega = 10^{-2}\omega_{CD}$ and the m=1 mode was assumed.

Figure D-3

When the 150 MW of RF was used, the neutral beams produced more fusions in their initial 50 ms than without the RF preheat. However, the 150 MW of RF power produced less than 0.1 MW of fusion power in the preheat phase while the neutral beams would have produced over 50 MW of power in this same period. Therefore, any increase in the efficiency of the neutral beams was not great enough to offset the initial loss of fusion power. TETR reached the same operating parameters as those without an RF preheat within 300 ms because both τ_p and τ_E are of the order of 100 ms, τ_p and τ_E are purposely kept short in order that a high flux of neutrons can be obtained for the various engineering and materials tests.

We then proceeded to investigate the possibility of increasing the amount of alpha fusions by dividing 150 MW of injected power between the RF and neutral beams. Figure D-4 is a plot of the power from the alpha fusions as the RF power varies from 0 to 50 MW while the total input power is kept constant. In Figure D-5 we notice that the injected power to the ions, and consequently the ion temperature, drops as the proportion of RF power increases. In Figure D-6 we see that though the injected power supplied to the electrons increases, P_B, the power supplied to the electrons from the neutral beams decreases, as does the beam power supplied to the ions. We also notice that as the amount of RF power increases, the power delivered to the electrons via alpha fusions and ion-electron collisions, as well as the diffusion power caused by colder electrons leaving an area rather than entering decreases. The net result of this is that as the RF power is increased, the ion temperature steadily drops from an average value of 13.4 keV to 10.0 keV while the electron temperature rises slightly from 9.2 keV to 9.4 keV. Therefore, there appears to be no advantage to using RF heating in this manner for the TETR tokamak.

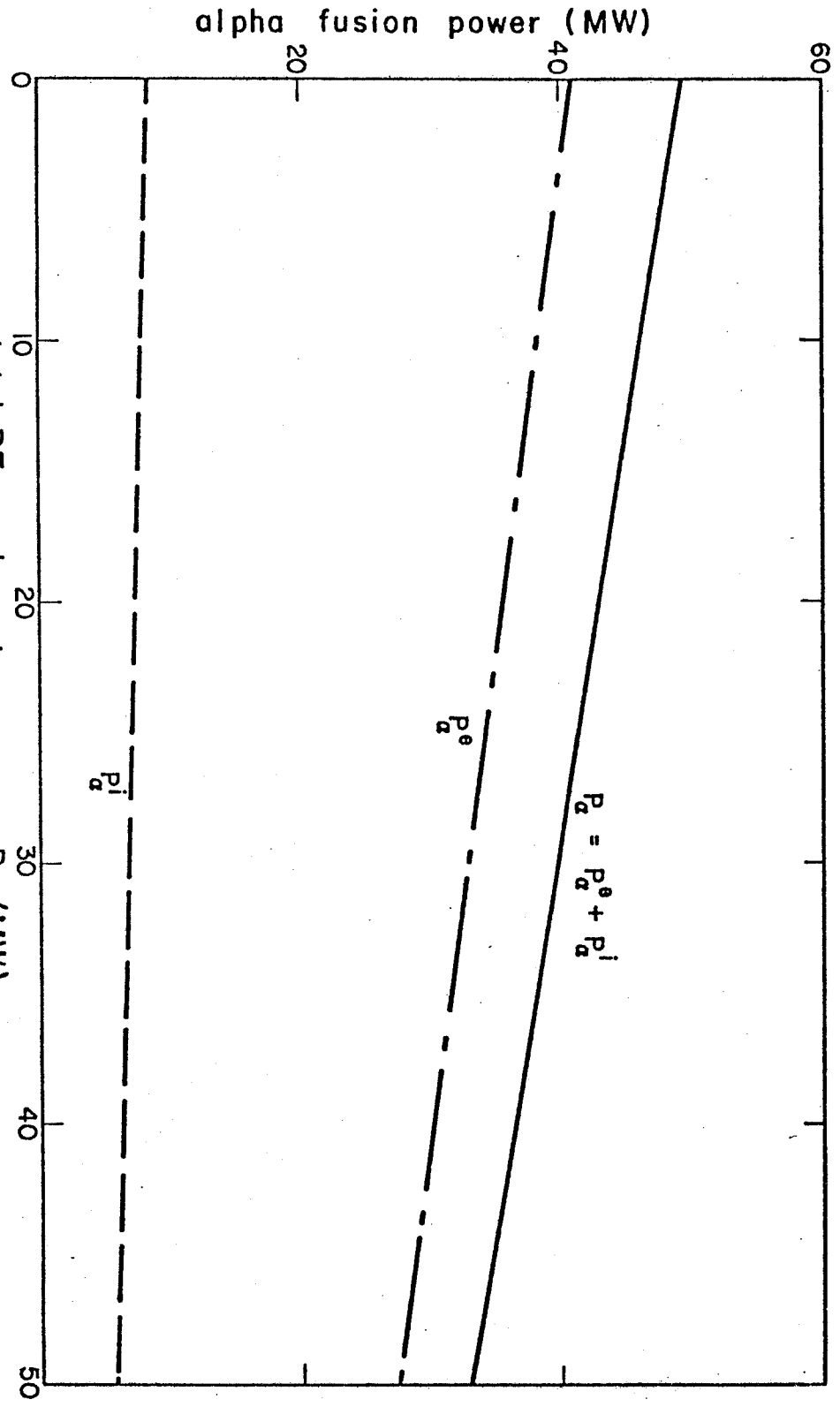

Alpha fusion power produced as a function of RF supplementary power. The total injected power is maintained at 150 MW. $\omega = 10^{-2}\omega_{CD}$, $k_{//} = 10^{-3}cm^{-1}$ and $t = 1.5$sec. In addition, an m=1 mode and the diffusion coefficients one-tenth those of trapped particle scaling were assumed.

Figure D-4

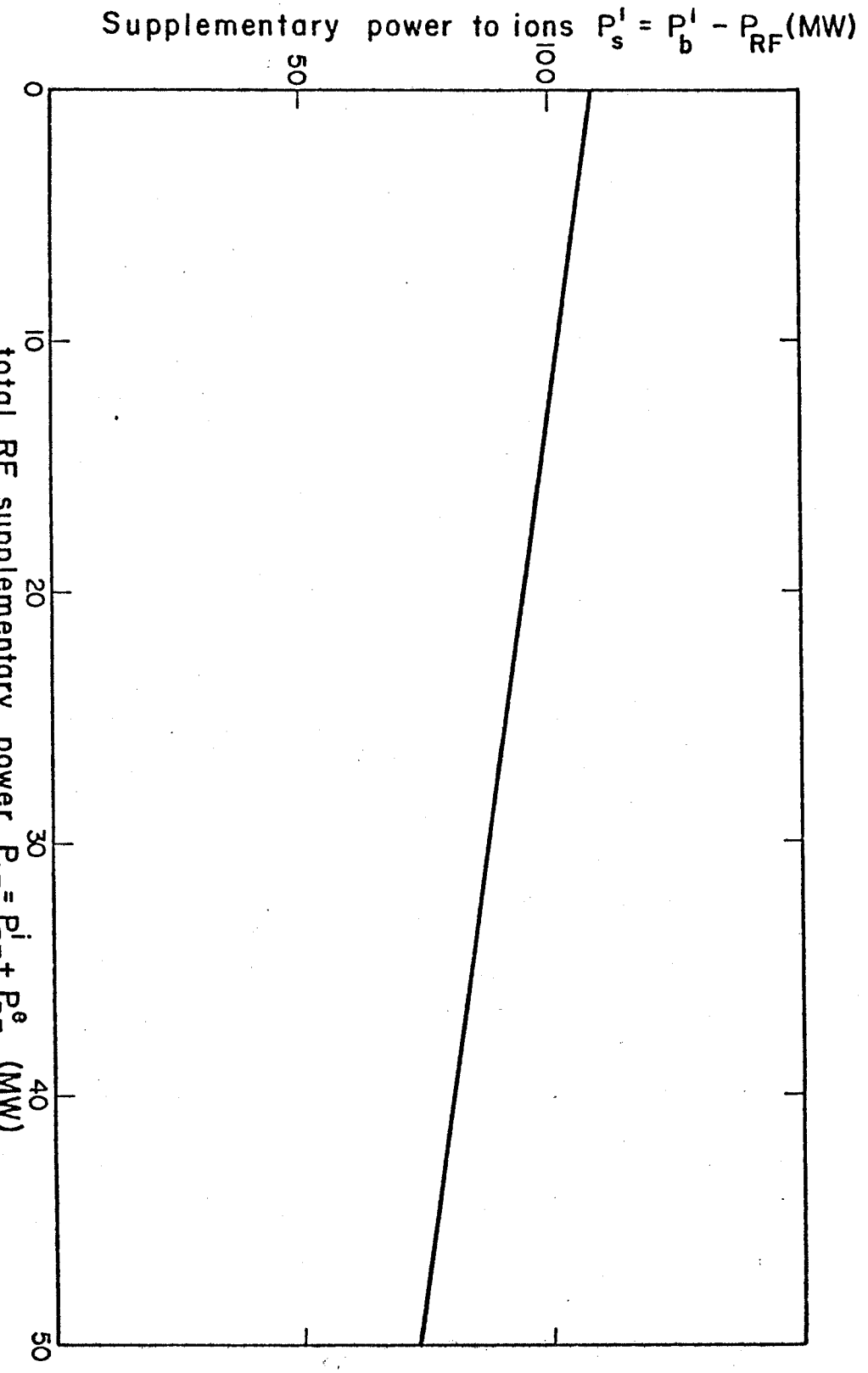

Power supplied to the ions from the neutral beams as the RF injected power varies from 0 to 50 MW. The total injected power remains constant at 150 MW. In this case, $\omega = 10^{-2}\omega_{CD}$, $k_{||} = 10^{-3}cm^{-1}$ and t = 1.5 sec. In addition, the m=1 mode and the diffusion coefficents one-tenth trapped particle scaling were assumed.

Figure D-5

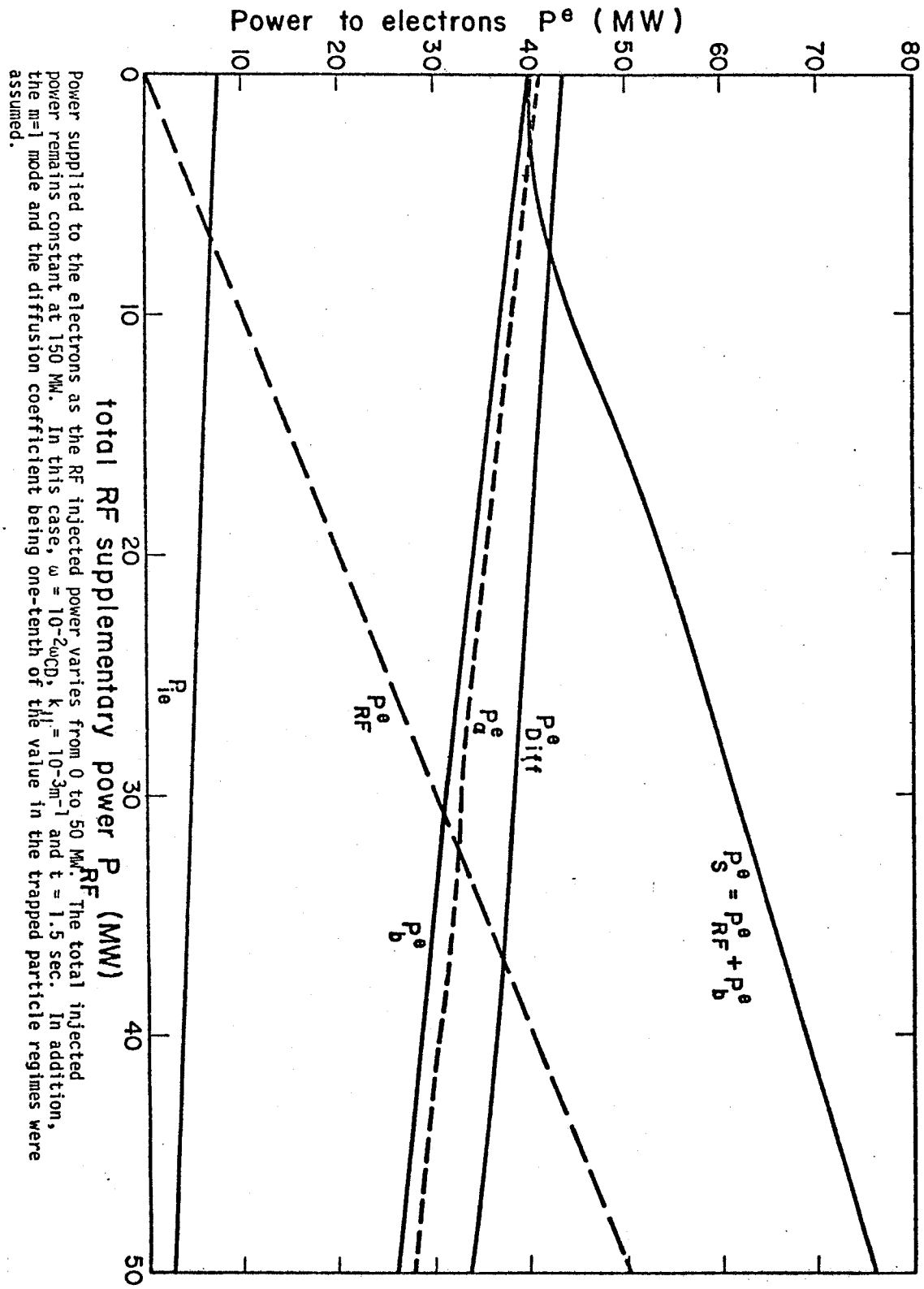

Power supplied to the electrons as the RF injected power varies from 0 to 50 MW. The total injected power remains constant at 150 MW. In this case, $\omega = 10^{-2}\omega_{CD}$, $k_{\parallel} = 10^{-3}m^{-1}$ and $t = 1.5$ sec. In addition, the m=1 mode and the diffusion coefficient being one-tenth of the value in the trapped particle regimes were assumed.

Figure D-6

Since τ_p and τ_E are short, the profile relaxation time is on the order of 300 ms as compared to a burn time of 60 s. Consequently, RF heating profile effects do not alter our results. However, transport scaling may be quite important. If different scaling is assumed so that the neutral beams could not heat the electron temperature past 8 keV, the RF power would make the beams more efficient in creating fusions. Above 8 keV, Q_F, the ratio between fusion output power and injected power only slightly increases as the electron temperature increases. However, when trapped particle scaling is assumed, the manner in which TETR operates essentially precludes RF efficient utilization of the fast Alfvén wave to heat the electrons and provide more fusion output power from the neutral beams.

References

(1) F.W. Perkins, "The ICRH Tokamak Fusion Test Reactor", Princeton Report, TM-284 (Aug. 1975).

(2) TETR FDM.

(3) T.H. Stix, "Fast Wave Heating of a Reactor Plasma: Consideration of Two Frequency Regimes", Proc. of the 3rd Symposium on Plasma Heating of Toroidal Devices, Varenna, Italy (Sept. 1976).

(4) A. Hasegawa and L. Chen, Phys. Rev. Letters 32, p. 454 (1974).

(5) L. Chen and A. Hasegawa, Phys. of Fluids 17, p. 1399 (1974).

(6) J.A. Tataronis, J. Plasma Physics 13, p. 87 (1975).

(7) A. Hasegawa and L. Chen, Phys. Rev. Letters 35, p. 370 (1975).

(8) A. Hasegawa and L. Chen, PPPL-1286 (Sept. 1976), Phys. of Fluids 19, 1924 (1976). F.W. Perkins, Bull. Am. Phys. Soc. 23, 864 (1978).

(9) T.H. Stix, Theory of Plasma Waves, McGraw-Hill Book Co., New York (1962), pp. 10, 707.

(10) B. Badger, et al., "UWMAK-III, A Noncircular Tokamak Power Reactor Design", Nucl. Eng. Dept Report UWFDM-150 (Univ. of Wisconsin-Madison, July 1976).

TABLE 1 TOKAMAK PARAMETERS

DEVICE	COUNTRY	R_o (cm)	a (cm)	B_T (kG)	I_p (kA)	$\bar{n}$ 10^{13} cm^{-3}	T_i (keV)	T_e (keV)	q	τ_E (ms)	YEAR
ALCATOR	USA	54	12	80	100	53	800	1200	6	20	1979
ATC	USA	88-35	17-11	17	80-200	1.5	250	1100	4.1	5-11	1976-7
DIVA	JAPAN	68	28x43 cross section	16-20	15	1.0	150	200	0.7	16-20	1978
ERASMUS	BELGUIM	50	50x50 cross section	3.6-4	30-50	0.2-1.2		300		0.7	1978
MACROTOR	USA	95	96x150 cross section	2	60	∿1.0		∿100			1978
MICROTOR	USA	30	20x25 cross section	10-25	30-100	>1.0	40-60	100-300		3.	1978
PLT	USA	130	40	25-46	540	3.5-10	1000	2500	3.6	40	1978-9
ST (phase I)	USA	109	13	16 (40 max)	65 (130max)	4.0	120	2500	2.4	10	1972-4
ST (phase II)	USA	109	13	16 (40 max)	65 (130max)	4.0	600	2500	2.4	10	1974-5
T-4	USSR	100	17	10-35	220	4.0	700	3000	4	16	1976
T-10	USSR	150	37	35-50	400	5.0	800	1200		60	1979
TFR (phase I)	FRANCE	98	20	34-49	130-150	1.0-1.7	500-600	1500	4.0	25	1976-8

TABLE 1 TOKAMAK PARAMETERS

DEVICE	COUNTRY	R_o (cm)	a (cm)	B_T (kG)	I_p (kA)	$\bar{n}$ 10^{13} / cm^3	T_i (keV)	T_e (keV)	q	τ_E (ms)	YEAR
TFR (phase II)	FRANCE	98	20	34-49	130-150	16-80	500-600	1500	4.0	25	1978
TM-1Vch (phase I)	USSR	40	8	12	10	>2		70		0.3	1974-6
TM-1Vch (phase II)	USSR	40	8	20	10	>2		70		1.0	1976
TO-1	USSR	60	18	7.5	10	1.0	100	250	2.5	2.5	1974
JET	EUROPE	296	140x125 cross section	30	2600	7.0					
NUWMAK	USA	512.5	112.5	60	5200	20	1000-13200	1000-15400	2.6	2000	∿2000
TETR	USA	325	75	42	2520	7.5	8600	7400	2.4	52	∿1985
TFTR	USA	248	85	52	2500	2		2500	4.1	20	∿1982
UWMAK III	USA	810	383	40.5	15800	6.5	1800-18400	1800-23000	∿1	1700	∿2000

TABLE 2 EXPERIMENTAL RF PARAMETERS

DEVICE (Ω)	f (MHz)	P_{RF} (kW)	COIL DESIGN	η_{wave} (%)	$\eta_{heating}$ (%)	ΔT_i (ev)	τ_{RF} (ms)	Q (expected)	POLOIDAL MODE	TOROIDAL MODE	MODE TRACKING
ATC (2)	25	<200 145 avg	135° copper strip	90	10-40	200	10		1		NO
DIVA (1) (2)	25-30 48-60	<200	1/2 turn coil	65	20	200	1		0,±1	20-30μs <12	YES
ERASMUS	3-15	∿100	faraday loop				∿10	50-70 (≥700)	0,1		NO
MACROTOR	0-20	<100	copper					∿40	2	seen	NO
MICROTOR	22	<100	copper		<70			50	2	seen	NO
PLT (1) (2)	55 25	5000	two 1/2 turn	(90)	(25-50)	(2000-4000)	300	HIGH	0,±1,±3	1 seen	YES
ST (phase I)	25	<30	1/2 turn inside	40 (Ω=1) 35-50 (Ω=2)		55	5-10	200-300	0,1		NO
ST (phase II)	25	75-150	two 1/2 turn faradays	90	20	100	5-10	200-300	0,±1 (mainly -1)	4-9	NO
T-4 (2)	23	50	uninsulated SS coil	90		200		300 (3000)			

TABLE 2 EXPERIMENTAL RF PARAMETERS

DEVICE (Ω)	f (MHz)	P_{RF} (kW)	COIL DESIGN	η_{wave} (%)	$\eta_{heating}$ (%)	ΔT_i (eV)	τ_{RF} (ms)	Q (expected)	POLOIDAL MODE	TOROIDAL MODE	MODE TRACKING
T-10	50-60	500	wide coil			(1000-2000)					
TFR (phase I)	50-75	<0.1	V-shape faraday				5-27	50	0	1,2,3	YES
TFR (phase II)	50-90	120	two 1/2 turn faradays	55		150-200	5-27	$<10^4$	0,±1	1,2,3	YES
TM-1Vch (phase I)	22	≤20	loop	40-50		80-90	0.4	6-15	1	seen	NO
TM-1Vch (phase II)	7-35	150(Ω=2) 1000 (Ω=1)	two asy-mmetric	80-90	30-40	100	0.6-.8		0,1	seen	NO
TO-1	48	≤5	loop			50	20-22	10-250			YES

TABLE 3 PROPOSED RF PARAMETERS

DEVICE	f (MHz)	P_{RF} (MW)	STRUCTURE	η_{wave} (%)	$\eta_{heating}$ (%)	ΔT_i (keV)	τ_{RF} (sec)	Q	POLOIDAL MODE	TOROIDAL MODE
JET	46	1	loaded waveguide 45x30cm or loop						$0 \leq \lvert m \rvert \leq 6$	
NUWMAK	92	75	waveguide	∿100	∿60	12.2	2	10-50	1,2	∿50
TETR	.3	50	waveguide	∿100	∿60	1.5	∞	160-3660	0,1	∿50
UWMAK III	60	200	waveguide	∿100	∿60	16	15	∿120	0,±1,±2	∿50

TABLE 4

REACTOR PARAMETERS

$a = 125$ cm	$\bar{n}_e = 1.95 \times 10^{14}$ cm^{-3}
$R = 500$ cm	$\bar{n}_e = \bar{n}_T = .975 \times 10^{14}$ cm^{-3}
$A = 4$	$\frac{n_{edge}}{n_{max}} = \frac{T_{edge}}{T_{max}} = .01$
$S = 1.33$	$T_i = T_e = 1.0$ keV
$I = 6.48$ MA	$f = 92$ MHz
$B_o = 60$ KG	$k_{\parallel} = 0.1$ cm^{-1}
$P \simeq 2300$ MW	$k_{\perp} \sim 1.6$ cm^{-1}
Toroidal mode number = 50	

	TABLE 5	TABLE 6
Tokamak Parameters		
Toroidal Field (kG)	60	60
Major Radius (cm)	500	500
Minor Radius (cm)	125	125
Output Power (MW_e)	2300	-
Reactor Q	~ 7	$\lesssim$ 1.1
Plasma Parameters		
Plasma Volume (cm^3)	1.54×10^8	1.54×10^8
Tritium Density (cm^{-3})	1×10^{14}	2×10^{14}
Initial Deuterium Density (cm^{-3})	1×10^{14}	1×10^{12}
Tritium Energy Containment Time (sec)	10	0.1
Deuterium Energy Containment Time (sec)	10	0.1
Tritium Particle Containment Time (sec)	10	0.1
Deuterium Particle Containment Time (sec)	10	∞ for $E_o > 15$ keV 0.1 for $E_o < 15$ keV
Initial Temperature ($T_d = T_t = T_e$) (eV)	667	667
Energy of Deuterium Beams (keV)	-	200
Beam Pulse Length (ms)	-	3000
RF Heating Parameters		
Toroidal Mode Number	50	50
Parallel Wavenumber (cm^{-1})	0.1	0.1
Minor Radius of Heating Calculation (cm)	50	50
RF Frequency (MHz)	57.5	5.75
RF Power (MW)	100	-
RF Pulse Length (sec)	2.5	3

Acknowledgements

I would like to thank Profs. John E. Scharer and Robert W. Conn for the leadership which they have provided me in my research. I would also like to express my gratitude to Drs. Tak Kuen Mau, Brian McVey, and Jay Kesner for their invaluable assistance in my work.

My thanks go out to Ms. Gail Herrington who typed much of this rather large document.

Finally, I wish to thank my wife, Kathy, who provided the motivation for me to finish this work.